Layer-by-Layer Self-assembled Weak Polyelectrolyte-based Novel Multilayered Film: Fabrication, Unique Properties and Applications

Yuan Weiyong

School of Chemical and Biomedical Engineering

A thesis submitted to the Nanyang Technological University

in fulfillment of the requirement for the degree of
Doctor of Philosophy

2010

Acknowledgements

First, I am honored to express my deepest gratitude to my dedicated supervisor, Prof. Li Chang Ming. Prof. Li has advised, inspired, and supported me throughout my PhD work, especially in times of difficulty. He has offered me valuable ideas, suggestions, and criticism, drawing upon his deep knowledge of the topic and his rich research experience. At the same time, he has offered me the freedom to develop my own ideas and pursue them. I treasure the research journey I have taken under his guidance, and his encouragement will continue to motivate me as I face scientific challenges in the future.

I also wish to extend my thanks to the research fellows and PhD students in our lab, especially those who have collaborated with me. I greatly appreciate the experimental assistance I have received from them, as well as the fruitful discussions we have shared. I will always cherish the moments we have spent together.

Last but not least, I would like to thank my family for providing support throughout my PhD program. My parents, my brother, and especially my wife have always been there to bolster my confidence. This thesis could not have been finished without them.

Table of Contents

List of Figures

List of Tables

List of Schemes

Summary

Layer-by-layer (LbL) self-assembled weak polyelectrolyte-based multilayered films have shown superior tunability and versatility to other polyelectrolyte multilayers. Previous works have focused primarily on the assembly of linearly grown synthetic weak polyelectrolyte multilayers. Further investigation is warranted of weak polyelectrolyte-based self-assembly systems such as natural weak polyelectrolyte multilayers, nanoparticle-participated weak polyelectrolyte multilayers, and exponentially grown multilayers, their unique properties, and novel applications.

In particular, in this PhD research project, a chitosan/alginate multilayer film was constructed via LbL self-assembly. The surface composition of the self-assembled multilayer film can be tailored through pH adjustment during the assembly process. The loading capacity of the antibody on the multilayered film and the binding activity of the antigen to the immobilized antibody can be well-tuned by pH control. This work can provide more scientific insight into the interaction between protein and polymer matrix and render a novel, simple approach to build high-performance biointerfaces through pH control for potential applications of highly sensitive immunosensors.

For the first time, a pH-controllable weak polyelectrolyte/metal nanoparticle composite film was successfully constructed on a solid substrate through LbL assembly, and its localized surface plasmon coupling (LSPC) was investigated. The degree of LSPC can be modulated by controlling the pH of the weak polyelectrolyte used. The LSPC proved tunable and stable, as demonstrated by a large shift of the longitudinal band peak position over a range of 625-741.5 nm as a

function of pH while shifting insignificantly at a fixed pH for a month. The modulation of LSPC of the LbL nanocomposite film can be ascribed to changes in the assembled weak polyelectrolyte, where the charge density and conformation can be easily controlled by pH to tailor the interparticle spacing in the nanoparticle clusters. This work provides a rational approach to the preparation of stable nanocomposites with easily tunable LSPC and affords scientific insight into the effect of film morphology on the optical properties of assembled nanoparticles. The spectral response to the environment has great potential in applications such as plasmonics, biosensing, and medical therapy.

A nanoparticle-participated three-component LbL assembly with a weak polyelectrolyte-nanoparticle blend and another weak polyelectrolyte was used to fabricate composite hollow capsules. The polyelectrolyte assembly pH and the blend ratio of polyelectrolyte to nanoparticles were tailored to construct blend multilayers on colloidal templates without aggregation. The microcapsules obtained after removal of the templates had well-dispersed assembled nanoparticles with desired concentration, size, and interparticle spacing. The prepared capsule demonstrates both superior tunable localized surface plasmon resonance (LSPR) and permeability synergistically from its assembled components, which have not been achieved by reported polyelectrolyte or polyelectrolyte/nanoparticle capsules. These properties can be controlled by adjusting the ratio of nanoparticle to polyelectrolyte in the blend solution. This work provides a novel and universal approach to the fabrication of well-dispersed microcapsules with tailored nanoparticles for various applications while offering scientific insight into the

nanoparticle-participated blend LbL assembly process. The prepared new polyelectrolyte/nanoparticle capsules could hold promise for intelligent drug delivery, biosensing, and bioimaging applications.

A hierarchical nanoporous ultrathin polymer film was fabricated through an exponentially growing LbL assembly of weak polyelectrolytes without any template and post-treatment. It demonstrated greatly enhanced loading capacity of charged small molecules, significantly extended release time, and greatly increased linear release range in a wide pH range with pH-dependent loading and release behavior in comparison to reported weak polyelectrolyte multilayer films. Thus, it offers great potential for controlled drug release applications.

This research not only developed several self-assembly systems with unique properties that could be controlled by assembly conditions at the molecular level, but also provided scientific insight into the mechanism of weak polyelectrolyte-based LbL self-assembly. Additionally, this work provides opportunities to fabricate LbL assemblies for various potential applications.

Chapter 1 Introduction

1.1 Introduction

The self-assembly of functional materials on substrates with chemistry, structure, and properties controlled at the nanometer level has attracted tremendous interest in recent years.[1-10] A rapidly developing technique with great potential to achieve this objective is layer-by-layer (LbL) assembly, which was first attempted by Iler et al. in 1966[11] and developed by Decher et al. in 1991.[12-14] The basic principle of LbL self-assembly is the sequential adsorption of oppositely charged species on substrates driven by electrostatic force.[15] It is easy to implement this technique, as it only requires one to expose suitable substrates to solutions of charged species for the electrostatic adsorption and to remove loosely adsorbed species due to other nonspecific interactions by rinsing after each assembly step.[15] No sophisticated equipment or strict conditions are required.[15] In addition to its simplicity, this technique is very versatile. Various charged species such as synthetic polyelectrolytes, biomacromolecules (such as proteins, DNA, and polysaccharides), and nanoparticles can be adopted as building blocks.[5-10] Materials with any geometry and chemical composition that can survive the assembly conditions can be used as substrates.[5-6, 8-9, 16] In recent years, besides electrostatic interaction, various driving forces such as hydrogen bonding,[8] covalent bonding,[17] coordination bonding,[18] and biomolecular recognition[19] have been used to drive the assembly process, greatly expanding the type of building blocks that may be used. The assembled building blocks can be self-organized on a substrate to form the

nanoscale-ordered structure in both vertical and lateral directions.[5, 20-22] Numerous unique properties of LbL-assembled multilayers have been discovered: the thickness can be controlled at the nanometer level simply by changing the layer number,[14, 23] and many physicochemical properties such as wettability,[23] stiffness,[24] permeability,[25] optical transparency,[26] and conductivity[27] can be manipulated and changed to a great extent. The combination of diverse chemistry, nanoscaled structures, and unique properties endow self-assembled multilayers with great potential in various fields including electronics,[28] optics,[29] photovoltaics,[30] sensors,[31] and biomaterials.[32]

The versatility of the LbL process lies principally in the molecular-scale control of physicochemical properties via the control of assembly conditions and versatile building blocks. As the charge density and conformation of weak polyelectrolytes are dependent on pH, the assembly of weak polyelectrolytes can be significantly tuned by pH.[23] Typical weak polyelectrolytes include synthetic polyelectrolytes such as poly(allylamine) (PAH), poly(acrylic acid) (PAA), poly(ethyleneimine) (PEI), and poly(methacrylic acid) (PMAA), and biomacromolecules such as chitosan, alginate, poly(L-lysine) (PLL), hyaluronic acid (HA), and gelatin. Rubner et al. at MIT systematically studied the effect of assembly pH on the chemical composition, surface morphology, thickness evolution, surface wettability, swellability, and roughness of weak polyelectrolyte multilayer films using synthetic weak polyelectrolytes such as PAH and PAA as model weak polyelectrolytes.[23, 33-38] Bilayer thickness, chemical composition, wettability, surface roughness, swelling capabilities, mechanical strength, and even conductivity can be controlled through

the assembly pH of weak polyelectrolyte at a molecular level.

However, previous studies on weak polyelectrolyte-based multilayers have focused on 2-synthetic weak polyelectrolyte systems. The structural and functional diversity of synthetic weak polyelectrolytes are limited, which greatly restricts the properties and applications of weak polyelectrolyte multilayers. Other building blocks such as nanoparticles could, in principle, be assembled with weak polyelectrolytes, but the multilayers both on substrate and in freestanding form are much less studied. These weak polyelectrolyte/nanoparticle multilayer films could combine the pH-tunability of weak polyelectrolyte with the unique physicochemical properties of nanoparticles, thus providing broad opportunities for new applications. Besides enriching the building blocks for weak polyelectrolyte-based LbL assembly, tuning the growth mode from traditional linear growth to others such as exponential growth could lead to novel multilayer films.

1.2 Motivations

Natural weak polyelectrolytes such as chitosan and alginate have great potential for biomedical and environmental applications, but their assembly kinetics, tunability, and mechanism via adjustment of assembly pH have not been systematically studied and require further investigation.

Strong polyelectrolyte has been used as a linker to assemble nanoparticles into multilayered films for synergistic effect from their unique physical and chemical properties, but it is difficult to tune the assembly due to the narrow adjustment range of the charge density of the strong polyelectrolyte. In addition, the

relationship between nanoparticle organization and multilayer properties is not well understood. The study of LbL assembly of weak polyelectrolytes and nanoparticles could provide a simple route to tune the charge density of polyelectrolytes at a wide range for the investigation of the structure and properties of nanoparticle assemblies.

Freestanding nanoparticle assemblies such as hollow spheres with tailored nanoparticle concentration, size, and interparticle spacing could have important applications such as drug delivery. However, a method for obtaining hollow capsules with these attributes using weak polyelectrolyte-based LbL assembly has not been reported. Weak polyelectrolytes provide a strategy to adjust the electrostatic interaction between nanoparticles and the colloidal template and therefore may have promise for the development of well-controlled polyelectrolyte/nanoparticle composite capsules with unique properties.

Exponentially growing LbL assembly could greatly accelerate the multilayer fabrication process while producing an extremely loose structure to allow a large amount of small molecules, proteins, and even nanoparticles to penetrate into the multilayers. The pH-controlled assembly of exponentially grown weak polyelectrolyte multilayers has not been fully studied. Its interaction with guest materials such as small molecules and proteins is not well understood. Investigation of these interactions could afford scientific insight into these unique systems as well as provide a novel, superior platform for broad biomedical applications such as drug delivery.

1.3 Objective of study

The objective of this project is to controllably fabricate weak polyelectrolyte-based novel multilayered films via LbL self-assembly at a molecular level, to study their structure and properties, to explore their potential applications, and to understand their assembly mechanisms. The study is composed of the following parts.

1) An investigation of the pH-controlled LbL assembly of natural weak polyelectrolytes and their biological properties by antibody immobilization. The multilayer construction process, chemical composition, and surface morphology of the multilayered films built at different assembly pH are studied to understand their self-assembly mechanism. The loading capacity and antigen binding activity are also studied.

2) An investigation of pH-controllable LbL-assembled weak polyelectrolyte and nanoparticle nanocomposite films. The nanoparticle organization at different assembly pH levels is used to study the self-assembly mechanism. The collective properties of nanoparticles in the nanocomposite film determined by the nanoparticle organization are also investigated to demonstrate pH-tunability.

3) The development of a new method for the fabrication of polyelectrolyte/nanoparticle composite capsules with the desired concentration, size, interparticle spacing, and nanoparticle dispersion via LbL assembly of weak polyelectrolyte-nanoparticle blend and another weak polyelectrolyte, and the further study of their synergistic properties.

4) The construction of unique nanostructured multilayer films via exponentially

growing LbL assembly of weak polyelectrolyte and the exploration of their potential application in drug loading and release. In particular, small molecule delivery is used to study the enhancement of drug loading capacity and release time, as well as pH-controlled loading and release.

1.4 Organization

This dissertation investigates the buildup, mechanism, and applications of novel LbL-assembled weak polyelectrolyte-based multilayers. Chapter 1 has introduced the background, motivation, and objective of this PhD research. Chapter 2 reviews recent research on weak polyelectrolyte-based multilayers, including the fundamental controllability of multilayer properties, different types of building blocks for the formation of multilayers, and applications. Chapter 3 describes the materials, equipment, and methodology used in this study. Chapter 4 describes an investigation of the pH-controlled construction of chitosan/alginate multilayer film and its application for antibody immobilization. Chapter 5 explores the pH-controlled LbL assembly of weak polyelectrolyte/gold nanoparticles for direct modulation of LSPC on solid substrates. Chapter 6 addresses three-component LbL assembly for the fabrication of weak polyelectrolyte/gold nanoparticle composite capsules with superior tunability and synergistic physical properties. Chapter 7 describes the fabrication of an exponentially grown weak polyelectrolyte multilayer with hierarchical nanoporous structure by pH-controlled LbL assembly and its application to the delivery of small charged molecules. Chapter 8 outlines general conclusions and provides possible directions for future research.

Chapter 2 Literature Review

2.1 Layer-by-layer assembly

In 1966, Iler first reported the formation of multilayers from alternate adsorption of two charged particles from solution.[11] Since the extension of this method to polyelectrolyte systems in 1991 by Decher et al.,[39] the technique has developed rapidly. The preparation process and principle of this technique are very simple, as shown in Figure 2.1.[15] First, a charged surface is immersed into a solution containing an oppositely charged polyelectrolyte. After a certain time, a molecularly thin layer of this polyelectrolyte will form due to the electrostatic force. After a water rinse, the loosely adsorbed polyelectrolyte is washed away. Subsequently, the substrate is immersed into another solution containing a polyelectrolyte charged oppositely to that of the previous polyelectrolyte. Another molecularly thin layer is formed after a certain time. With the process repeated, a structured film with a controlled thickness can be formed easily.

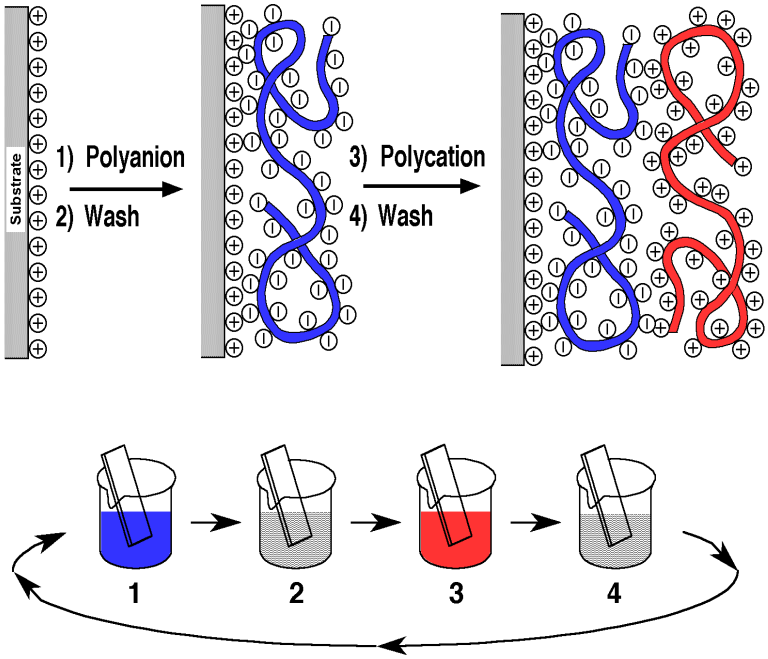

Figure 2.1 Schematic diagram of the LbL process. Reproduced with permission from [15]. Copyright 1997 American Association for the Advancement of Science.

There are many advantages of the LbL technique:[5, 40-41] The process is easy; no sophisticated equipment is needed; many building blocks such as synthetic polyelectrolytes, biomacromolecules (such as DNA, proteins, and polysaccharides), and nanoparticles can be used in the assembly; various materials with essentially any geometry can be used as substrates; and the physicochemical properties of assembled film can be controlled easily at a molecular level by adjusting the assembly condition and building blocks. The driving forces of LbL films are not limited to electrostatic interactions.[6] In recent years, they have been extended from electrostatic force to hydrogen bonding, coordination bonding, biological recognition, covalent bonding, and hydrophobic interaction. The simplicity, versatility, and robustness of this technique have made it attractive to more and more scientists. Potential applications of this technique have been developing

rapidly and include biosensors, catalysis, membrane separation, soft electrode, modulation of cell surface interaction, and drug delivery.[42-46]

2.2 Weak polyelectrolyte as a building block for LbL assembly

Weak polyelectrolytes are polymers whose charge density is widely tunable through the adjustment of solution pH. Weak polyelectrolyte chains with higher charge density are more rigid, whereas chains collapse with more coiled conformation when the charge density is lower.[47-48] Thus, the conformation and size of weak polyelectrolytes can also be modulated accordingly by solution pH. Weak polyelectrolytes represent a broad range of polymers including polyamines, polycarboxylic acids, DNA, numerous polysaccharides, polypeptides, and conducting polymers (a few examples are listed in Figure 2.2). A lot of novel weak polyelectrolytes with diverse functions are also synthesized, greatly expanding the range of weak polyelectrolytes.[49-52] With their diversity in chemical species and tunability in charge density, conformation, and size, weak polyelectrolytes have attracted tremendous interest in terms of fundamental science[47, 53-55] as well as practical applications.[56-58]

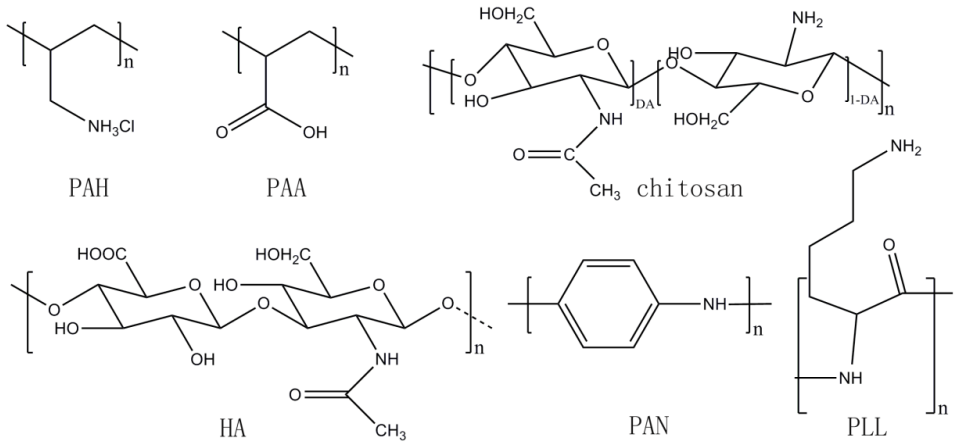

Figure 2.2 Typical examples of weak polyelectrolytes

Recently, a lot of effort has been made to adopt weak polyelectrolytes as building blocks for LbL assembly. Many unique characteristics and advantages have been revealed for weak polyelectrolyte-based LbL assembly. First, the pH-tunable charge density of weak polyelectrolytes renders their assembly behavior and the final physicochemical properties of multilayers highly sensitive to assembly pH.[23, 35, 59] Second, the assembled multilayers may be responsive to environmental pH, as both the electrostatic interaction between building blocks and polyelectrolyte conformation can be readily changed by the environmental pH.[34, 37, 60-61] Third, although pH plays a dominant role in determining multilayers' properties, other factors also affect them.[62-64] Last but not the least importance, novel applications are enabled due to the multilayers' diverse chemistry, unique tunable structures, and rich suite of properties.[25, 57, 65-67]

The area of weak polyelectrolyte-based multilayers is expanding very rapidly. Previously, this type of research focused primarily on linearly grown, all-weak-polyelectrolyte multilayers.[23, 35, 59] More recently, however, LbL assembly involving weak polyelectrolytes and many other components including strong

polyelectrolytes,[37, 68-69] neutral polymers[8, 70-71] and nanoparticles[72-74] has been investigated. These multilayers can inherit the advantages of weak polyelectrolytes and incorporate the unique characteristics of the other components; therefore, they may have novel structures, properties, and applications.[25, 38, 72, 75] Weak polyelectrolyte systems that show exponential growth during the LbL assembly process have also been explored recently.[63, 76-78] Their properties can be distinct from those of linearly grown weak polyelectrolyte multilayers, and they can easily incorporate other components such as nanoparticles to further enrich their properties.[21, 60, 76-77, 79-85]

2.3 Superior controllability of structure and properties of weak polyelectrolyte multilayers

2.3.1 pH-controlled properties of weak polyelectrolyte multilayers

Several studies have shown that the bilayer thickness, chemical composition, and layer interpenetration of weak polyelectrolyte multilayers can be controlled accurately at a molecular level.[23, 86-87] Rubner et al. have studied the LbL assembly of the synthetic weak polyelectrolytes PAH and PAA.[23] When the pH is in the range of 2.5 to 4.5, the thickness of the PAH layer and PAA layer is solely dependent on the solution pH. With an increase in the assembly pH, the PAA layer's thickness decreases due to increased charge density and reduced loop and tail segmental density. For the PAH layer, however, thickness remains essentially unchanged, as the polymer chain is nearly fully charged in this pH range. More interestingly, the thickness ratio of the PAH and PAA layer determines the

interpenetration between layers. Thus, by simply controlling the assembly pH to control the layer thickness, one can accurately control the interpenetration level between layers.

The swelling capability of polyelectrolyte multilayers in aqueous solutions plays an important role in applications such as membrane separation,[88] biomaterials,[36] sensors,[73] and drug delivery.[89] Barret et al. have studied the swelling dynamics of PAH/PAA multilayers.[90] The swelling extent, swelling rate, and the time to reach maximum swelling can all be tunable by assembly pH, possibly as a result of pH-tunable ionic cross-linking and loop density. To further understand the swelling of weak polyelectrolyte multilayers, Barret et al. also studied PAH/HA multilayers.[91] Solution pH plays important roles in multilayer swelling in addition to other factors such as ionic strength and thickness. The largest swelling extent occurs at the low or high assembly pH when multilayers have low ionic cross-linking density and a large number of loops and tails are available for proton exchange (Figure 2.3). The highly pH-dependent swelling behavior of weak polyelectrolyte multilayers was also observed for PLL/HA multilayers,[35] which always swell much more when assembled at pH 9 than at pH 5 at all the swelling pH levels studied, due to weakly charged PLL molecules at pH 9 forming loosely cross-linked multilayers with HA.

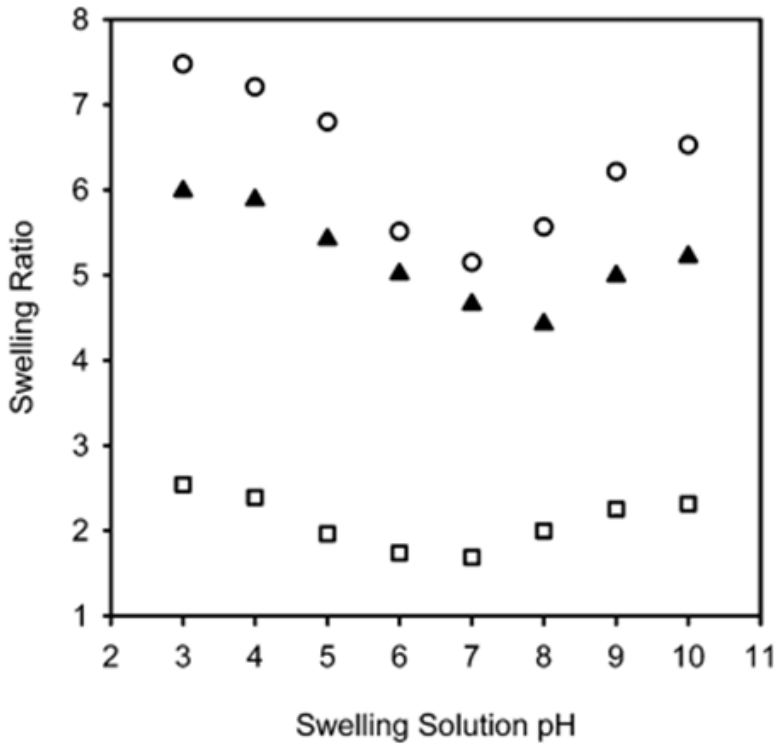

Figure 2.3 The swelling of $(PAH/HA)_{15}$ film assembled at pH 4.0 (○), pH 7.0 (□), and pH 10.0 (▲) at different swelling solution pH. The uncertainty in the swelling ratio is ±0.6-1.0%. Reproduced with permission from [90]. Copyright 2005 American Chemical Society.

The mechanical properties of polyelectrolyte multilayers can be related to interchain ionic cross-linking and molecular conformation in multilayers, which are tunable via the assembly pH for weak polyelectrolyte multilayers. PAH 7.5/PAH 3.5 multilayers have a much lower hardness and elastic modulus than PAH 6.5/PAA 6.5 multilayers due to the loopier conformation of polymers in PAH 7.5/PAH/3.5 multilayers, which adapt more easily to the force added. [92] Significant effects of ionic cross-linking on Young's modulus of weak polyelectrolyte multilayers in an aqueous environment have been reported. Young's modulus can be enhanced by several orders of magnitude for the PAH/PAA system by simply increasing the assembly pH from 2.0 to 6.5, due to greatly increased ionic cross-

linking density inhibiting the swelling in aqueous solution.[93] The importance of ionic cross-linking density on the elastic modulus has also been studied by Barret et al. using PAH/PAZO as a model system.[94] The elastic modulus of the multilayer film assembled with a strongly charged PAH (assembly pH 5.0 and 7.0) is on the order of 50 times greater than that assembled with a weakly charged PAH (assembly pH 9.0 and 10.5).

The conductivity of weak polyelectrolyte multilayers can also be controlled by assembly pH. Rubner et al. have studied the dielectric property of PAH/PAA multilayers. With an increase in the assembly pH from 3.5 to 6.5, the charge density of PAA increases to form more ionic association with PAH. Consequently, fewer small ions are incorporated, making the film less conductive.[27] Hammond et al. have studied the ionic conductivity of a series of multilayers.[71, 95-96] For the weak polyelectrolyte pair LPEI/PAA, the ionic conductivity of multilayers assembled at pH 5 is one order of magnitude greater than that of multilayers assembled at pH 2. It is possible that at pH 5, there is high content of mobile and uncoordinated PEI chains to enhance ion mobility more efficiently than carboxylic acid groups.[95] The pH tunability of ionic conductivity for hydrogen-bonded weak polyelectrolyte involved multilayers such as PEO/PAA multilayers[96] or MEEP/PAA multilayers has also been demonstrated by the same group.[71] The hydrogen bonding-driven LbL assembly involving weak polyelectrolytes will be discussed later.

Weak polyelectrolyte multilayers can be responsive to environmental pH. Novel structures have been observed through the simple pH treatment of weak

polyelectrolyte multilayers. A microporous film was obtained after brief immersion of the PAH/PAA multilayer (assembled at pH 7.5 for PAH solution and 3.5 for PAA solution) in water with a pH around 2.4.[34] Further optimization of the assembly pH and posttreatment procedure (acid treatment plus a brief rinse in water) would generate a nanoporous film that exhibits excellent antireflective properties.[26] The transition from nonporous to nanoporous status is reversible only by changing the environmental pH (Figure 2.4). Hammond et al. have studied the morphological change of the exponentially grown PEI/PAA multilayer after post pH-treatment.[60] With only slight change to the assembly pH and posttreatment pH, various morphologies with pores from the nanometer scale to the micrometer scale were observed. For example, the PEI/PAA multilayer assembled at pH 5 exhibited nanoporous morphology after posttreatment at pH 1.75 but a heterogeneous structure with distinct nanopore and micropore regions at pH 2. Instead, a craterlike micropore was obtained at pH 3. The pore volume was as high as 72% at posttreatment pH 2 and was even 77% at pH 2.25.

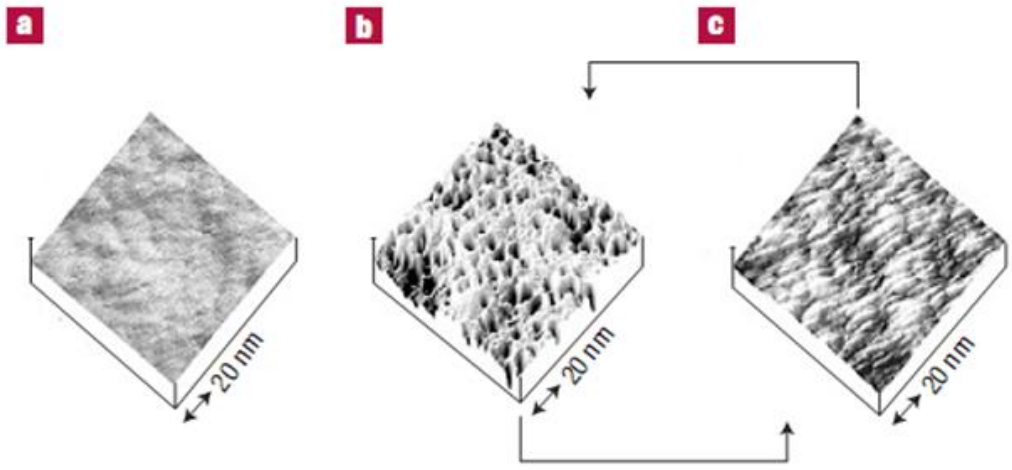

Figure 2.4 AFM images of PAH/PAA multilayers on silicon substrates. a, original non-porous structure. b, nanoporous structure after pH treatment. c, non-porous structure created during pH cycling. The z range is 100 nm. Reproduced with permission from [26]. Copyright 2002 Nature Publishing Group.

Properties such as wettability, swelling, and permeability can also be tuned by the environmental pH. The water contact angle of PLL/HA multilayers can be changed at different environmental pH values.[35] At high environmental pH, the PLL has more $-NH_3^+$ group deprotonized to increase hydrophobicity, while HA has more -COOH group ionized to increase hydrophilicity. Rubner et al. have studied the swelling of PAH7.5/PAA3.5 multilayers on plane substrate and PAH7.5/PAA3.5 nanotube array attached on substrate.[61] The thicknesses of both PAH7.5/PAA3.5 multilayers and PAH7.5/PAA3.5 nanotube array can reversibly change when subjected to pH above around 5.5 and 2 alternatively (Figure 2.5). Mauser et al. have studied the swelling behavior of P4VP/PMA multilayer capsules under different pH values.[97] The shell swells significantly at pH 2 and pH 8.1 due to the net strong electrostatic repulsion between building blocks at these two extremes. The shell is stabilized by hydrophobic force at these conditions. Park et

al. have fabricated stable weak polyelectrolyte multilayers with benzophenone-modified PAA (PAA-BP) and benzophenone-modified PAH (PAH-BP) followed by photo-cross-linking to show a pH-sensitive bipolar ion-permselective property.[50] Tong et al. have successfully fabricated stable cross-linked PEI and PAA multilayer capsules with pH-sensitive permeability.[98]

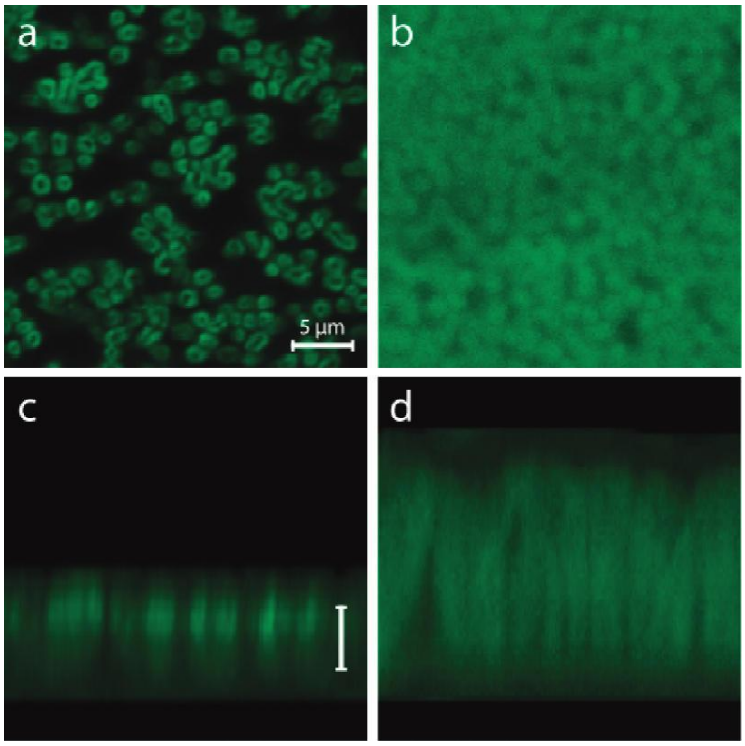

Figure 2.5 CLSM images of $(PAH7.5/PAA3.5)_{20}$ tube arrays. (a, b) Higher-magnification plan-view in pH 5.5 and 1.8 water, respectively. Both images were scanned at half tube length (not compiled from multiple scans at different heights). (c, d) Compiled side-view images of panels a and b, respectively. Scale bars: 5 μm. Reproduced with permission from [60]. Copyright 2009 American Chemical Society.

2.3.2 Other factors that can tune the properties of weak polyelectrolyte multilayers

Although the properties of weak polyelectrolyte multilayers are dominated by pH, they can also be affected by other factors such as the hydrophobicity of

polyelectrolytes,[99-100] ionic strength,[62, 101-102] molecular weight,[33, 52, 63] cross-linking,[64, 103-104] and the addition of other components into a weak polyelectrolyte solution.[75, 105-106]

Illergard et al. have studied the effect of hydrophobilization on the LbL assembly of PVAm and PAA by modifying the PVAm with alkyl chain.[99] The hydrophobilization of PVAm does not have a significant effect on its dispersion in solution and its LbL growth behavior with PAA, but the surface morphology can be greatly changed with aggregation between the hydrophobically modified PVAm at the same salt concentration. The multilayers assembled with hydrophobically modified PVAm and PAA have a higher contact angle than that with unmodified PVAm and PAA. Dai et al. have changed the hydrophobicity and charge density of PAA by esterification.[100] As a consequence, the hydrophobicity of PAH/d-PAA multilayers increases a great deal compared to PAH/PAA multilayers. Furthermore, the permeability of LbL-assembled PAH/d-PAA multilayers to $Ru(NH_3)_6^{3+}$ and $Fe(CN)_6^{3-}$ is greatly reduced. Hydrolysis after cross-linking renders the film selectively permeable to $Ru(NH_3)_6^{3+}$ over $Fe(CN)_6^{3-}$ due to the high density of COO^- produced from the ester group.

The properties of weak polyelectrolyte multilayers can be further tuned by adjusting the salt concentration. Caruso et al. have fabricated a nanoporous PAH/PAA film by assembling the PAH and PAA multilayers in a salt solution, followed by washing with pure water.[62] Kovacevic et al. have studied the effect of salt concentration and type on the formation and stability of weak polyelectrolyte multilayers.[101] A critical “glass transition ionic strength” is needed to dissolve the

fabricated multilayers, and this ionic strength is dependent on not only the salt concentration, but also the salt type and polymer type. Rubner et al.[102] have investigated the salt-controlled etching of PAH/PAA multilayers. The relative thickness change after etching was determined by NaCl concentrations, the increase of which can decrease the residual relative thickness.

The molecular weight of polyelectrolytes has a great effect on the LbL assembly of weak polyelectrolytes. For the typical PAH/PAA multilayer system, when a nearly fully charged polyelectrolyte PAA (pH=5) is alternatively assembled with a fully charged polyelectrolyte PAH (pH=5) layer, the adsorbed layer exhibits loopy conformation, and its thickness is proportional to $M^{0.3}$ (M is the molecular weight of the adsorbed polymer).[33] For the exponentially grown weak polyelectrolyte multilayers CH/HA, the thickness change versus molecular weight similarly obeys the scaling law, and the scaling exponent is 0.35 ± 0.06. No effect of molecular weight on the exponential growth rate was observed.[63] Furthermore, the transition from islands to vermiculate structure is dependent on the molecular weight. A smaller molecular weight will generate larger wormlike domains.[63] Sun et al. have studied the effect of molecular weight on the growth mode of LbL assembly of PAH/PAA.[52] Although the PAH/PAA multilayers assembled from commercially available high-molecular-weight PAA show linear growth behavior, the PAH/PAA multilayers from synthesized low-molecular-weight PAA exhibit exponential growth. The exponential growth of weak polyelectrolyte multilayers will be discussed in detail below.

Cross-linking of weak polyelectrolyte multilayers has a profound effect on their

properties. A photo-cross-linkable weak polyelectrolyte poly(acrylic acid-ran-vinylbenzyl acrylate) (PAArVBA) was assembled with PAH via LbL technique.[64] After photo-cross-linking, the multilayers showed a significantly lower degree of swelling compared to the as-prepared multilayer. Furthermore, the ability to form a microporous structure by low pH treatment and water rinsing is lost for the cross-linked multilayers. PLL/HA multilayers were cross-linked with EDC and sulfo-NHS.[103-104] The degree of cross-linking can be broadly controlled by the concentration of EDC, resulting in a wide range of modulation of the Young's modulus over 2 orders of magnitude. Consequently, the adhesion and spreading of human chondrosarcoma cells and differentiation of Myoblast can be controlled.

The properties of weak polyelectrolyte multilayers can also be tuned by adding one or more other polyelectrolytes into the weak polyelectrolyte assembling solutions. The obtained so-called polyelectrolyte blend multilayers can not only maintain the properties of weak polyelectrolyte multilayers, but also incorporate other unique characteristics.[75, 105-106] PAH/PAA-PSS multilayers assembled from PAH and PSS added PAA combine the pH-responsive property of weak polyelectrolytes with the stabilization effect of strong polyelectrolytes (PSS).[105] Film thickness and film composition can be simply controlled by adjusting the ratio of PAA to PSS.[105] By controlling the surface composition, one can even manipulate the interaction between protein and the multilayers.[107] PGA-PSS/PAH multilayers have been studied to tailor the growth mode by adjusting the ratio of PGA and PSS in solution.[106] After adding PSS into PGA, the growth shows an exponential trend followed by a linear trend with decreased slope. More PSS induce a greater

difference in the slope. Many other three-component systems have also been studied, including PSS-HA/PLL,[108] DNA-PSS/PAH,[109] and PGA-PLA/PLL.[110] In principle, this combination can be extended to the LbL assembly of an unlimited number of components to realize multifunctionality.[75]

2.4 LbL assembly incorporating weak polyelectrolyte and other components

Recently, the study of the LbL assembly of weak polyelectolytes has been extended from pure weak polyelectrolyte multilayers to multilayers composed of weak polyelectrolytes and other functional materials. In these multilayers, not only are the intrinsic properties of weak polyelectrolytes retained, but other unique properties might also be obtained.[25, 38, 72, 75] In this section, the LbL assembly of weak polyelectrolytes and other components such as strong polyelectrolytes, neutral polymers, and nanoparticles will be reviewed.

2.4.1 LbL assembly of weak polyelectrolyte and strong polyelectrolyte

Many studies have shown that the pH-tunable properties of weak polyelectrolytes can be retained in weak polyelectrolyte/strong polyelectrolyte multilayer systems.[68-69, 111] Rubner et al. have studied the effect of weak polyelectrolyte charge density on the growth of weak/strong polyelectrolyte multilayers.[111] With an increase in charge density, the bilayer thickness decreases with a particularly dramatic change point at the weak polyelectrolyte ionization degree of around 70-90%, very similar to that of PAH/PAA multilayers.[33]

Elzbieciak et al. have investigated the LbL assembly of PEI and PSS by changing the PEI assembly pH.[69] Multilayers with usual growth were obtained at low PEI pH while nonmonotonous grown multilayers were produced at high PEI pH. The multilayers assembled from high-pH PEI showed higher permeability than those assembled from low-pH PEI. In addition to synthetic weak and strong polyelectrolytes, natural weak/strong polyelectrolyte multilayer systems have been studied. Fu et al.,[87] Boddohi et al.,[68] and other researchers[112-113] have studied the LbL assembly of a chitosan/heparin system. As the pH increases, the chitosan charge density decreases but the heparin charge density remains nearly the same, leading to increased multilayer thickness.[68, 87] Other properties of chitosan/heparin multilayers such as surface roughness and wettability can be controlled by assembly pH as well.[87] Besides the retained weak polyelectrolyte properties, weak/strong polyelectrolyte multilayers have advantages and properties compared to the pure weak polyelectrolyte multilayers. For example, the strong polyelectrolyte can increase the stability of multilayers,[75] the multilayers are more likely to be grown linearly with a more regular layered structure,[114-115] and a thinner film with a more compact structure can be obtained.[25, 116]

2.4.2 LbL assembly of weak polyelectrolyte and neutral polymer

Multilayers composed of weak polyelectrolytes and neutral polymers are driven primarily by hydrogen bonding.[8] In sharp contrast to electrostatically assembled multilayers, in which the ionization degree of most weak polyelectolytes will increase due to the formation of ion pairs compared to that in solution,[111, 117] the ionization degree of weak polyelectrolytes in hydrogen-bonded multilayers can be

suppressed to enhance the pH-responsive properties of weak polyelectrolytes.[8, 118-119] For example, the neutral polymer/poly(carboxylic acid) multilayers dissolve after assembly or cannot be assembled above a certain pH.[8, 71, 120] The lightly cross-linked hydrogen-bonded multilayers composed of polyacrylamide and weak polyelectrolyte such as PAA and PMAA can be swollen to a great extent in the physiological environment to significantly resist cell adhesion.[38] A lot of unique properties have been revealed for these hydrogen-bonded multilayers. PVPON/PAA multilayers after incubation show Fabry-Perot fringes that are sensitive to the water content of the film.[121] The study of Fabry-Perot fringes shows that the optical thickness of the incubated film is linear to the ambient humidity; thus, the multilayers can serve as humidity sensors. The PMAA/PVME and PMAA/PVCL hydrogen-bonded multilayers retain the thermoresponsive property of PVME and PVCL, thus offering great potential for drug delivery.[122] For a more comprehensive understanding of hydrogen-bonding driven assembly, a specific review can be referred.[8]

2.4.3 LbL of weak polyelectrolytes and nanoparticles

Nanoparticles have received particular attention in recent years due to their large surface area and unique physical and chemical properties.[123-126] Recently, the LbL assembly of weak polyelectrolytes and nanoparticles has attracted a great deal of interest, as it can combine the advantages of the LbL assembly of weak polyelectrolytes with the unique properties of nanoparticles.[72-74, 127-128] Li et al. have studied the pH-controlled assembly of PEI and Laponite clay.[72] The thickness of the films can be tuned by the assembly pH. Furthermore, the films have a high

degree of hardness and highly reduced moduli and can improve the thermal stability of cotton fabric due to the incorporation of clays. Geest et al. have assembled PAH and gold nanoparticles on $CaCO_3$ microparticles.[74] After removing $CaCO_3$ microparticles, the PAH/Au nanoparticle microcapsules were obtained, showing pH-responsive properties. At low environmental pH, the gold nanoparticle is less negatively charged but the PAH is more positively charged, leading to a net electrostatic repulsion to swell/break the capsules. The same phenomenon can also be observed at high pH when the PAH is less positively charged and the gold nanoparticle is fully charged. Furthermore, the capsules can be disrupted under the irradiation of IR light due to the incorporation of gold nanoparticles. The multi-responsive microcapsules have great potential for drug delivery. Jiang et al. have studied the SPR response of PAH/Au multilayers to environmental pH.[73] Similarly, at high or low pH, the multilayers swell due to the electrostatic repulsion increasing the interparticle spacing of Au nanoparticles. Thus, the LSPR peak blue shifts accordingly compared to that at neutral pH. The response of the SPR (ATR) signal enhancement to environmental pH can also be controlled by fabricating the hybrid PAH/PSS and PAH/Au multilayers, as the PAH/PSS can reversibly swell and deswell with pH change to adjust the distance between Au nanoparticles with Ag substrate.

2.5 Exponentially grown multilayers incorporating weak polyelectrolytes

Traditional LbL systems usually exhibit the linear growth of thickness governed

by the kinetically frozen internal structures and charge reversal.[15, 114-115] Recently, the multilayers obtained from exponentially growing LbL assembly have attracted tremendous interest.[21, 60, 63, 76, 78, 82-84, 116] The thickness of these multilayers can increase exponentially with the bilayer number, greatly accelerating the fabrication process.[76, 84, 129] Furthermore, these multilayers usually exhibit distinct structures and unique properties compared to linearly grown multilayers.[80-82, 130] Until now, although some strong polyelectrolytes have been reported to exhibit exponential growth behavior in extreme conditions, most reported systems are weak polyelectrolyte incorporated systems, including PLL/HA,[78] PLL/PGA,[131] chotosan/HA[63], PEI/PAA,[76] and PDDA/PAA.[130]

Many studies have been conducted to explore the mechanism of exponential growth. The interdiffusion of one or two of the building blocks during assembly has been recognized as the main mechanism for most systems.[21, 76, 78, 131-132] Picart et al. have studied the mechanism of exponential growth of PLL/HA multilayers.[78] When the multilayer film is in contact with PLL, PLL will not only compensate for the surface charge, but also penetrate as free PLL chains into the film, some of which diffuse out of the film during rinsing. When the PLL-terminated multilayer film is further immersed into HA solution, the HA will complex with not only the surface PLL, but also the free PLL inside the film. As the free PLL is proportional to the film thickness, the thickness will show exponential growth (Figure 2.6).[78-79] In certain systems such as PLL/PGA, not only PLL, but also PGA can diffuse in and out of the film.[131] The interdiffusion of polyelectrolytes to drive exponential growth is also observed in synthetic weak polyelectrolyte incorporated systems

such as PEI/PAA multilayers,[76] in which PEI is an interdiffusing component, and PDDA/PAA multilayers,[130] in which PAA is an interdiffusing component. The factors that influence the interdiffusion of weak polycations have been systematically studied by Hammond et al. using PXV/PAA as a model system.[114-115] Loose ionic cross-linking of the multilayers and preferential interaction between studied polycations with polyanions in the film favor the interdiffusion of polycations.[114] The charge density of polycations is also important.[115] For all of the polycations studied, including LPEI, BPEI, PAH, and PAMAM, there is a critical ionization degree below which the interdiffusion is possible. The interdiffusion capability is also related to the intrinsic properties of the polymer itself.[115] For example, PEI has a stronger diffusion capability than PAH, possibly due to its more hydrophilic properties. Laugel et al. have managed to relate exponential growth to the polyanion/polycation complexation enthalpy.[116] The exponentially grown film has an endothermic or weakly exothermic complexation reaction. Furthermore, the growth of model exponential PGA/PAH multilayers at high salt concentration is very sensitive to temperature, but its enthalpy changes little with temperature. Thus, the exponential growth process is mainly driven by entropy.

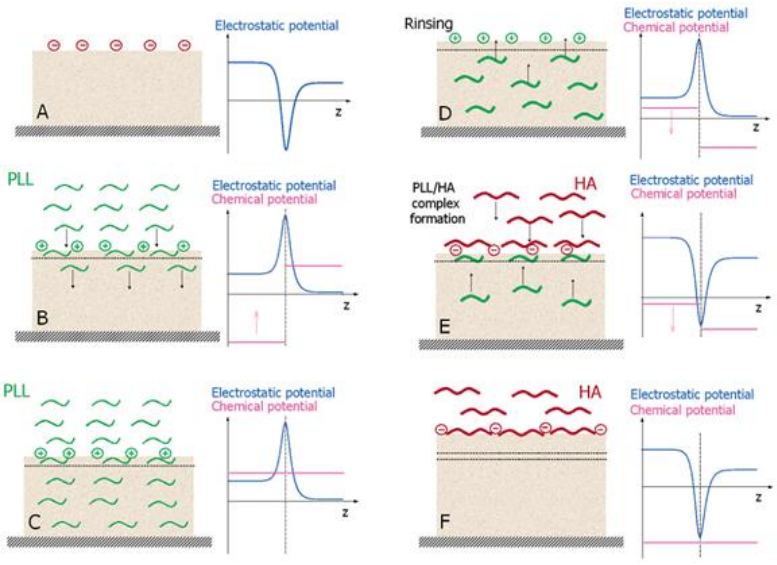

Figure 2.6 The buildup mechanism of PLL/HA film. (A) At the end of a HA deposition step with a negative electrostatic potential at the top of the film. (B) and (C) PLL interacted with the surface HA and diffused into the film. The chemical potential of free PLL chains increased until equal to that of the PLL chains in the solution. (D) Free PLL chains diffused out during rinsing with diminishing chemical potential. (E) and (F) HA chains interacted with the outermost PLL and diffusing PLL (due to the disappearance of positive electrostatic barrier) during HA assembly step to form PLL/HA complexes as the outermost layer. Reproduced with permission from [78]. Copyright 2004 American Chemical Society.

With weak polyelectrolytes incorporated, the exponential growth of multilayers is highly dependent on pH. Fu et al. have systematically studied the pH effect on the LbL assembly of PEI and PAA.[76] When both PEI and PAA solutions are at neutral pH, the growth is nearly linear. Either decreasing the assembly pH of PAA or increasing the assembly pH of PEI will significantly accelerate the assembly process. Thickness of several micrometers after less than 10 deposition cycles can even be achieved. The amplified exponential growth can be explained by the enhanced PEI interdiffusion and pH-tunable charge density of both the film and the polyelectrolyte. Burke et al. have studied the effect of pH on the growth of exponential PLL/HA multilayers.[35] Of the multilayers assembled at pH 5.0, 7.0,

and 9.0, the thickest film was obtained at pH 9.0, while the thinnest film was assembled at pH 7.0. This is because at pH 9.0 or 5.0, the PLL or HA is less charged to be adsorbed on the surface with loopier conformation and a larger amount. Other factors such as salt concentration,[79, 116] molecular weight,[63] and temperature[133] can also affect exponential growth behavior. Richert et al. have studied the effect of salt concentration on the growth of CHI/HA multilayers.[79] With an increase of salt concentration from 10^{-4} M to 0.15 M, the growth mode shifts from linear to exponential. At low salt concentration (10^{-4} M), CHI/HA multilayers are difficult to form, whereas the continuous film is quickly formed after just a few deposition steps at high salt concentration. The effect of molecular weight on the growth and morphology of exponentially grown CH/HA multilayers has been studied by Kujuwa et al..[63] A higher thickness is achieved when the molecular weight is higher. Furthermore, the transition from isolated islands to interconnected domains occurs earlier for the multilayers assembled from small molecular weight pairs. Laugel et al. have studied the effect of temperature on the growth of exponential multilayers.[116] The thickness of exponentially grown PGA/PAH (50 mM salt concentration) multilayers is much more sensitive to temperature than that of PGA/PAH (1mM salt concentration) due to the entropy-driven assembly behavior of exponentially grown multilayers.[116]

A lot of unique properties of exponentially grown multilayers have been revealed in recent years. The multilayers are extremely loose with high density of loop and tail segments, allowing molecules with large molecular weight and even nanoparticles to penetrate in.[80-82, 130] Wang et al. have found that the oligo-peptide

can penetrate into PLL/HA exponentially grown multilayers for loading.[81] Kotov et al. have fabricated PDDA/PAA exponentially grown film to load nanoparticles including quantum dots,[130] silver nanoparticles,[80] and even SWNT.[82] The exponentially grown multilayers have highly mobile polyelectrolyte chains, which have been employed to drive the self-assembly of nanostructures.[21, 77] Hammond et al. have found that the rod-shaped M13 viruses could form an ordered monolayer on the surface of PEI/PAA multilayers during the assembly process.[77] This ordering process occurs largely due to the high mobility of PEI in the multilayer and is driven by the competitive interaction between viruses and polyelectrolytes, interpolyelectrolyte interaction, and the intrinsic nature of viruses (Figure 2.7). Kotov et al. have realized a periodical structure composed of alternative nanometer-scale inorganic layer and micrometer-scale polymeric layer.[21] This structure is attributed to the strong, unequal diffusion rate of polymers and is determined by the relative position of the meeting point of the in-and-out flux of polymers to the film center and MTM layer. Due to the incorporation of weak polyelectrolytes, the diffusion and mobility of weak polyelectrolytes in exponentially grown multilayers can be controlled through the assembly pH. Hammond et al. have employed the pH-controlled surface mobility of polyelectrolytes to control the assembly of M13 virus.[134] When the pH increased from 3 to 5, the charge density of PEI becomes lower to form a thicker PEI layer with enhanced lateral mobility to increase the order of M13 assembly. The same group has also controllably fabricated the micro/nano porous structure using the pH-controlled assembly of PEI/PAA followed by a low-pH treatment.[60] The low-

pH treatment breaks the ionic interaction in the multilayers, causing phase separation to form the hierarchical structures. The formation process is fast due to the quick diffusion of polyelectrolytes. Fu et al. have exploited the pH-enhanced exponential growth of PEI/PAA multilayers to fabricate a hierarchical micro/nano composite structure successfully.[76] The fast growth of multilayers is largely due to the enhanced diffusion of polyelectrolyte with the alternate switching of assembly pH. After hydrophobilization, the multilayer surface can easily exhibit superhydrophobicity.

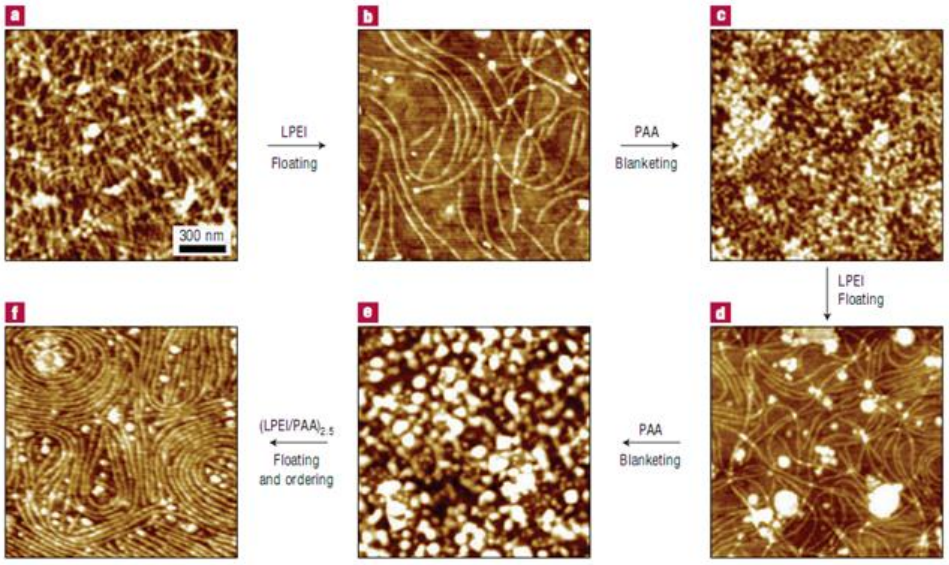

Figure 2.7 Height-mode AFM images of virus organization on multilayers during the assembly process. (Z-range, height scale, 20 nm). a, initial disorderly adsorbed viruses on $(LPEI/PAA)_{3.5}$. b–e, alternating depositions of LPEI and PAA onto the prepared virus layer of a. f, after further deposition of $(LPEI/PAA)_{4.5}$ onto the surface of e. The scale bar in a refers to all parts. Reproduced with permission from [76]. Copyright 2006 Nature Publishing Group.

2.6 Applications of weak polyelectrolyte-based multilayers

Due to their molecular-level controlled structures and rich suite of unique properties, LbL-assembled multilayers including weak polyelectrolyte-based

multilayers have found a lot of applications in optoelectronics,[28, 30-31] biomedicine,[6, 9] membrane separation,[25, 135] and other areas.[5, 41, 136] In this section, we will focus on those applications that we think are most relevant to weak polyelectrolyte-based multilayers.

2.6.1 Drug delivery

PAH/PAA multilayers assembled at pH 2.5 have a large number of uncompensated carboxylic acid groups that can be ionized at high pH to bind permeable cationic molecules. Based on this principle, Rubner et al. have studied the drug loading and release behavior of PAH/PAA multilayers using Methylene Blue (MB) as an indicator.[57] MB can be loaded into multilayers at neutral solution (nonbuffered or buffered), and the release of MB can be controlled via environmental pH. Barret et al. have studied the loading and release behavior of PAH/HA films with two dyes, Indoine Blue and Chromotrope 2R.[89] PH plays a dominant role in the loading and release. The maximum loading can be obtained at the pH value the maximum attraction between dyes and films, the minimum repulsion between dyes and films and greatest J-aggregation of dyes is achieved, while the fastest release can be achieved at the pH value the repulsive force is largest. Poly(AAc-co-NIPAAm)/polyVAm multilayer film has proven able to load anionic dyes.[137] The responsiveness to pH or ionic strength is related to the charge of the dyes that are used. The release rate and released amount of MO, a dye with a single charge unit, cannot be controlled. However, the release of AR, a dye with double charge units, can be controlled via both ionic strength and pH. As the ionic strength or pH increases, the interaction between AR and film is weakened,

resulting in a faster release. The pH-switchable swelling of PAH/PSS multilayers has been employed to load and release rose bengal as a model anionic drug.[37] At an adequately low pH, the multilayers can become swollen with positive charges to load rose bengal. Interestingly, the release of rose bengal can last days to weeks in pH 7.4 buffered solutions, in sharp contrast to common weak polyelectrolyte multilayers, which can release drugs completely in only a few minutes. Microporous and nanoporous films obtained from post treatment of PAH/PAA multilayer films have also been utilized for drug delivery applications.[138] Both loading and release can be controlled. For example, closed pores cannot load drugs, whereas the total amount of drugs loaded into microporous or nanoporous films can be tuned by the bilayer number. The release profile can be controlled by adjusting the pore size of the films: the microporous film shows a Fickian diffusion mode, while the nanoporous film shows a linear release mode. It is noteworthy that drug release from some of these multilayers can last over 20 days in PBS (Figure 2.8).

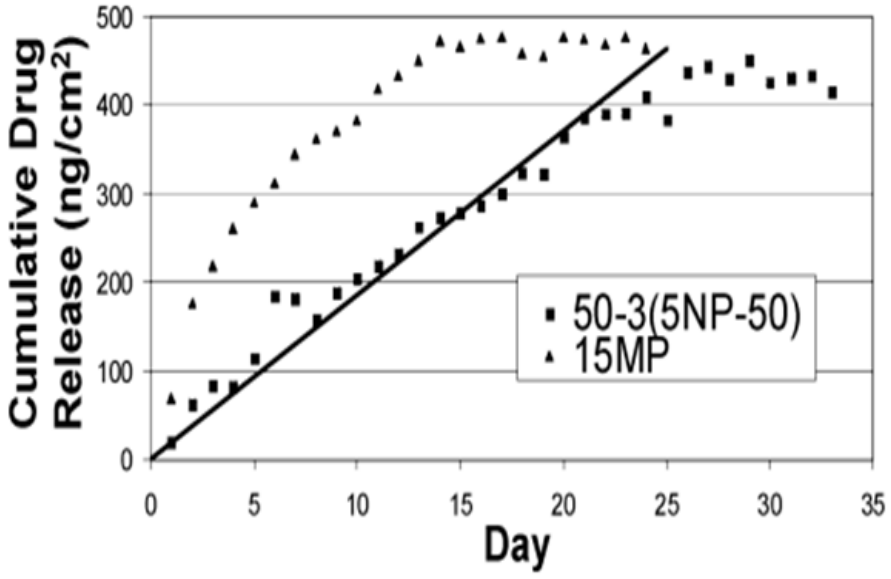

Figure 2.8 Cumulative cytochalasin D release from 50-3(5NP-50) and 15MP films versus time (drug loaded from a 0.2 mg/mL DMSO solution in both cases). Reproduced with permission from [137]. Copyright 2006 American Chemical Society.

2.6.3 Tunable biointerfaces

Weak polyelectrolyte-based multilayers can also be used as tunable biointerfaces. Rubner et al. have studied the adhesion behavior of NR6WT fibroblasts on PAH/PAA multilayers.[36] By controlling the assembly pH, one can tune the ionic cross-linking density accordingly. It is interesting to note that the cell adhesion can be modulated by the ionic architecture of multilayers. The cells can easily attach to multilayers assembled at pH 6, or at pH 7.5 for PAH and pH 3.5 for PAA, both of which are highly ionically cross-linked. However, few cells can attach to the multilayer assembled at pH 2.0, which is loosely cross-linked. This is due to the highly swollen and gel-like nature of the film, which appears to be regarded as water by cells. The highly cell-resistant film is also fabricated by assembling PAAm and PAA or PMA via hydrogen-bonding driven LbL deposition, which

swells greatly in a physiological environment.[38] Fu et al. have fabricated chitosan/heparin multilayers at different assembly pH levels to exhibit both anti-adhesion and antibacterial properties to reduce infection induced by a medical device.[87] Both the antibacterial property and the anti-adhesion property can be controlled through adjustment of the assembly pH (Figure 2.9).

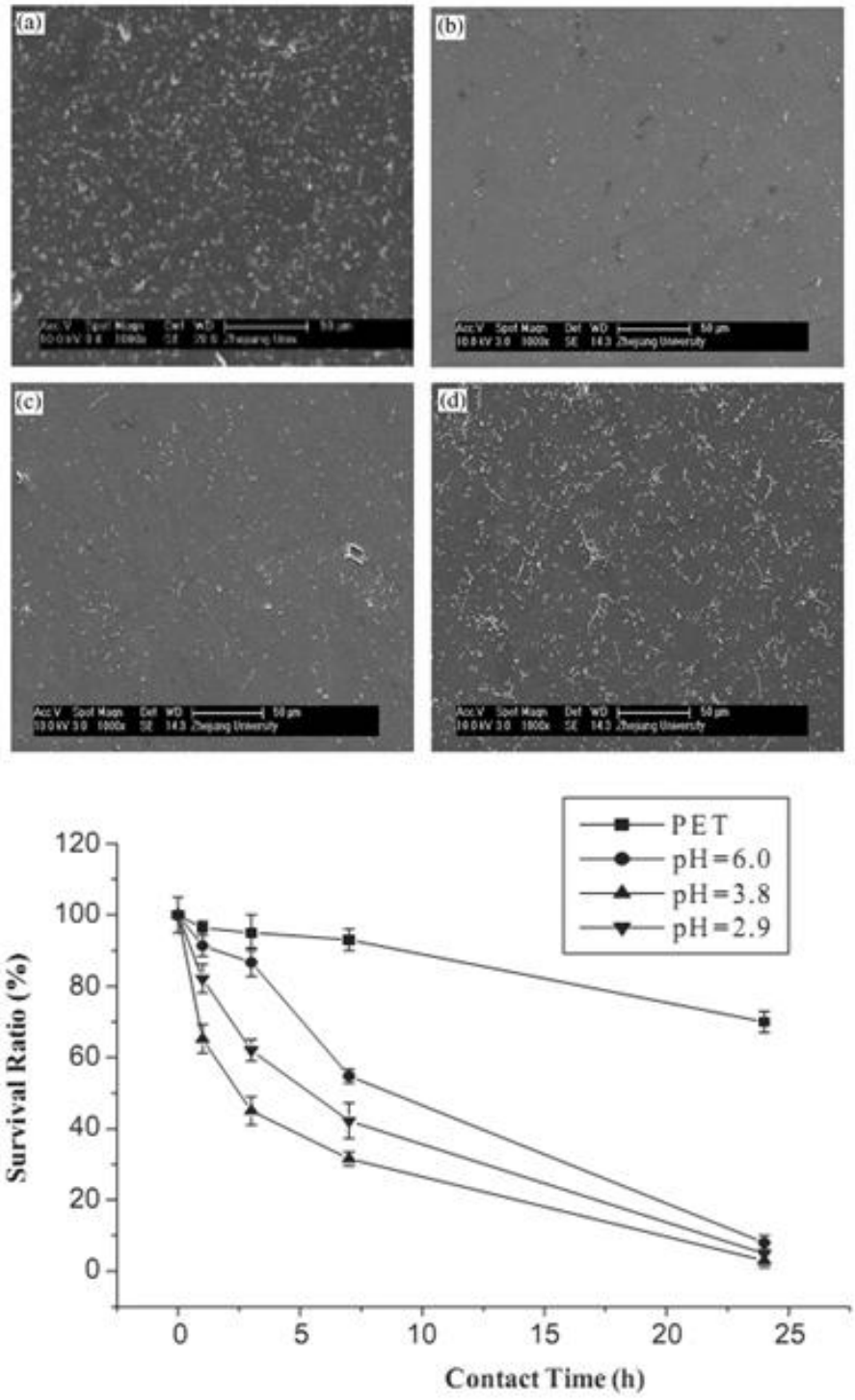

Figure 2.9 Top images: SEM images of (a) pristine PET, (b) the $(heparin/chitosan)_6$ multilayer film assembled at pH 2.9, (c) the $(heparin/chitosan)_6$ multilayer film assembled at pH 3.8, and (d) the $(heparin/chitosan)_6$ multilayer film assembled at pH 6.0 after exposure to 5×10^7 cells/ml E. coli for 4 h. Bottom image: Change in the viable E. coli cells with time exposed to the modified films. Reproduced with permission from [86]. Copyright 2009 Elsevier.

2.6.4 Synthesis of nanostructures by nanoreactors

The weak polyelectrolyte multilayers can be used as nanoreactors to synthesize various nanostructured materials. Available carboxylic acid groups in the PAH/PAA multilayers assembled at low pH can be used to bind cationic precursors such as Ag^+ to synthesize silver nanoparticles.[67, 139] Furthermore, by simply manipulating the assembly pH to tune the free available carboxylic acid groups, one can control silver concentration and nanoparticle size.[67] Semiconductor nanoparticles such as PbS[139] and ZnS[140] can also be synthesized by sulfidation of loaded metal ions. The anionic precursors can be loaded after pH-induced molecular rearrangement. The PAH7.5/PAA3.5 multilayers at very low pH conditions (pH~2.3) produce free ammonium groups due to the protonization of carboxylate groups and the rearrangement of the multilayers for successful loading of $AuCl_4^-$ to synthesize gold nanoparticles (Figure 2.10).[141] In addition to PAH/PAA multilayers, many other multilayers have been used to synthesize nanomaterials. All-polysaccharide multilayers assembled from chitosan and heparin have been used to synthesize metal nanoparticles with controlled metal concentration and nanoparticle size by controlling the assembly pH and loading pH.[142] The synthesis of silver nanoparticles has also been demonstrated in TiO_2-incorporated chitosan/heparin multilayers based on the same principle.[143] The synthesis of two types of nanoparticles in one polyelectrolyte multilayer has been demonstrated by using the PSS-PAA/PAH multilayer capsules as a template.[144] Another route to in situ synthesis of the nanoparticles involves the incorporation of the precursor during the assembly process, followed by in situ reduction. Multilayers of $(PdCl_4^{2-}/PEI)_n$ and

$(PAA/PEI\text{-}Pd\ (II))_n$ have been fabricated by Kidambi et al.[145] After reduction of the precursor by $NaBH_4$, Pd nanoparticles are successfully synthesized in both of these multilayers. Jiang et al. have assembled PAA-Ag^+ and $H_3PW_{12}O_{40}$ and PEI sequentially, and the $Ag_3PW_{12}O_{40}$ nanoparticles can be synthesized successfully.[146]

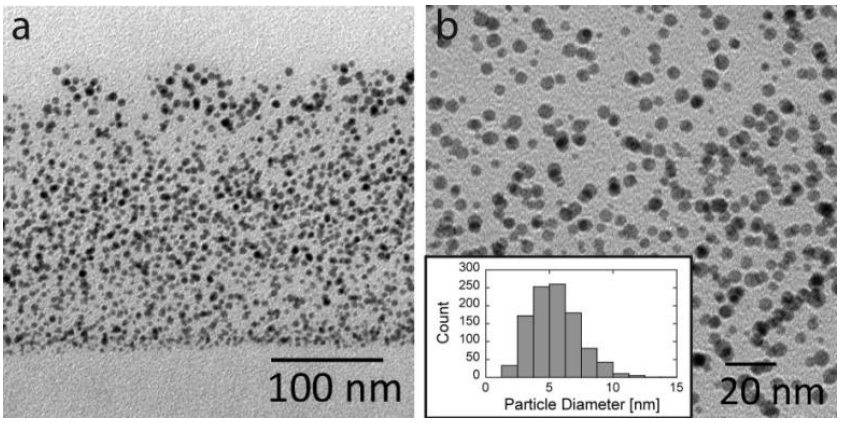

Figure 2.10 (a) Cross-sectional TEM image of a $(PAH7.5/PAA3.5)_{20}$ PEM (as-assembled dry film thickness 292 nm) loaded with pH 2.3 gold salt and UV-reduced. (b) TEM image at higher magnification. Inset: Particle size distribution. The average particle size is 5.5 ± 1.9 nm. Reproduced with permission from [140]. Copyright 2008 American Chemical Society.

2.6.5 Solid state electrolytes

With great improvement to ionic conductivity in recent years, weak polyelectrolyte-based multilayers have become promising candidates for solid state electrolytes. Rubner et al. have fabricated a PAH/PAA multilayer at assembly pH 3.5 to obtain an ionic conductivity of 2×10^{-7} S cm^{-1} at a relative humidity of 85-90% at 23˚C.[27] Later, Hammond et al. fabricated LPEI/PAA and LPEI/PAMPS multilayers with ionic conductivities as high as 1.0×10^{-5} S cm^{-1} and 1.5×10^{-5} S cm^{-1} at 100% relative humidity after optimization, respectively.[95] The higher ionic conductivity of LPEI/PAA multilayers relative to PAH/PAA multilayers might be due to the better hydrophilicity and stronger cation complexation capability of

LPEI compared to PAH. Ionic conductivity has been further increased by the same group using hydrogen-bonded PEO/PAA multilayers to achieve 5.5×10^{-5} S cm^{-1} at 100% RH and room temperature.[120] This high ionic conductivity is due to the greatly inhibited PEO crystallinity and good hydrophilicity of PEO and PAA. To further improve ionic conductivity, MEEP, a polymer with a highly flexible chain and good ionic conductivity, has been assembled with PAA to form MEEP/PAA multilayers via hydrogen bonding-driven LbL assembly.[71] The multilayers have over 1 order of magnitude higher ionic conductivity than PEO/PAA multilayers. Such a high ionic conductivity can be ascribed to the good ion-conductive property of MEEP and high water transport property of the multilayers. To date, some of these multilayers have been used as solid state electrolytes in practical electrochemical systems. For example, a PEO/PAA multilayer film has been deposited on nucleopore membranes for the application of hydrogen fuel cells.[65] The ionic conductivity and the blocking effect of fuel crossover of PEO/PAA multilayer film render it a good candidate for fuel cell applications. The assembled fuel cell generates a power density of 17 mW cm^{-2} and PEM conductivity of 2.4×10^{-4} S cm^{-1} at 55% RH.

2.6.6 Membrane separation

LbL assembly provides a versatile route to the design of a filtration membrane with enhanced flux and selectivity. Miller et al. have systematically tailored nanofiltration properties using different polyelectrolyte multilayers including PSS/PDDA, PSS/chitosan, and chitosan/HA.[25] As the charge density of chitosan is slightly lower than that of PDDA, the PSS/chitosan multilayer film has a lower rate

of rejection for the studied glucose/raffinose system but has a similar or slightly lower water flux, which might be due to its relatively high thickness. The chitosan/HA multilayers have the lowest rejections and highest water fluxes. Even the rejection of dextran with M_w 4000-6000 and myoglobin with M_w 17000 is less than 15%. The low rejections and high water fluxes are due to the diffusive ability of chitosan during assembly, which increases permeability greatly. Such films have great potential for protein separation. To understand the permeability of these multilayer films, Miller et al. have further correlated the permeability with swelling.[88] The low charge density results in a high water swelling film with increased water uptake, which reduces rejections and increases fluxes. However, in the case of permeation in ethanol, there is no clear relationship between flux and swelling. Aravind et al. have coated PSS/chitosan multilayers on a polyether sulfone microfiltration membrane and studied its effect on protein separation.[147] Deposition of only a few layers of PSS/chitosan can sieve a protein such as BSA successfully. For all the proteins, both the charge factor and the size factor play important roles in permeation. For example, the permeation of BSA and ovalbumin at their isoelectric point is dependent on their size. For the permeation of ovalbumin and lysozyme through the multilayers with the same bilayer and at given pH, the charge factor seems to outweigh the size factor.

2.6.7 Sensors

Weak polyelectrolyte-based multilayers have also shown great potential in sensor applications. Wang et al. have immobilized a fluorescent probe, H-PURET, on the electrospun nanofibers through LbL assembly using PAH as a partner.[66] Due

to strong interaction between analytes and the fluorescent conjugated polymer and the ultrahigh area-to-volume ratio, the fluorescence of the fabricated materials can be efficiently quenched by cyt c and MV^{2+}, leading to high sensitivity for the sensors. Wosnick et al. have alternately assembled PDDA and Poly(phenylene ethynylene), a weakly charged anionic polymer, on silica microspheres.[51] Although the fluorescence of multilayer-coated microspheres is similar to that of free polymers in solution, the sensitivity of fluorescence to nitroaromatic quenchers is significantly enhanced, which is due to combined effects such as hydrophobicity, penetration of analytes, and electronic contact between analytes and fluorescent probes. Surface modification of PDMS by the LbL assembly of PEI and PAA followed by cross-linking with EDC and NHS endows PDMS with long-term hydrophilicity.[148] After immobilization of BSA, anti-BSA, and protein G, an affinity surface is obtained for favorable antibody immobilization and low nonspecific binding.[148] Via the ELISA method, detection of TGF-β is successfully realized with high sensitivity and good stability. Furthermore, a PDMS microfluidic sensing device is fabricated by incorporating protein G-immobilized hydrogel plugs into the PEI/PAA multilayer modified PDMS channel.[149] ERα can be detected with good sensitivity and high specificity.

2.7 Summary

In brief, weak polyelectrolyte-based multilayer assembly has been studied extensively, and significant progress has been achieved in this area. However, there is still a great need to further develop novel multilayers for unique properties and

practical applications and to understand their self-assembly mechanisms. LbL assembly of 2-natural weak polyelectrolyte has not been fully studied. It is believed that different natural weak polyelectrolyte pairs display distinct assembly kinetics and properties and that some of them might exhibit great potential for certain applications, particularly biomedical applications. For nanoparticle-incorporated weak polyelectrolyte systems, there is still no systematic study on the use of weak polyelectrolyte charge density to control nanoparticle organization and their collective properties. Furthermore, the fabrication of free-standing forms of weak polyelectrolyte/nanoparticle multilayers has not been fully conducted. Although some exponentially grown weak polyelectrolyte multilayers have been studied, the effect of pH on the assembly, especially in terms of the surface nanostructure and their applications in such as pH-responsive drug delivery, requires further study.

Chapter 3 Experimental Approaches

3.1 Materials and equipment

3.1.1 Materials

Chitosan (medium molecular weight), alginate (sodium salt, 20-40 cP, 1% in H_2O (lit.)), rabbit IgG (purified immunoglobulin, technical grade), anti-rabbit IgG (whole molecule), goat IgG (purified immunoglobulin, technical grade), anti-goat IgG (whole molecule), bovine serum albumin (BSA) (minimum 98%, electrophoresis), Poly(ethyleneimine) solution (50% in water, M_w~750 K), sodium citrate tribasic dehydrate, Poly(acrylic acid) solution (PAA, 35% in water, M_w~100 K), FITC-dextran (M~2000 K), FITC-dextran (M~250 K), Poly(diallyldimethylammonium chloride) (PDDA) solution (20 wt.% in water, medium molecular weight), Poly(sodium 4-styrene-sulfonate) (PSS) (M_w~70 K), crocein orange G (CG), and phosphate buffered saline (PBS) (pH 7.4, 10 mM, NaCl 138 mM) were all purchased from Sigma-Aldrich. Hydrogen tetrachloroaurate (trihydrate) was received from Acros, USA. Methylene blue (MB) was obtained from Research Chemicals Ltd.. Deionized water (18.2 MΩ•cm) was obtained from a Millipore Milli-Q water purification system.

3.1.2 Equipment

Surface plasmon resonance equipment (The Autolab SPRINGLE system, Echo Chemie B.V., The Netherlands) was used to track the LbL assembly process and biomolecular adsorption and binding process.

The contact angle was measured with the FTA 1000 contact angle system (First Ten Angstroms) to probe the wettability of a surface.

Field emission scanning electron microscopy (FE-SEM) was performed with a JEOL (JSM-6700F) microscope equipped with an energy dispersive X-ray (EDX) analysis unit at an acceleration voltage of 5 kV and a working distance of about 8 mm to observe the surface morphology and element distribution.

The UV-visible (UV-vis) spectra were recorded by a UV-2450 spectrophotometer to study the buildup process of LbL assembly, LSPR peak intensity and position, and the drug loading and release.

Confocal laser scanning microscopy (CLSM) images were obtained with a Carl Zeiss LSM 510 META confocal microscope to study the formation of microcapsules and the permeability of microcapsules.

Transmission electron microscopy (TEM) was performed with a JEOL 2010 microscope operated at 200 kV to characterize the morphology and internal structure of materials.

Atomic force microscopy (AFM) images were obtained with a Nanoman AFM (Veeco Metrology Group, USA) to study material surface morphology.

3.2 Methodology

3.2.1 Substrate cleaning before LbL assembly

Silicon wafers and glass slides used in this work were immersed in a freshly prepared piranha solution (H_2SO_4/H_2O_2, 7:3 v/v) for 1 hour of cleaning, followed sequentially by rinsing thoroughly with DI water, immersing in H_2O_2: NH_3: H_2O

(1:1:5) overnight, rinsing again with DI water, and drying with N_2. The SPR gold chip was dipped into acetone and ethanol for 3 min each, followed by thoroughly rinsing with DI water for 3 min and drying with N_2.

3.2.2 pH adjustment of solutions

The pH of chitosan and alginate phosphate-citrate buffer solutions was adjusted using pure HAc or 0.5 M NaOH. The pH values of PBS, PEI PBS solution, PEI water solution, and alginate PBS solution were adjusted by 1 M HCl or 1 M NaOH.

3.2.3 Material characterization techniques

SPR is a technique for the real-time and label-free monitoring of biospecific binding events and macromolecular interactions. The principle of SPR measurement is based on the phenomenon of surface plasmon resonance on the metal surface. The refractive index of the sensor surface changes upon binding of macromolecules to the surface. As a result, the SPR wave will change and the angle will change accordingly. There is a linear relationship between the amount of bound material and the shift in SPR angle. In this study, in situ SPR was used to study the LbL assembly of chitosan and alginate in a real-time and antigen-antibody interaction.

UV-vis spectroscopy is a technique for the measurement of optical absorption, transmission, and reflection when UV or visible light is passing through a material, from which the chemical composition, localized SPR peak position and intensity, and concentration can be qualitatively or semi-quantitatively determined. In this work, UV-vis spectroscopy was used to study the LbL assembly process, LSPR

intensity, LSPR coupling strength of gold nanoparticles, and drug loading and release. Glass slides were used as the LbL substrate for all UV-vis measurement.

Confocal laser scanning microscopy (CLSM) is a technique to obtain high-resolution fluorescence images of biological entities or materials with optical sectioning ability. The position and relative concentration of fluorescent probes in materials can be accurately determined by CLSM. Thus, this technique has been used frequently to investigate biological events or material properties. In this study, CLSM was adopted for the study of the permeability of microcapsules.

SEM and AFM are techniques for the study of surface morphology. Here, we exploited them for the exploration of material morphology. Before FE-SEM imaging, the film surface was coated with a thin layer of Pt by an Auto Fine Coater (JEOL) at a current of 20 mA for 100 s. For AFM characterization of powder form of materials, the dilute suspension was dropped on mica. For the multilayer sample, the SPR chip was used as the substrate for LbL assembly.

TEM have the ability to probe the internal structure of materials. In this study, it was adopted to investigate the nanoparticle concentration, size, and distribution in the hollow capsules. For the TEM sample preparation, 40 μL of capsule suspension were dropped on the carbon-coated copper grid and then air-dried.

Contact angle measurement can be used to evaluate the wettability of a surface. Here, it was used to characterize the LbL assembly process. Silicon wafer was used as the substrate to fabricate the multilayer film for the measurement. Before the measurement, the film-coated silicon wafers were dried in a vacuum at room

temperature. The measurement of the contact angle was performed with the sessile drop method. The volume of the liquid droplets was kept constant at 1 µL.

Chapter 4 pH-controlled construction of chitosan/alginate multilayer film: characterization and application for antibody immobilization[a]

4.1 Introduction

A biointerface with immobilized antibodies on various substrates plays an important role in many fields such as biochip developments, biosensor design and bioseparation.[150-154] However, an efficient biointerface not only needs a high loading of antibody, but also requires retaining the antibody affinity to its antigen. The latter is often suffered from unfavorable orientations, structural changes or steric hindrance after immobilization.[153, 155] Various biointerfaces have been extensively studied for efficient antibody immobilization and its applications.[156-157] Self-assembled monolayer (SAM) on different substrates such as gold and silica is commonly used due to its well-defined surface structure at a molecular level and controllability of surface properties by varying terminal groups and compositions,[158] but it is limited by low loading capacity and few workable substrates.[159] Biomacromolecules have been investigated to build biointerfaces for supporting antibodies in applications of in vitro and in vivo sensors.[160] Such kind of biointerfaces might enhance the loading capacity of antibody and meanwhile reduce the non-specific adsorptions.[161] However, there is need to improve the tunability of the assembled film for enhancing its surface property, loading

[a] Reproduced in part with permission from [W. Yuan, H. Dong, C. M. Li, et al., Langmuir, 23 (2007), 13046–13052.] Copyright [2007] American Chemical Society

capacity and antigen binding activity.

Polyelectrolyte LbL self-assembled biointerfaces have attracted great interest in recent years due to their prominent advantages of using various substrates and allowing nanoscale control of the thickness, compositions, and molecular organization of the film.[15, 23, 43, 162-164] Much attention of the assembly has been paid on using weak polyelectrolytes due to the particular versatility and tunability with only controlling the pH.[23, 93, 165] The effect of pH is much stronger than that of ionic strength and other factors on an electrostatic self-assembly process of a weak polyelectrolyte.[23, 165-166] Meanwhile, the building blocks for constructing the multilayer have been recently expanded from the synthetic polymer[167-168] to biomacromolecules such as polysaccharides, proteins, polynucleotides, enzymes and polypeptides for functional biocompatible surfaces.[169-171] However, only a few reports studied the pH controlled assembly of such biomacromolecules.[35] As biocompatible and environmentally benign materials, chitosan and alginate are both widely used in biomedical fields such as drug delivery and tissue engineering.[172-173] Both chitosan and alginate are weak polyelectrolytes and thus their charge density can be easily tuned by pH. It is anticipated that the chitosan/alginate multilayer film could offer the unique properties for immobilization of antibody with retaining its binding activity. Although the self-assembled multilayer film of chitosan and alginate has been reported,[174] there is no report to study its assembly kinetics, tunability, mechanism and antibody immobilization via the adjustment of assembly pH, which all are of importance for construction of excellent biointerfaces in different applications.

SPR spectroscopy is a powerful analytical tool for in-situ and real-time monitoring of biomolecular interaction on the surface.[175-176] Since the assembly pH has great effect on the charge density, molecular conformation and even their interaction of chitosan and alginate, in situ SPR could offer an approach to effectively study the interaction in a real time and provide solid data to study the mechanism of the assembly of chitosan and alginate. In this work, the pH-controlled self assembly of chitosan and alginate was monitored by in situ SPR spectroscopy. The surface composition of chitosan/alginate multilayer film was analyzed via the combination of SPR and contact angle measurement. Further, antibody was immobilized in the multilayer film and the loading amount of antibody and its binding activity was quantitatively measured by SPR spectroscopy. To establish the relationship of antibody immobilization and its binding activity on antigen versus the surface property, SPR kinetics analysis is performed.

4.2 Multilayer films assembly and antibody immobilization

4.2. 1 Films assembly on a SPR chip

The baseline of SPR was measured by injecting 200 μL DI water into the chamber and wait until the resonance angle was stable. After draining off the water, 1mg/mL PEI aqueous solution was injected into the chamber and kept for 10 min followed by water wash for three times. Then, the water was replaced with phosphate-citrate buffer to measure SPR as the baseline for solutions prepared with phosphate-citrate buffer. Alginate and chitosan were alternatively injected into the

chamber and incubated for 15min. Before switching the assembling solutions, the gold chip was washed with phosphate-citrate buffer for three times. In this report, $(chitosan/alginate)_n$ is used to represent the multilayer film, where n corresponds to the number of bilayer built. Once the SPR response angle was near 1000 m°, the location of spindle was adjusted to refresh the dynamic range. In data process, the Origin software was used to combine the SPR curve with different dynamic range artificially (By superposing the first baseline of the subsequent sensorgram with the last baseline of determined sensorgram.). Typical SPR curve was shown in the following section.

4.2.2 Antibody immobilization and measurement of antibody-antigen binding activity via SPR

The baseline was obtained by injecting 200 μL phosphate-citrate buffer onto the multilayer film coated gold chip until the signal was stable. After the buffer was drained, 200 μL anti-Rabbit IgG solution with desired concentration was injected and incubated for 30 min. Then the gold chip was further washed with buffer for three times.

To obtain the antibody-antigen binding activity, the antibody immobilized film was blocked with 0.1% BSA phosphate-buffer solution for 1 h followed by buffer-washing for 3 times. Then 112 μg/mL Rabbit IgG prepared in 0.1% BSA phosphate-citrate buffer was injected into the chamber and incubated for 15 min followed by washing with 0.1% BSA phosphate-citrate buffer for 3 times and phosphate-citrate buffer for 3 times, respectively.

4.3 Fabrication and characterization of chitosan/alginate multilayer film

To demonstrate the tunability of surface property for the chitosan/alginate multilayer film, the alginate was adopted as the last assembled layer and different multilayer films were built under different pH combinations. Since the last assembled layer has the most significant effect on the surface property,[23] only the pH of alginate was adjusted (3.0, 4.0, and 5.0) while keeping the chitosan pH constant at 3. The effect of assembly pH on the growth of the multilayer film and the surface composition of the outermost layer were studied via SPR spectroscopy.

Figure 4.1 shows the SPR spectrum of the assembly process of chitosan and alginate, in which the three assembly curves obtained with different pH follow a same trend: an initial stepwise increase in the resonance angle with each successive deposition of alginate and chitosan followed by a leveling off of the resonance angle. The incubation time is long enough for all the three systems to achieve equilibrium.

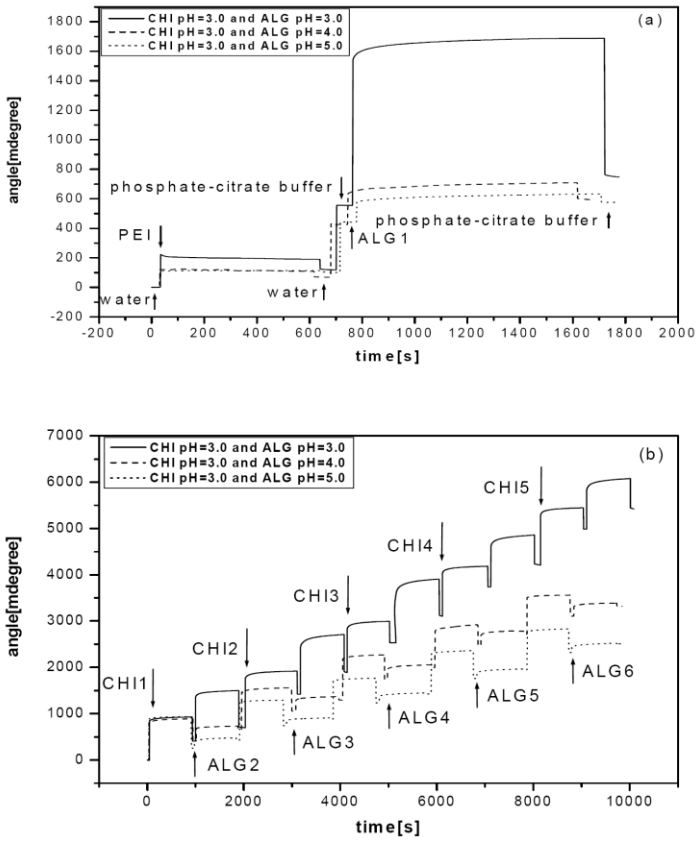

Figure 4.1 SPR spectrum of the assembly of chitosan and alginate at different assembly pH. a. First bilayer. b. From 2nd bilayer to 6th bilayer. (CHI: chitosan, ALG: alginate. Note: graph b was combined from two sensorgrams with the first baseline of the second sensorgram superposed with the final baseline of the first sensorgram via the Origin software. One refreshment of dynamic range was performed to make the measurement always in the SPR detection limit.).

There is a linear relationship between the amount of bound material and shift in SPR angle[177] (in our SPR equipment, a change of 120 millidegrees represents a change in surface materials of approximately 1 ng/mm^2.). The SPR angle shift in millidegrees is therefore used to quantify the binding of macromolecules to the sensor surface. The SPR angle shift in millidegrees is used to quantify the binding of macromolecules to the sensor surface. Figure 4.2 shows the relationship of resonance angle shift with the bilayers. From the 2nd bilayer, all three curves

follow exactly the linear trend, which indicates that the two polyelectrolytes can be assembled successfully at all the three pH values. PEI was used as a prime layer since it not only has great affinity to various substrates including the gold surface but also can introduce positive charge to the surface for further assembly.[178-179] The deviation of the first bilayer from linear relation is possibly ascribed that PEI is used as the prime layer instead of chitosan and the substrate (gold chip) may have some effect on the assembly since it may not be fully covered by the polyelectrolytes.

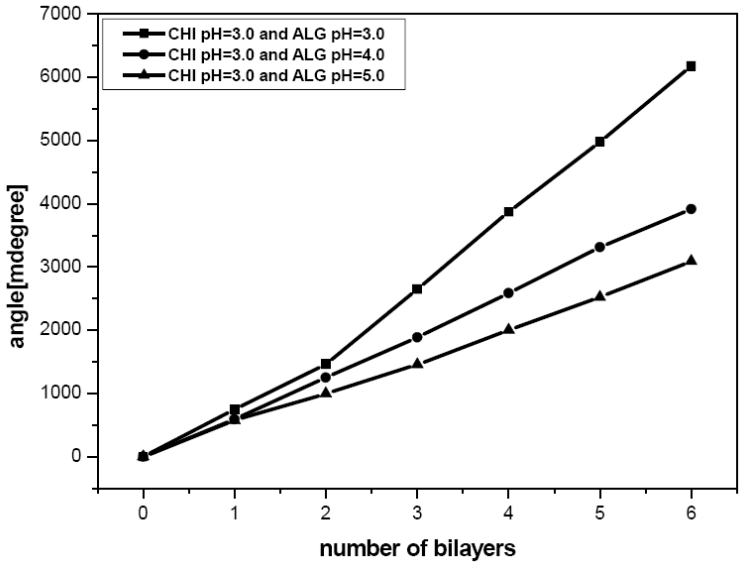

Figure 4.2 SPR responses versus the number of bilayer. The outermost layer is alginate layer.

According to Fresnel equation,[180] the thickness of polymer films on the gold chip is proportional to the change of resonance angle and inversely proportional to the difference between the two refractive indexes of the polymer film phase and the aqueous solution phase. At each pH, the same polyelectrolyte/buffer solution was used throughout the assembly experiment. Thus the relative thickness ratio can be reflected by the ratio of resonance angle change. Figure 4.3 shows the average ratio

of the resonance angle change of each bilayer for all the three conditions in the linear range. With the increase of the alginate pH, this ratio increases and meanwhile the thickness of alginate layers decreases. For the assembly of alginate, at higher assembly pH, the charge density is higher, while for the chitosan, the charge density usually keeps the same. To overcompensate and reverse the charge sign,[23] less alginate relative to chitosan should be assembled. Furthermore, higher charge density makes alginate chain more extended to form a thinner layer.[23, 181] Yoo et al.[23] has reported that for the LbL assembly of weak polyelectrolytes such as PAA and PAH, the thickness ratio of single layer takes dominant role in determination of the surface composition. When the thicker layer is the outermost layer, much fewer chain segments from the underlying thin layer penetrate into the surface of the thicker layer. As the thickness of the underlying thinner layer increases, more chain segments penetrate into the surface layer. The amount of penetration and thus the surface composition is determined by the relative thicknesses of the two layers. Fu et.al[181] studied the assembly of chitosan and heparin and realized the control of surface composition via assembly pH. The main reason was also the change of relative thickness caused by the assembly pH. In our case, since the thickness ratio of the underlying chitosan layer and the outermost alginate layer increases with the increase of the assembly pH while the absolute thickness of the outermost alginate layer decreases, more chitosan molecules can penetrate to the outermost layer at higher alginate assembly pH, indicating that the surface composition can be controlled.

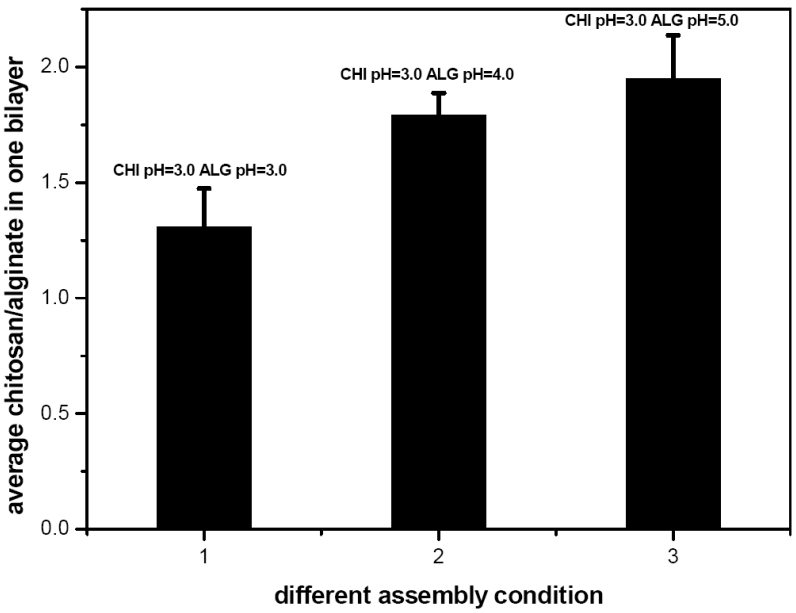

Figure 4.3 The average ratio of resonance angle change of chitosan to that of alginate layer.

The surface wettability is very sensitive to the surface compositions of the outermost layer.[23] Figure 4.4 shows the contact angle of the multilayer films with layer number from 1 to 6. The measurement is only recorded for the first six layers since from SPR result is already in the linear range of growth and the surface property should not be changed. The multilayer film with layer number 6 is also adopted as the sample for all the following experiment. For all the conditions, the contact angles exhibit the zigzag feature with the layer number, indicating the alternate assembly of chitosan and alginate on the surface. This agrees well with the SPR result. Furthermore, it can be seen that the wettability can be tuned by the assembly pH, from the third layer. The contact angles of both the odd layers and even layers increase with the assembly pH, which is mainly resulted from the difference of surface composition. With the increase of assembly pH of alginate, the relative thickness of chitosan layer to neighboring alginate layer increases.

Since the contact angle of chitosan is bigger than alginate, the overall contact angle thus increases. However, the conclusion is not applicable to the first two layers, which is influenced by the substrate and the prime PEI layer. The contact angle result further demonstrates that the surface composition can be simply controlled by the adjustment of assembly pH.

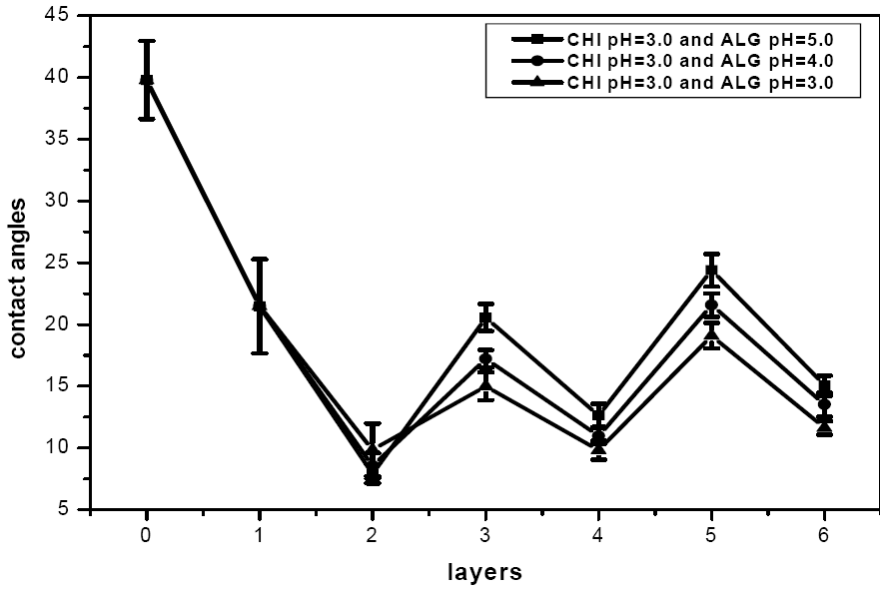

Figure 4.4 Contact angle of chitosan/alginate multilayer films with certain number of layers. The substrate without modification (pristine silicon wafer) is as the layer zero.

The surface morphologies of the multilayer films at different assembly pH were characterized via AFM (Figure 4.5). Interestingly, the surface morphology shows a regular evolution with the change of assembly pH. There are small globules on all the multilayer films, which are composed of chitosan/alginate complex. With the increase of the assembly pH, the size of globules becomes larger. Although the assembly pH of chitosan is the same at all these conditions, when the next alginate layer is assembled on the chitosan, the different assembly pHs induce the change of conformation of chitosan molecules. When the assembly pH of alginate is 3, the

assembled structure is relatively homogeneous, which means that the alginate molecules are adsorbed homogeneous on the surface. With the increase of assembly pH, chitosan develops more loopier and globular conformation. Thus the assembled alginate molecules produce more globular complex with chitosan molecules.[23, 33, 35] The higher assembly pH also induces the aggregation of chitosan molecules (the electrostatic repelling becomes weaker at the higher assembly pH), and therefore the chitosan/alginate complex becomes more aggregated.

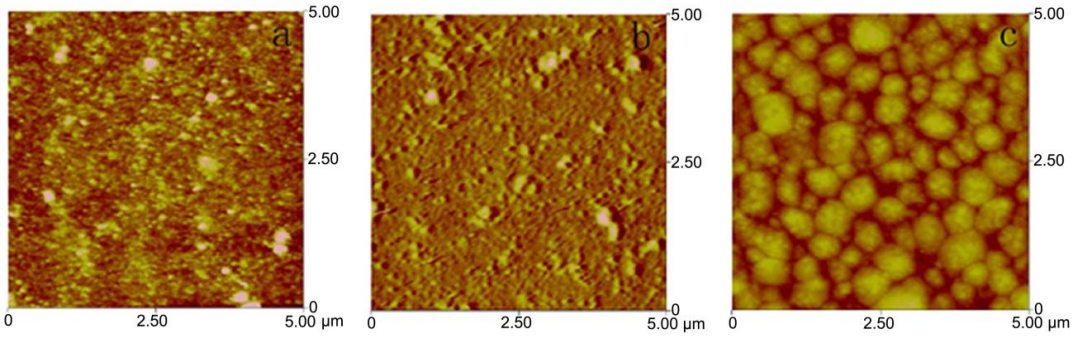

Figure 4.5 AFM images acquired in the phosphate-citrate buffer (pH=5.0). The layer number of all these multilayer films is 6. The assembly pH of chitosan of all these multilayer films is 3.0. The assembly pH of alginate is a. 3.0 b. 4.0 c. 5.0. The Z range (maximum height) is a.30 nm b.100 nm c.400 nm.

4.4 Antibody immobilization

In-situ SPR measurements can provide the kinetics and equilibrium information of the antibody adsorption on the multilayer surface. The phosphate-citrate buffer (pH unadjusted) was used in the experiment to dilute the antibody and the pH was kept below the isoelectric point (IEP) of antibody (IEP=6.0-6.5).[155, 182] at which the antibody was positively charged and can be electrostatically adsorbed on the negatively charged assembled multilayer film surface. It is reported that the protein

is adsorbed either on the outmost surface or into the bulk film.[183] However, in our study, there is no enhancement of the antibody adsorption when the number of the film increases from 6 layers to 12 (alginate layer as the outermost layer) (data not shown), indicating that the antibody adsorption only occurs on the outmost surface. The 6-layer film with alginate as the outermost layer was employed to study the behavior of antibody adsorption. Figure 4.6 (a) shows the adsorption process under different assembly pH values illustrated by in situ SPR measurements in solutions containing different concentrations of antibody. The highest antibody concentration used is 0.2 mg/ml, which is a high enough concentration to form a saturated coverage of protein on a surface.[184] The amount of the saturated antibody adsorption is often defined as the loading capacity of the surface. The results demonstrate that the loading capacity of the multilayer films decreases with the increase of the assembly pH of alginate. SPR and the contact angle results show the amount of chitosan interpenetrated to the outermost layer increases with the increase of assembly pH of alginate. The higher loaded alginate and lower interpenetrated chitosan at a lower assembly pH cause higher charge density of the films, on which more antibody can be adsorbed. In our work, anti-Goat IgG was also immobilized onto the films under different pH, of which the loading capacity also increases with the decrease of assembly pH (data not shown here). It needs to be noted that the antibody loading capacity achieved here is already very high (The highest loading capacity is 8.7 ng/mm^2, which is much higher than the SAM based biointerface.[185]) Such a high loading capacity could be contributed from the high surface area due to nanoscale surface roughness and the strong electrostatic force.

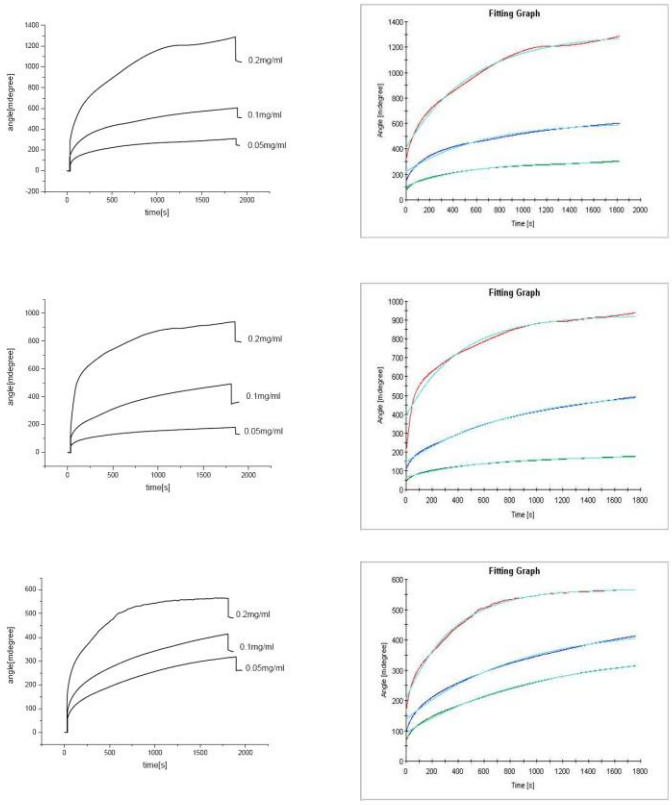

a b

Figure 4.6 SPR spectrum (a) and fitting result (b) of antibody adsorption with different antibody concentrations at different assembly pH. The assembly pH of alginate was 3.0, 4.0 and 5.0 from up down. The assembly pH of chitosan was fixed at 3.0.

The adsorption and dissociation rate constant can be calculated from the SPR binding curves obtained under different concentrations of antibody on the film surface. The affinity of the antibody to the films can thus be evaluated via these two parameters.

The interaction of protein with surface ligand can be simply formalized as

$$A+B \underset{k_d}{\overset{k_a}{\rightleftharpoons}} AB$$

Where *A* is the protein in aqueous solution, *B* is the active sites on the film surface, *AB* is the adsorption complex. k_a and k_d are association rate constant and dissociation rate constant respectively. For electrostatic force dominated adsorption, the concentration of *B* is proportional to the charge density of the surface. It is worthy of a note that although the surface charge density increases with the decrease of pH, the affinity doesn't necessarily increase accordingly. This means that the increase of charge density only represents the increase of concentration of active sites on the surface while the affinity constant could be reasonably considered to be constant.

The *AB* formation rate can be expressed as follows[176]

$$\frac{d[AB]}{dt} = k_a[A]([B]_0 - [AB]) - k_d[AB] \quad (1)$$

Where *[AB]* and *[A]* is the concentration of *AB* and *A* respectively. $[B]_0$ represents the concentration of *B* at time zero.

Let *R* denote the SPR response, which is proportional to the concentration of *AB*.

Let $$E = \frac{k_a[A]R_{\max}}{k_a[A] + k_d}$$

and $$k_s = k_a[A] + k_d \quad (2)$$

(1) can be further transformed into

$$R_t = E[1 - e^{-k_s t}] + R_0 \quad (3)$$

Where R_0 is the SPR response at t=0.

The parameter E, k_s, and R_0 can be obtained by fitting the adsorption curve using Eq. (3) (Figure 4.6 (b)), which is very well in agreement with the measured SPR curves. Then k_a and k_d can be further determined by fitting Eq. (2) with k_s vs. [A] (Table 4.1). It is known k_a/k_d represents the affinity of A to B. There are deviations between the fitting and experimental curves at the beginning. This is possibly due to a time needed for the antibody to uniformly distribute on the surface after injection. It can be seen that when the chitosan is on outermost layer, the antibody can still be adsorbed on the surface, although much less than that of the alginate. This is likely ascribed to other intermolecular forces such as hydrogen bonds and hydrophobic interactions. The fitted result shows that k_a/k_d increases with the increase of assembly pH (Table 4.1), but contradictorily, the antibody adsorption capacity decrease with the increase of pH (Figure 4.6 (a)). Through the kinetic analysis in our work, although the antibody adsorption capacity is determined by both the affinity and the concentration of binding sites on the surface, the later is dominated and the capacity can be mainly controlled by assembly pH as we discussed above.

Table 4.1 Calculated k_a and k_d at different assembly condition.

	CHI3.0/ALG3.0	CHI3.0/ALG4.0	CHI3.0/ALG5.0
k_a / $(M.s)^{-1}$	$3.289620\times10^{1}\pm1.853\times10^{0}$	$1.675277\times10^{3}\pm2.400\times10^{0}$	$1.938116\times10^{3}\pm2.564\times10^{0}$
k_d / s^{-1}	$1.673580\times10^{-3}\pm2.102\times10^{-6}$	$2.152858\times10^{-4}\pm2.491\times10^{-6}$	$2.086533\times10^{-4}\pm2.146\times10^{-6}$
(k_a/ k_d) /M^{-1}	1.965619×10^{4}	7.781642×10^{6}	9.288691×10^{6}

4.5 Antigen binding activity

BSA is commonly used as a blocking agent to inhibit the nonspecific adhesion. The films were immersed in BSA-phosphate-citrate solution for 1h without any antibody immobilization and washed with phosphate-citrate buffer followed by adsorption of antigen for SPR measurement. The SPR angle shift monitored is insignificant (Figure 4.7 inset).

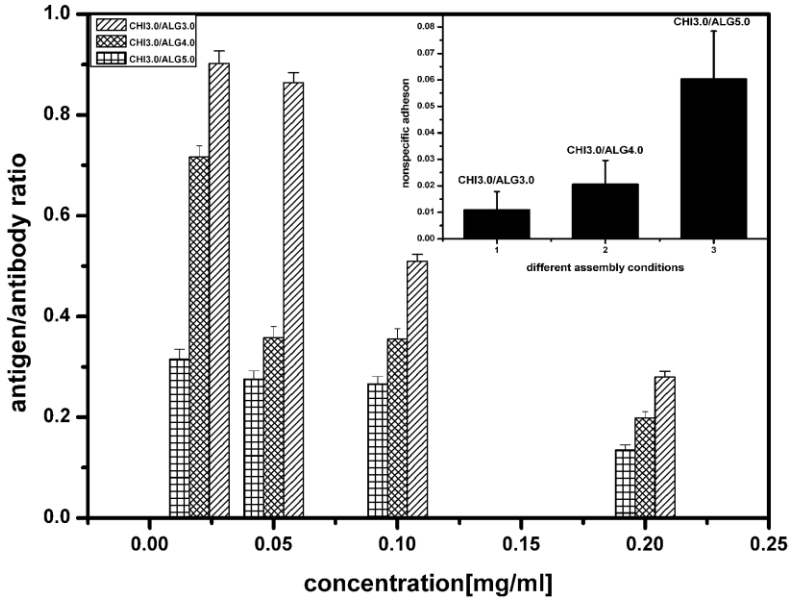

Figure 4.7 The antigen/antibody ratio obtained from SPR resonance angle change. The four antibody concentrations adopted were 0.2 mg/ml, 0.1 mg/ml, 0.05 mg/ml and 0.025 mg/ml. Inset: The nonspecific adhesion represented as amount of antigen binding to multilayers without antibody/amount of antigen binding to multilayers with antibody at different assembly condition.

The ratio of bound antigen to the adsorbed antibody is frequently used to evaluate the antigen binding activity (immunological activity) of the antibody.[155, 185] Figure 4.6 shows the surface concentration of the antibody on the multilayer film can be changed via the change of its concentration in solution. Interestingly,

the antigen binding activity is greater with its smaller solution concentration (Figure 4.7), possibly indicating a steric hindrance effect of highly concentrated reactants on the surface. This indicates the antigen binding activity can be easily controlled by the surface density of the antibody. Figure 4.7 shows that even with different immobilization concentrations, the ratio of antigen to antibody is larger when the assembly pH of alginate is lower. The same experiment was conducted with anti-Goat IgG and showed the similar trend as that of the anti-Rabbit IgG. As previously stated, the SPR simulation results show that the affinity of the antibody to the multilayer films increase with the increase of assembly pH of alginate. Stronger physical interaction may cause more structural change of protein and will lead to the loss of antigen binding activity. The ratio of antigen to antibody is 0.9 (Figure 4.7) at pH 3 of both alginate and chitosan, which is highest binding activity reported up to date.[155, 185] This excellent biointerface could be used to fabricate immunosensors with high sensitivity and good specificity.

4.6 Conclusions

Chitosan and alginate were assembled at different pH to form a multilayer film. Experimental results show that the surface composition of the film can be controlled by the assembly pH, in which with decrease of assembly pH of alginate, less positively charged chitosan can interpenetrate to the outermost alginate layer, resulting in increase of negative charge density from alginate for more antibody immobilization. The multilayers give much higher loading capacity than SAM based biointerface. More importantly, the antibody immobilized on these

multilayers have high and pH-tunable antigen binding activity. The highest binding ratio of antigen to antibody achieves 0.9, which is the best value reported in the literatures up to date. This work can provide more scientific insight into the interaction between protein and polymer matrix and render a simple novel approach to build a high performance biointerface on various substrates through pH control for potential applications of highly sensitive immunosensors.

Chapter 5 Direct Modulation of Localized Surface Plasmon Coupling of Au Nanoparticles on Solid Substrates via Weak Polyelectrolyte-mediated Layer-by-Layer Self Assembly[b]

5.1 Introduction

Various metal nanoparticles have attracted great research interest in recent years because of their unique optical, electrical, and magnetic properties for broad applications in optoelectronics, catalysis, sensors and therapeutics.[186-193] One of the most interesting phenomena of metal nanoparticles is the localized surface plasmon resonance (LSPR), which is uniquely an effect of the nano size regime.[194] The LSPR peak, an intense surface plasmon absorption band occurs at a frequency of the electromagnetic wave identical to that of the collective oscillation of the conduction electrons in metal nanoparticles. The frequency of the LSPR peak can be tuned by varying the size, shape, dielectric environment, and interparticle spacing of the nanoparticles.[194-196] Among these factors, the interparticle spacing is particularly significant and has been studied extensively.[7, 195-198] When two metal nanoparticles close to a certain distance, localized surface plasmon coupling (LSPC) is observed[195-197, 199-200] to change the oscillation frequency of the surface plasmon, thus resulting in a shift of the longitudinal LSPR band. LSPC is important for many practical applications such as surface enhanced Raman scattering,[201-203] second harmonic generation,[204-205] photonic wave guiding,[206-207] and laser-

[b] Reproduced in part with permission from [W. Yuan, C. M. Li, Langmuir, 25 (2009), 7578–7585.] Copyright [2009] American Chemical Society

responsive drug delivery.[208-209] To realize all these applications, it is desirable to have tunable LSPC on a solid substrate as a component in a device[201-207] or as a prime step to fabricate a free-standing functional nanocomposite film.[208-209] LSPC has been studied by a number of theoretical models with changing interparticle distance in 2 dimensions (2D) on a substrate,[197, 199, 210-211] indicating that the LSPR peak positions are mainly determined by the interparticle spacing. Recent experimental results also show that the aggregation of nanoparticles into a three dimensional (3-D) structure can red shift LSPR peaks significantly.[212-213]

Both top-down and bottom-up methods have been explored to construct nanoparticle-based structures to generate LSPC. Electron beam lithography is used to fabricate 2D patterns on solid substrates to control the interparticle distances for LSPC modulation,[197, 199] but it is expensive and can only make an array structure on a small area with limited tunability. Recently, more works have focused on control of interparticle spacing in various self-assembled ordered nanostructures.[196, 198, 214-218] A "brick and mortar" solution-based self-assembly approach has been introduced to control the interparticle distance of Au, silica and magnetic nanoparticles.[196, 214, 216, 218-220] Poly(amidoamine) (PAMAM) dendrimer has been used to tune Au nanoparticle interparticle spacing by varying size of the dendrimers.[220] Alternatively, lysozyme has been employed as a model protein to control the interparticle spacing by changing the molar ratio of protein to Au nanoparticle, or by controlling the assembly temperature.[196] The self-assembly methods used currently to tune LSPC are mainly conducted by either solution condition or nanoparticle surface modification,[221] thus limiting the tunability. It

remains a great challenge to extensively tune LSPC directly on a solid substrate for practical applications and fundamental studies.

Layer-by-layer (LbL) self-assembly can build composite films containing different molecules or/and metal nanoparticles by simple wet chemistry.[5, 40, 212] It could be an effective approach to tune LSPC because of its superior capability in construction of different nanostructures on various solid substrates.[43-46, 181, 212, 222-223] The thickness, chemical composition, surface morphology and nanostructure of a LbL assembled film can be controlled at a molecular scale with nearly no limit of geometry and type of the substrate materials. Different building blocks such as biomacromolecules, nanoparticles, nanosheets, and carbon nanotubes can be incorporated into a multilayer film.[5, 40-41] In LbL assemblies, weak polyelectrolytes, including many synthetic ones and biomacromolecules, are particularly versatile construction blocks[23, 35, 224] because their charge density and conformation in an assembled structure can be simply controlled by pH. The LbL assembly of two weak polyelectrolytes has been investigated using poly(acrylic acid) (PAA) and poly(allylamine) (PAH) as model molecules.[23, 33-34, 225] In the previous chapter, a multilayer film assembled with chitosan and alginate was constructed by this approach and exhibited pH dependence of the loading capacity and bioactivity of the antibody. However, no work has been reported on the modulation of LSPC in an assembled nanocomposite film with weak polyelectrolyte and metal nanoparticle.

In this work, poly(ethyleneimine) (PEI) and Au nanoparticle solutions were used to self-assemble a weak polyelectrolyte/metal nanoparticle nanocomposite

film. The monodispersed, citrate-stabilized Au nanoparticle is selected as the model metal nanoparticle due to its prominent LSPR.[226-228] PEI is a typical weak polyelectrolyte with a wide range of pH-tunable charge density and conformation (See Scheme 2.1 for structure of PEI). The negatively charged Au nanoparticles should be able to interact with the posively charged PEI by electrostatic force. Furthermore, by changing the assembly pH, their interaction could be tuned easily. For the first time, we investigated the possibility of modulation of LSPC on a self-assembled nanocomposite film through pH-tailored interparticle spacing. The mechanism of LSPC modulation in the LbL assembly was studied. The stability of the self-assembled nanocomposite was also investigated.

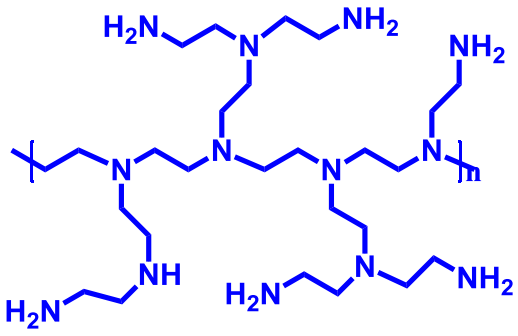

Scheme 5.1 molecular structure of PEI.

5.2 Synthesis of gold nanoparticles and LbL assembly of PEI and gold nanoparticles

5.2.1 Synthesis of Au nanoparticles

The Au nanoparticles were synthesized according to Natan's method,[226] but with modifications. In the synthesis, 0.75 mL 1% sodium citrate was added to 50 mL 0.3 mM boiling $HAuCl_4$ solution. With the reaction progress, the color changed to blue

and then to red-violet in about 100 s. After boiling for an additional 10 min, the heat source was removed. The produced colloid solution was stirred for 30 min and then stored in the dark at room temperature. The size of the formed Au nanoparticles was 18 ± 3 nm (70 particles sampled) (see Figure 5.1 for TEM). The pH of the gold nanoparticle solution was 4.4 and was kept constant in all experiments.

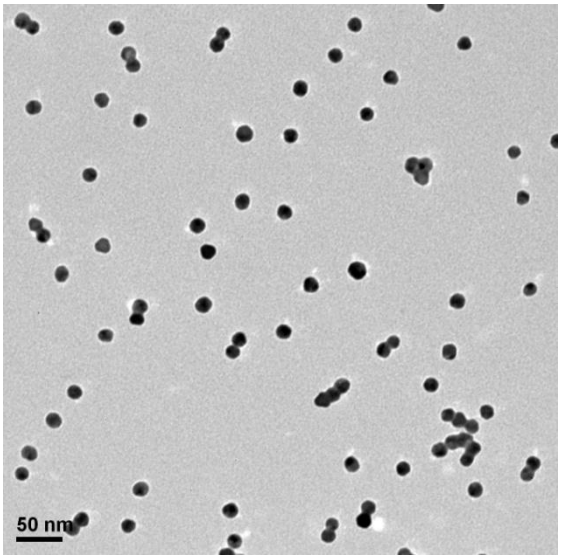

Figure 5.1 TEM images of gold nanoparticles.

5.2.2 LbL assembly of PEI and Au nanoparticles

The substrate, a cleaned glass slide or silicon wafer was immersed in 1 mg/mL PEI at a given assembly pH for 10 min followed by washing with DI water, and then blowing dry with N_2. Subsequently, the substrate was immersed in the as-prepared Au nanoparticles solution for 15 min, and then washed with DI water and dried with N_2. By repeating this cycle for several times, multilayer films with PEI-Au nanoparticle bilayers were obtained. In this report, $(PEI/Au)_n$ is used to represent a multilayer film with n bilayers.

5.3 Characterization of (PEI/Au nanoparticles)$_n$ multilayers

The UV-Vis spectra (Figure 5.2a) of the PEI-Au nanocomposite films with different bilayers assembled at pH 3.4 (PEI) on glass slides illustrate two peaks, which can be assigned to the transverse and longitudinal modes of the LSPR.[199, 212, 229] With increase of the assembly layers, the intensity ratio of transverse to the longitudinal band decreases (Figure 5.2b) until the transverse band is almost covered by the longitudinal band, indicating a high degree of clustering and LSPR coupling. This trend is also observed for assembled PEI/Au nanoparticle nanocomposites at different pHs (data not shown).

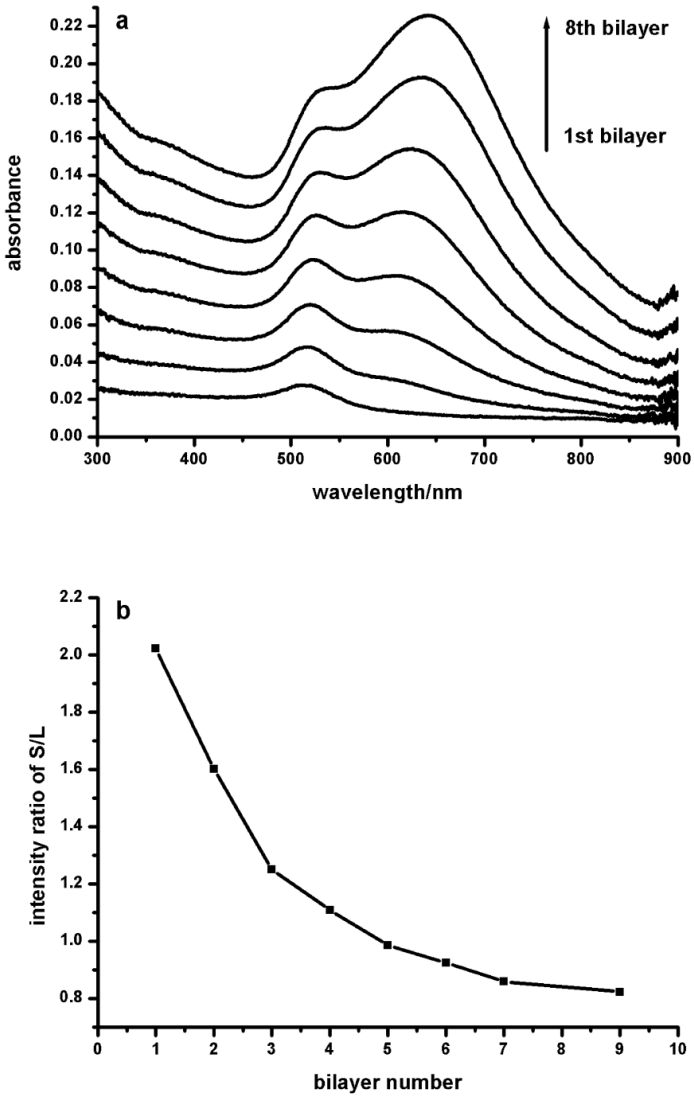

Figure 5.2 Typical UV-Vis spectra evolution of the nanocomposite films during the assembly process (a) and the peak intensity ratio of transverse band to longitudinal band (b). The outermost layer is Au nanoparticle layer. The PEI assembly pH is 3.4.

The LSPR peak intensity can be used to characterize the LbL assembly. For both transverse and longitudinal bands of all the PEI/Au nanoparticle films assembled at different pHs (Figure 5.3), the peak intensity shows good linearity versus the bilayer number, demonstrating that the Au nanoparticles are successfully

assembled on the substrate; however, the rate of change of intensity versus bilayer number, for both transverse and longitudinal bands, decreases with increase of the assembly pH in a range up to 6.8, followed by insignificant change with further increase of the assembly pH (Figure 5.3). This result indicates that the surface density of the assembled Au nanoparticles can be tuned by the assembly pH in a range lower than 6.8. All the assembled composite films displayed good linear relationships of surface nanoparticle density vs. bilayer number and thus the nanocomposite films with first three bilayers were selected for further studies in this work.

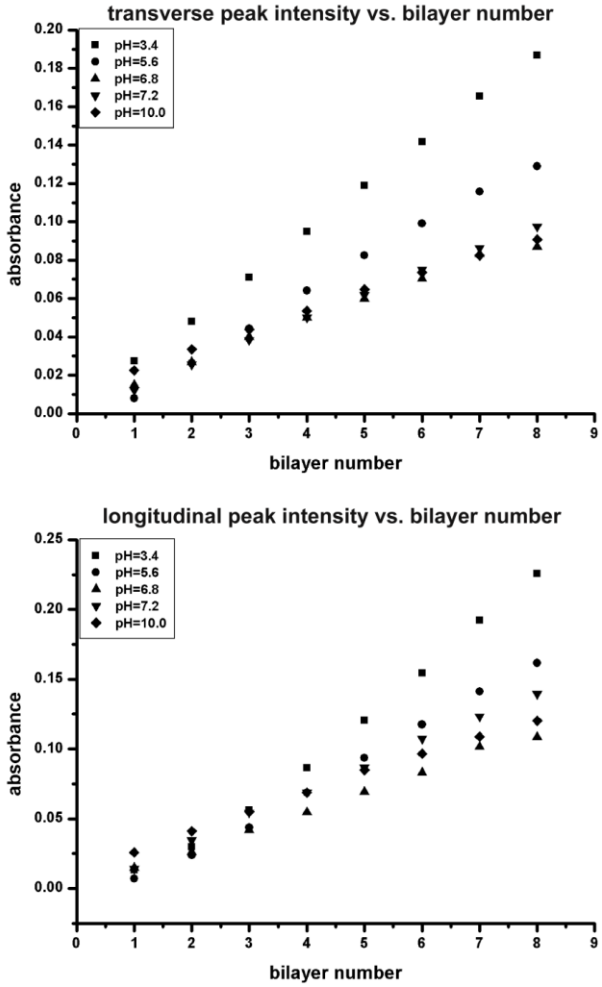

Figure 5.3 The transverse LSPR peak intensity versus bilayer number and longitudinal peak intensity versus bilayer number at different assembly pH.

The FE-SEM images (Figure 5.4) of various bilayered nanocomposite films assembled at different pHs show that the nanoparticles assembled at pH lower than 6.8 display a uniformly distributed 2-D assembly pattern and nearly no aggregation. The surface nanoparticle density increases with increase of the bilayer number but decreases with increased assembly pH. These results are in good agreement with the UV-Vis result discussed above. However, at pH 6.8 small aggregates start to form (Figure 5.4C1, 2, 3) and are significantly increased with

apparent 3-D growth for larger sizes when increasing pH to 7.2 (Figure 5.4D1, 2, 3). At pH 10, nearly all the nanoparticles are assembled into 3D large aggregates (Figure 5.4E1, 2, 3). As the pK_a of PEI in solution falls in the pH range of about 6.8-7.2,[115, 230] it is very likely that the dramatic change of the assembled nanostructure is caused by the sharp drop in the PEI ionization around its pK_a, which will be discussed later.

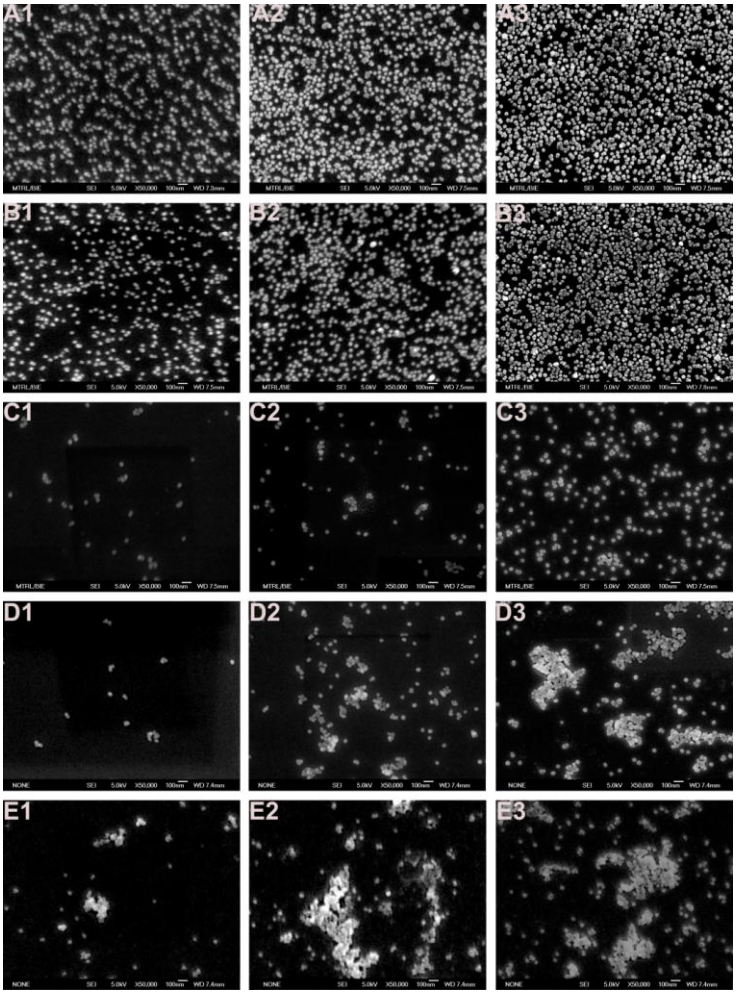

Figure 5.4 FE-SEM images of the nanocomposite films with different bilayers at different assembly pHs. A1, A2, A3, B1, B2, B3, C1, C2, C3, D1, D2, D3, E1, E2, E3 are the images of the first, second and third bilayer assembled at pH 3.4, first, second and third bilayer at pH 5.6 and first, second and third bilayer at pH 6.8, first, second and third bilayer at pH 7.2, first, second and third bilayer at pH 10.0 respectively.

The change of the assembled nanoparticles surface density with the assembly pH can be explained by the pH-dependent ionization of PEI, which is lower at higher pH, resulting in a lower surface charge density[33, 165-166, 231] to electrostatically assemble less negatively charged citrate-stabilized gold nanoparticles[232] (the charge is constant due to its fixed pH). Thus, the main factor affecting the LbL nanoparticle assembly is likely the positive surface charge density. However, with further increase of pH to 6.8 and above, the change of the assembled nanoparticle density is insignificant, possibly due to the high assembly pH, at which the poor PEI ionization causes low surface positive charge for less Au nanoparticle adsorption via electrostatic attraction, while the high content of loop and tail conformations promotes 3D aggregation of the assembled nanoparticles.[231] These results demonstrate that, in an assembly pH range lower than 6.8, the assembled surface density of PEI and Au nanoparticles can be tuned by changing the assembly pH. Two modes, normal growth and lateral expansion, are used to explain the LbL assembly of polyelectrolyte and nanoparticles.[188, 233-234] The increase of assembled nanoparticle surface density with an increase of the number of bilayers on the substrate is characteristic of the lateral expansion mode.[188, 233] In more detail, small nanoparticle clusters and some isolated nanoparticles are formed at all the assembly pHs in the first bilayer. With increase of bilayer number, the clusters grow laterally and new clusters are formed, while the percentage of isolated nanoparticles reduces. The FE-SEM morphology results discussed above also support this growth mode.

5. 4 LSPC of the multilayers

Figure 5.5a illustrates that the longitudinal band peak position of the multilayer films has very little change with the bilayer number (first two bilayers are not shown due to no well-defined peaks) at high assembly pH (7.2 -10.0), and only displays slight red-shifts, in films at assembly pH values lower than 6.8, showing that the number of bilayers assembled has little effect on LSPR maximum wavelength. However, the longitudinal band peak position shows significant red-shift with increase of the assembly pH (Figure 5.5a and b). This can be attributed to increased particle-particle interactions (clustering) within these films. Furthermore, the tunable range of LSPR by assembly pH is broad. With increase of the assembly pH from 3.4 to 10.0, the longitudinal band peak position red-shifts from 642 to 737 nm for the eighth bilayer, and 625 to 741.5 nm for an optimized 5 bilayer film, demonstrating the largest tuning range of the longitudinal band peak position to date.[196, 212] It is of great importance to tune the LSPR maximum to the near infrared (NIR) region where it has the strongest tissue penetration capability (700-900 nm),[235-236] and thus renders the greatest potential for applications in NIR bioimaging and phototherapy.[190, 235-236] Interestingly, dramatic 3-D aggregation growth occurs in the pH range of 6.8 - 7.2, with a large red shift of the longitudinal band peak position, indicating strong LSPC. The high sensitivity of LSPR peak position to the assembly pH may suggest that the assembled nanocomposite film could be used as a pH sensor, particularly a micro pH sensor, which is currently under investigation in our lab.

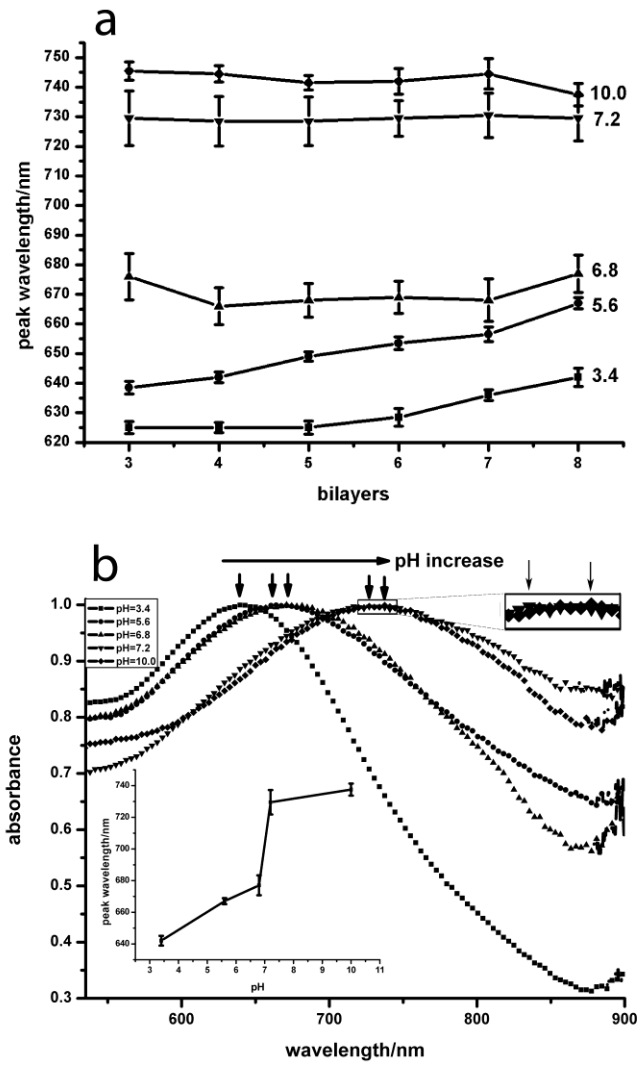

Figure 5.5 a. Longitudinal band peak positions of the nanocomposite films obtained from the UV-Vis spectra versus the bilayer number at different assembly pH. b. Typical UV-Vis spectra of 8 bilayer films at different assembly pH. Inset is longitudinal band peak positions of the nanocomposite films with the same bilayer number (8 bilayers) versus pH. The error bar is calculated from three times of measuring of films prepared from the same batch of gold nanoparticles.

A Gaussian distribution function was used to fit the UV-Vis absorbance spectra of multilayers assembled at different pH. The simulated curves fit well with the experimental spectra with distinguished separated transverse and longitudinal bands (an example of the spectra fittings is shown in Figure 5.6), from which the

bandwidths were easily obtained. Since the transverse band doesn't show obvious changes with assembly pH and assembled bilayer number, only the fitted longitudinal bandwidths are displayed in Figure 5.7. As in Figure 5.7, the longitudinal bandwidth has no obvious relationship with the bilayer number, but it significantly increases with increase of the assembly pH over a pH range of 3.4 - 7.2. This is in accordance with reported work[197, 237] showing that LSPC enhancement of metal nanoparticles not only causes the longitudinal peak red shift, but also leads to the bandwidth increase. A broader longitudinal band of a nanoparticle-composed structure can also be caused by decreased distribution uniformity,[237-238] as shown in Figure 5.4. Interestingly, with further increase of pH (from 7.2 to 10.0), the bandwidth decreases while the LSPC peak still red-shifts. Although this is not fully understood, one of the possibilities is that highly aggregated nanoparticles at high pHs result in more uniform interparticle spacing distribution for a narrowed bandwidth.

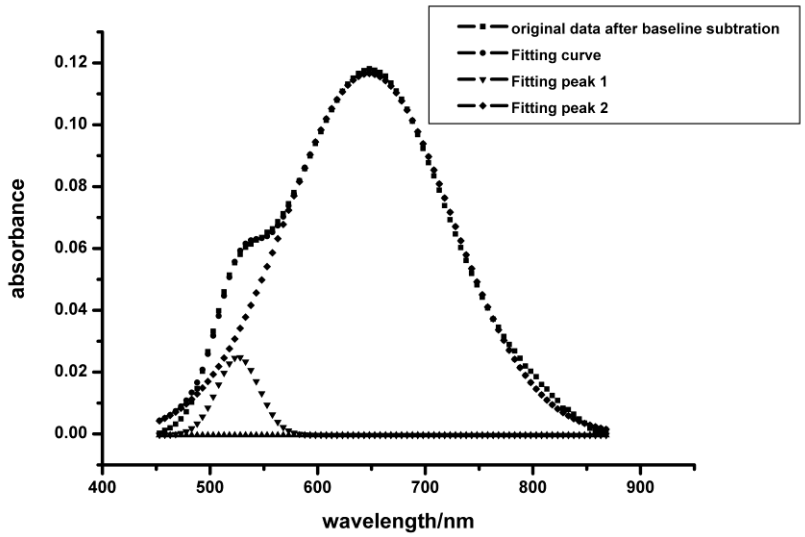

Figure 5.6 UV-visible spectra fitting of pH 3.4 film using Gaussian distribution function.

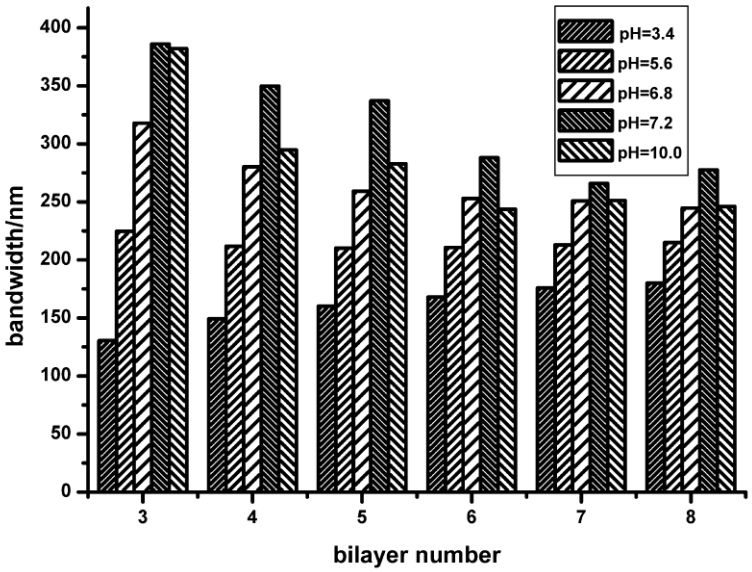

Figure 5.7 Simulated longitudinal bandwidth versus the bilayer number for each assembly pH.

The LSPC result discussed above may provide insight into the effect of morphology on the optical properties of metallic nanoparticles in LbL films. LSPC is mainly dependent on the interparticle spacing of metal nanoparticles,[197, 199, 210] and its significant peak red-shift can be caused by 2D and 3D aggregation.[212-213, 238-239] For films assembled at pH 3.4, 5.6 and 6.8, the interparticle spacing in the nanoparticle clusters was measured by using the Photoshop 'measure tool' and analyzed statistically (Figure 5.8). The analysis of interparticle spacing was limited to within the nanoparticle clusters with interparticle distances smaller than 55 nm (three times of the nanoparticle diameter), at which strong LSPC can be observed.[212] The results show that with increase of the assembly pH over this range, the interparticle spacing decreases (Figure 5.8), confirming that smaller interparticle distances result in stronger LSPC. The pH-tunability of interparticle spacing for LSPC in the nanoparticle clusters can be attributed to a combined effect

of polyelectrolyte conformation and surface charge density. There are three adsorbed polyelectrolyte conformations: trains, loops and tails.[23, 33, 234, 240] It is known that the lower the charge density of polyelectrolyte, the more the loop and tail conformations are. Contrarily, the higher the charge density of polyelectrolyte is, the more the train conformations are.[23, 33] At low assembly pHs (from 3.4 to 6.8), the adsorbed weak polyelectrolyte has high surface charge density, leading to increased interparticle spacing.[231] Meanwhile, the train conformation of weak polyelectrolyte observed at low pH promotes 2D assembly of the nanoparticles.[231, 241-242] When the assembly pH (pH 6.8 - 7.2) approaches the solution pK_a of PEI, the PEI ionization sharply drops to cause significantly reduced surface charge density. Both low surface charge density and high content of loop and tail conformations of the weak polyelectrolyte greatly increase the 3D aggregation of nanoparticles, and thus significantly decrease the interparticle spacing producing strong LSPC. This is very likely the reason that the 3D aggregates are dramatically developed and strong LSPC occurs in the high assembly pH range. The LbL assembly process for controlling the interparticle spacing and aggregation is represented in Scheme 5.2.

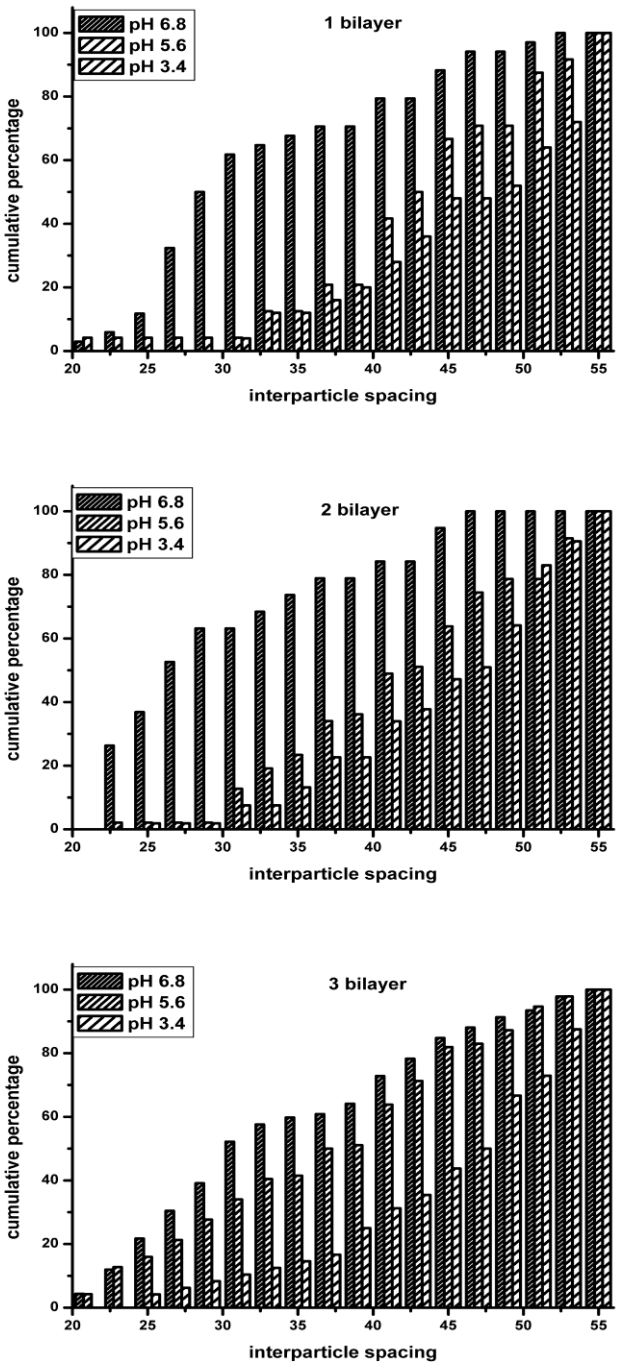

Figure 5.8 Statistical analysis histogram of the interparticle spacing smaller than 55 nm from the 50000× resolution images of pH 3.4, pH 5.6 and pH 6.8 films with the same bilayer number (1st, 2nd, and 3rd bilayer). Cumulative percentage (y-axis) means the percentage of nanoparticles with interparticle spacing smaller than certain values (x-axis).

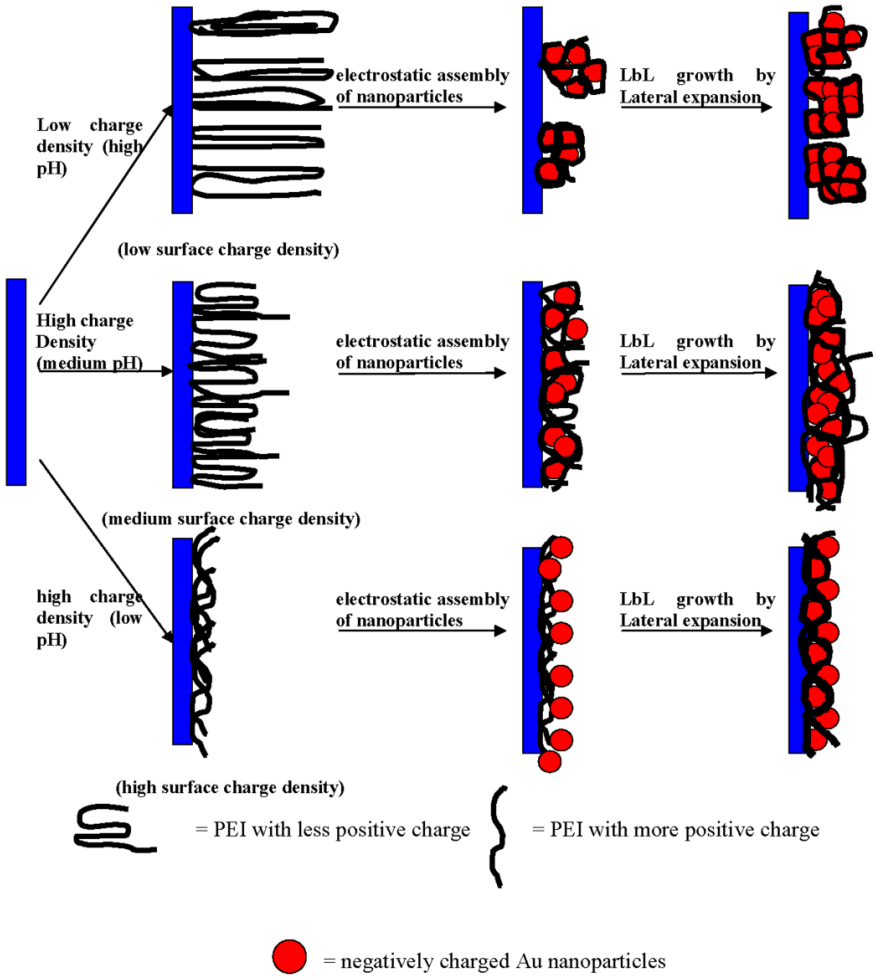

Scheme 5.2 Scheme of weak polyelectrolyte mediated LbL assembly to control the interparticle spacing in the nanoparticle clusters and aggregation.

5.5 Stability of the multilayers

The weak polyelectrolyte/nanoparticles nanocomposite films fabricated were tested for their stability. After immersing the films in 10 mM PBS, acid solution with pH 3.5, or alkaline solution with pH 10, respectively, for one month, the peak wavelength shifts were measured (Figure 5.9). The results show that the longitudinal peak position of the films assembled at pH 3.4 shifts 0.1 nm (Figure 5.9A1), 3.6 nm (Figure 5.9A2), and 5.3 nm (Figure 5.9A3) of their original values,

after immersion in pH 10 alkaline solution, pH 3.5 acid solution and PBS solution for one month, respectively. The films assembled at a high assembly pH (pH 10) are less stable than that assembled at pH 3.4. The peak shifts 7.0 nm and 6.9 nm of their original value after the films were immersed in pH 10 alkaline solution (Figure 5.9C1) and PBS (Figure 5.9C3) respectively for one month. The worst absolute red shift of LSPC after one month is ~7.0 nm, about 6% of the broad modulation range of the longitudinal peak wavelength by the assembly pH (116 nm). Thus, the assembled film is reasonably stable for practical applications. The good stability of the nanocomposite films fabricated in this work is very likely ascribed to the synergistic effect of long range electrostatic force and the short range interactions such as the van der Waals interactions due to the nonionized NH_2 and the dipole interaction between nanoparticles.[231] At low assembly pH, the electrostatic force likely plays a more important role in the stabilization of the multilayer films, while at high assembly pH, the van der Waals interaction becomes strong due to more nonionized NH_2 groups incorporated into the nanocomposite film. Meanwhile a smaller interparticle distance makes the dipole interaction stronger. Both the van der Waals force and the dipole interactions could stabilize the assembled films at high assembly pH.

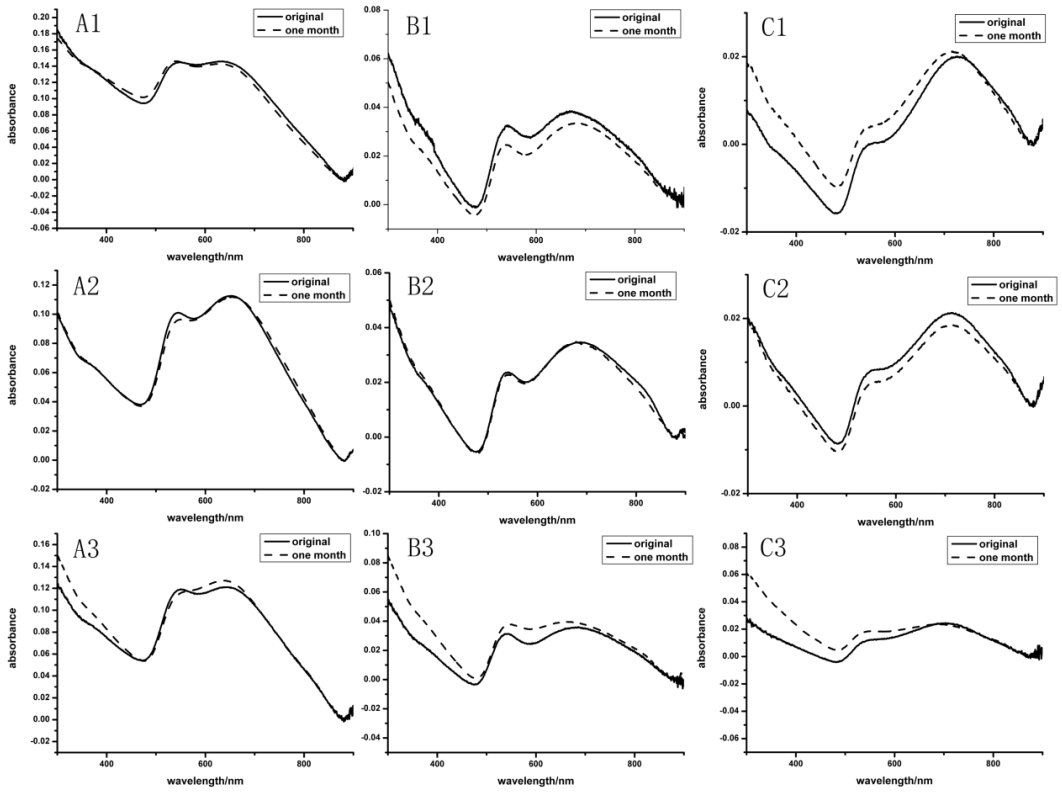

Figure 5.9 UV-vis spectra of nanocomposite film assembled at different pH before and after immersion in different medium (pH 10.0 alkaline solution, pH 3.5 acidic solution and pH 7.4 PBS (10mM)). A1-A3, B1-B3, and C1-C3 are the UV-vis spectra of pH 3.4 film in pH 10.0, pH 3.5, and PBS, pH 5.6 film in pH 10.0, pH 3.5, and PBS, and pH 10.0 in pH 10.0, pH 3.5, and PBS, respectively.

5.6 Conclusions

In brief, pH-controllable weak polyelectrolyte/Au nanoparticle nanocomposite films were successfully constructed through LbL assembly to investigate LSPC. The degree of LSPC can be extensively modulated by adjusting the weak polyelectrolyte assembly pH to achieve the largest tuning range of the longitudinal band peak (625 nm to 741.5 nm) to date, thus rendering great potential for various applications. The great LSPC modulation in the LbL nanocomposite film can be ascribed to the assembled weak polyelectrolyte, of which the pH dependant charge

density and conformation can easily tailor the interparticle spacing in the nanoparticle clusters.

This work provides insights into the effect of morphology on the optical properties of a self-assembled film, and also opens a simple and economical path to realize the modulation of the optical property directly on substrates. This method can be extended to other weak polyelectrolyte and nanoparticle systems for different devices.

Chapter 6 Tunability and Synergistic Properties of Controllably Layer-by-Layer Assembled Polyelectrolytes/Nanoparticle Blend Hollow Capsules

6.1 Introduction

Hollow spheres (capsules) have broad important applications in drug delivery, biosensors, catalysis, reactors, and artificial cells due to their versatile wall functions, capability to load active substances and unique permeability.[136, 243-244] Recently, the polymer/nanoparticle composite capsules have attracted particular attention by their unique properties contributed from both polymer and nanoparticle, in which the polymer provides flexibility and versatility and the nanoparticle offers superior electrical, optical, and magnetic properties while maintaining functionalities of the hollow spheres.[74, 144, 245-250] Furthermore, some particular synergistic properties of polymers and nanoparticles might be harvested.

As a fast developing and well-recognized technology, colloid-templated LbL assembly has now become an economic and versatile method to fabricate the hollow capsules.[136, 244, 251] The wall thickness of LbL assembled capsules can be controlled at a nanometer scale, while various chemical species can be incorporated with tunable nanoscale structures and functions.[5-6, 136, 244, 251-252] This method has been used to fabricate polymer/nanoparticle composite capsules but its direct alternate assembly of polyelectrolytes and nanoparticles may induce severe aggregations between nanoparticles and between colloids as well,[74, 246, 253] thus impairing the nanoparticle properties and the intactness of the capsule walls.

Compared to the direct assembly method, in-situ synthesis of nanoparticles in LbL-assembled polyelectrolyte multilayer shells by introducing precursors can have well-separated nanoparticles with controlled nanoparticle concentration and nanoparticle size.[193, 245] However, it is rather difficult to produce binding sites of precursors on the shells for the *in situ* synthesis through additional introduced reactions without aggregating the colloidal templates;[193, 245, 254-255] Alternatively, infiltration of nanoparticles through highly loose/porous polyelectrolyte shells has been reported, but it is not suitable for most polyelectrolyte systems and most nanoparticles, and only very small nanoparticles can be used.[256] Up to now, it still remains a great challenge to develop a well-controllable method to fabricate polyelectrolyte/nanoparticle composite capsules with desired concentration, size and interparticle spacing of nanoparticles and good dispersion, and to further study the synergistic property of the multicomponents in the composite capsules for achieving superior performance in practical applications.

Three-component LbL polyelectrolyte assembly via alternate deposition of a two-component polyelectrolyte blend and a third polyelectrolyte has attracted much interest recently due to its demonstrated superior tunability and versatility to traditional 2-component LbL assembly methods.[75, 110, 257-261] Particularly, the assembled film thickness, chemical composition, wettability, stability, and biological interaction can be simply tuned by the blend ratio.[75, 258-259] This 3-component polyelectrolyte blend assembly has been recently performed on colloidal template to fabricate microcapsules with tunable chemical composition, thickness and stability.[260] Nanoparticle is a building block in 2-component LbL

assembly, thus it might be used as one blend component to fabricate polyelectrolyte/nanoparticle composite capsules. There is a work on preparation of a 3-component capsule by using blended polyelectrolyte/nanoparticle solution assembled with another polyelectrolyte to prevent the nanoparticle aggregation.[253] However, the assembly process including the effect of assembly conditions on formation of the composite capsule has not been systematically studied. In comparison to an all-polyelectrolyte system, the challenge lies in that the nanoparticles in the blend with the same sign of charge as the polyelectrolyte component are normally assembled much slower than the polyelectrolyte one and even difficult to be assembled due to their larger size, much less binding sites and the fast charge overcompensation by polyelectrolyte, thus making it difficult to realize the controllability.[262-265] Thus, it is even more challenging to use this nanoparticle-participated blend assembly method to fabricate capsules with tunability of the assembled nanoparticles concentration, size and interparticle spacing and superior synergistic property of polyelectrolyte-nanoparticle.[74, 253-255]

The main advantage of the weak polyelectrolyte based LbL assembly is its pH-tunable charge density to adjust the electrostatic interaction between assembled components over a very broad range.[33, 35, 59, 76, 86, 254, 266] Parameters such as surface charge density, chemical composition, and permeability of the assembled multilayers can all be simply controlled by assembly pH.[23, 50, 59] In this work, we systematically investigate the nanoparticle-participated 3-component LbL assembly process to build a polyelectrolyte/gold nanoparticle hollow nanocomposite capsule system by using PEI and a PAA-gold nanoparticle blend (both PEI and PAA are

typical weak polyelectrolytes). Gold nanoparticle was used as a model nanoparticle because of facile synthesis, superior physic-chemical properties and unique biological applications.[267-268] Both the pH of weak polyelectrolyte and blend ratio of weak polyelectrolyte to nanoparticles were studied to manage the relative assembly rate of polyelectrolyte to nanoparticles and thus enhance assembly of gold nanoparticles for successful blended LbL assembly, meanwhile to maintain the dispersion of colloidal templates. To control the buildup of capsules at a molecular level, the effect of blend ratio on nanoparticle concentration and interparticle spacing in the weak polyelectrolyte/nanoparticle composite capsules are investigated. To control the buildup of capsules at a molecular level, the effect of blend ratio on nanoparticle concentration and interparticle spacing in the weak polyelectrolyte/nanoparticle composite capsules are investigated. The synergistic properties of weak polyelectrolyte and gold nanoparticles are explored. Encapsulation of antibody was conducted to demonstrate the potential applications of the assembled nanocomposite capsules.

6.2 Preparation of PEI/PAA-gold nanoparticles microcapsules

6.2.1 Synthesis of Au nanoparticles and $CaCO_3$ microparticles

Gold nanoparticles were synthesized according to Natan's method with minor modifications.[269] Typically, 0.75 ml and 0.375 ml of 1% sodium citrate were added to 50 ml 0.3 mM boiling $HAuCl_4$ solution respectively to prepare two differently sized Au nanoparticles. After 10 min boiling, the heat source was removed. The colloid solution was further stirred for 30 min and then stored in dark under room

temperature. Two kinds of gold nanoparticles prepared had the sizes of 18 nm ± 3 nm (70 particles sampled) (Figure 5.1) and 50 nm ± 5 nm (50 particles sampled) (Figure 6.1) respectively in terms of the TEM images. Unless described particularly, 18 nm nanoparticles were used in all the experiments.

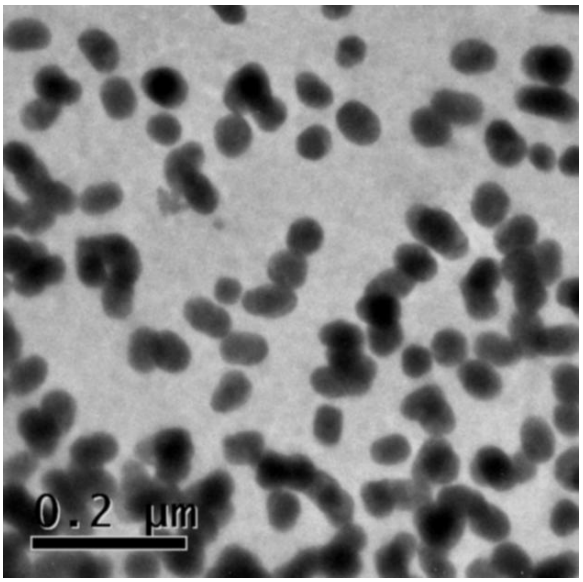

Figure 6.1 TEM images of large-sized gold nanoparticles.

$CaCO_3$ microparticles were prepared according to the reported method with minor modification.[270] Briefly, 0.33 M $CaCl_2$ and 0.33 M Na_2CO_3 were mixed under vigorous stirring for 3 min. Then three centrifugation and washing steps were performed with DI water to remove the unreacted species. Finally, the particles were washed with acetone and air dried. The size of $CaCO_3$ microparticles was about 4.0 μm ± 1.2 μm, as shown in the SEM image (Figure 6.2).

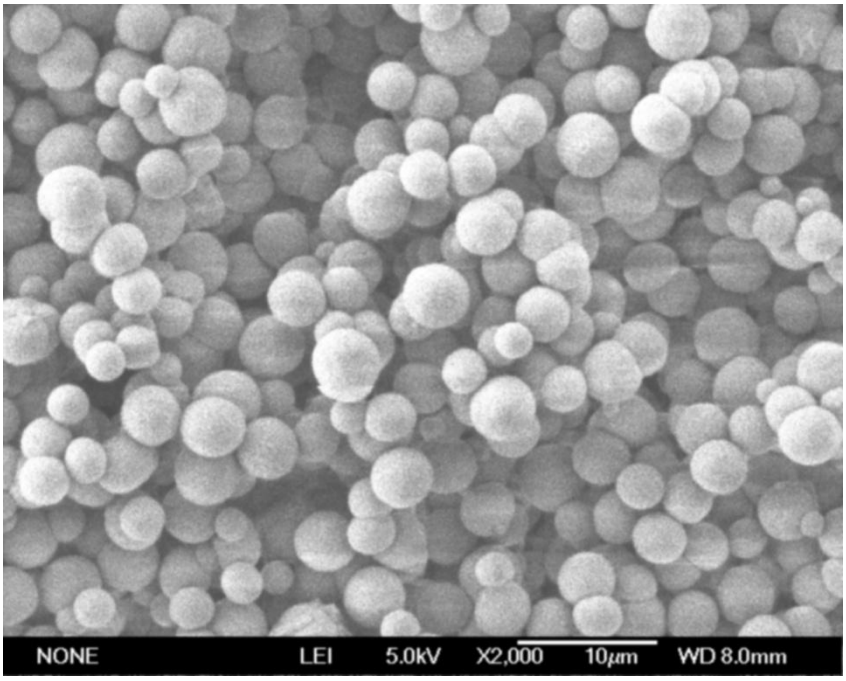

Figure 6.2 FE-SEM images of $CaCO_3$ microparticles.

6.2.2 LbL blend assembly

The PAA-gold nanoparticles blend solutions with varied blend ratio were prepared by adding different concentrations of PAA in the as-prepared gold nanoparticle solution. The pH of the blend solutions was adjusted using HAc or 0.1 M NaOH.

For the LbL assembly on plane substrates, the cleaned glass slides or silicon wafer were immersed in 1 mg/ml PEI solution (pH=9.0) for 10 min, followed by washing with DI water and blow-drying with N_2. Subsequently, the substrate was immersed in the PAA-gold nanoparticle blend solution (pH=10) for 15 min, followed by washing with DI water and blow-drying with N_2. Multilayer films with different bilayers were assembled by repeating the cycles. $(PEI/PAA\text{-}Au)_n$ is used to represent a multilayer film with n bilayers.

For the LbL assembly on $CaCO_3$ microparticles, 10 mg $CaCO_3$ microparticles were dispersed in 1 ml of 1 mg/ml PEI solution (pH=9.0) and shaken for 10 min using a vortex shaker. Then the microparticles were repeatedly centrifuged (200 g) and washed with DI water for 3 times, and were dispersed in 1 ml of the PAA-gold nanoparticles blend solution (pH=10) with shaking for 15 min, followed by three times of centrifugation (200 g) and washing with DI water. By repeating such cycles, multilayer shells with certain bilayers on $CaCO_3$ microparticles were produced.

6.2.3 Fabrication of polyelectrolyte-nanoparticle blend nanocomposite capsules

The multilayer-coated $CaCO_3$ microparticles were dispersed and shaken in 2% glutaraldehyde solution for 16 h to crosslink the multilayer films, followed by three steps of centrifugation (200 g) / washing with DI water to remove the free glutaraldehyde. Then, the multilayer-coated $CaCO_3$ microparticles were dispersed and shaken in 0.2 M EDTA solution (pH 7.5) for 30 min, followed by centrifugation (1200 g) and re-dispersion in 0.2 M fresh EDTA (pH 7.5) for 30 min. This procedure was repeated for 4 times to ensure complete removal of $CaCO_3$ microparticles.[270-271] Finally, the obtained capsules were repeatedly centrifuged (1200 g) and washed with DI water for 3 times.

6.3 Factors to affect microcapsule fabrication

The main factors to affect the nanoparticle incorporation for construction of PEI/PAA-gold nanoparticles blend multilayers were studied by using different assembly pH and PAA concentration (blend ratio) (Figure 6.3). At PEI pH of 9, PEI concentration of 1 mg/ml and PAA of 1 mg/ml, a PAA-gold nanoparticle blend solution with pH larger than ~ 4 could make incorporation of gold nanoparticles into the assembly impossible. Even after 8 bilayers, no localized surface plasmon resonance (LSPR) peak could be observed from the UV-vis spectroscopy (Figure 6.3a). Only by further decrease of assembly pH to ~ 3.2 that significant amount of gold nanoparticles can be assembled (Figure 6.3a). This is caused by a nearly neutral PAA at ~pH 3.2 or lower (PAA pK_a=~4.5[23]) with lower assembly rate by electrostatic attraction to compete with Au nanoparticles.[253, 272] It is interesting to note that the gold nanoparticles assemble exponentially with the bilayer number, which is possibly due to the exponential growth nature of PEI and PAA polyelectrolyte pair to provide increasingly rougher surface with increase of bilayer number for more gold nanoparticle adsorption.[60, 76] PAA has much faster assembly rate than gold nanoparticles due to its high charge density at assembly pH higher than 4 and small size. Thus, the polyelectrolyte concentration could also be used to tune the relative assembly rate of PAA and gold nanoparticles for successful assembly of gold nanoparticles. Indeed, when lowering the PAA concentration to ~ 0.1 mg/ml at pH 10, which keeps its fully charged state, the gold nanoparticles begin to be incorporated into the multilayers. The UV-vis spectra of the weak polyelectrolyte/nanoparticle nanocomposite films with different bilayers assembled

varied PAA concentrations in Figure 6.3b shows that the LSPR peak intensity increases with increase of the bilayer number, indicating successful assembly of gold nanoparticles with all these conditions. Furthermore, the LSPR peak intensity increases significantly with decrease of the PAA concentration. These results indicate that the tunable incorporation of gold nanoparticles in the assembly could be ascribed to the competitive adsorption between PAA and gold nanoparticles.[253, 272-273] It can be seen that at relatively high PAA concentration (0.01 and 0.1 mg/ml), the gold nanoparticles also assemble exponentially, which should be due to the same reason as stated above (exponential growth of PEI and PAA multilayers). Interestingly, increase of assembly pH of PEI can also significantly enhance the gold nanoparticles assembly. The nanoparticles assembled at PEI pH 9 significantly increase by ~ 9 times than that at pH 3.5 (Figure 6.3 (a), and also see Figure 6.4 for UV-vis spectra). In contrast, at PEI pH 3.5 and PAA pH 10 at which PAA is fully charged, the gold nanoparticles are very difficult assembled even with 0.001 mg/ml PAA (Figure 6.3 (b), and also see Figure 6.5 for UV-vis spectra). This is caused by more incorporated PEI with more loop and tail structure at a higher pH for more active sites.[33, 76, 274] Thus, the weak polyelectrolyte adopted here plays an essential role to enhance the assembly of gold nanoparticles, making the tunability of gold nanoparticle assembly possible. In the reported 3-component assembly for nanocomposite capsules, strong polyelectrolyte is used. it is much more difficult to incorporate substantial amount of gold nanoparticles for tuning the capsule composition due to the much stronger electrostatic interaction between two polyelectrolytes than that between nanoparticle and polyelectrolyte;[25, 116] even

with very small blend ratio of polyelectrolyte to nanoparticles the incorporated nanoparticles are still low due to much less active sites of the dominated train conformation in the strong polyelectrolyte-assembled multilayers.[23, 33] The LbL assembly on colloidal particles may impose restrictions on the tuning conditions for the nanoparticles assembly. It was found that at PEI pH as high as 9, the PAA-gold nanoparticles blend solution could not be too low (such as lower than 4), which would induce severe aggregations between colloidal templates. This might be due to the too low surface charge and/or too rough surface of coated colloids.[76, 193, 254] Furthermore, further increase of PEI pH could also increase the aggregation, possibly due to the same reason (too low charge density and/or too rough surface). Thus, in all the remaining experiments, the PEI pH was set at 9 to increase the incorporation of gold nanoparticles, but not aggregate the $CaCO_3$ microparticles, the pH of PAA-gold nanoparticles blend solution was chosen at 10 to make PAA fully charged to prevent the aggregation, and very small concentrations (0.01 mg/ml or less) of PAA were used to enhance the gold nanoparticle incorporation.

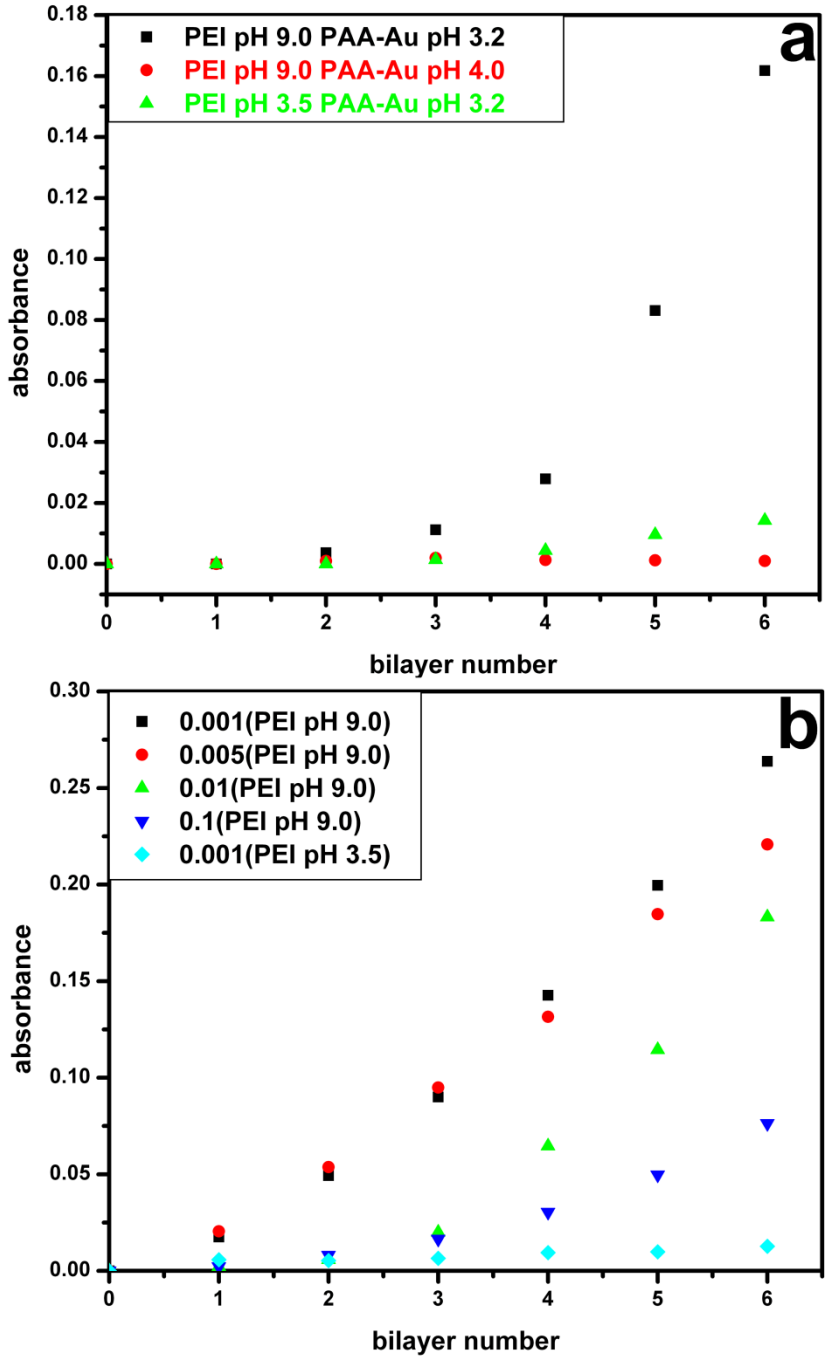

Figure 6.3 The LSPR intensity versus the bilayer number of the multilayers assembled at different pH and different PAA concentration. (a) PAA concentration of 1mg/ml and different PEI and PAA pH. (b) PEI pH of 9 and PAA concentration of 0.001 mg/ml, 0.005 mg/ml, and 0.01 mg/ml, and PEI pH of 3.5 and PAA concentration of 0.001 mg/ml. (0.001, 0.005, 0.01, 0.1 represent 0.001 mg/ml, 0.005 mg/ml, 0.01 mg/ml, and 0.1 mg/ml PAA in the blend solution with fixed gold nanoparticle concentration (the same below).).

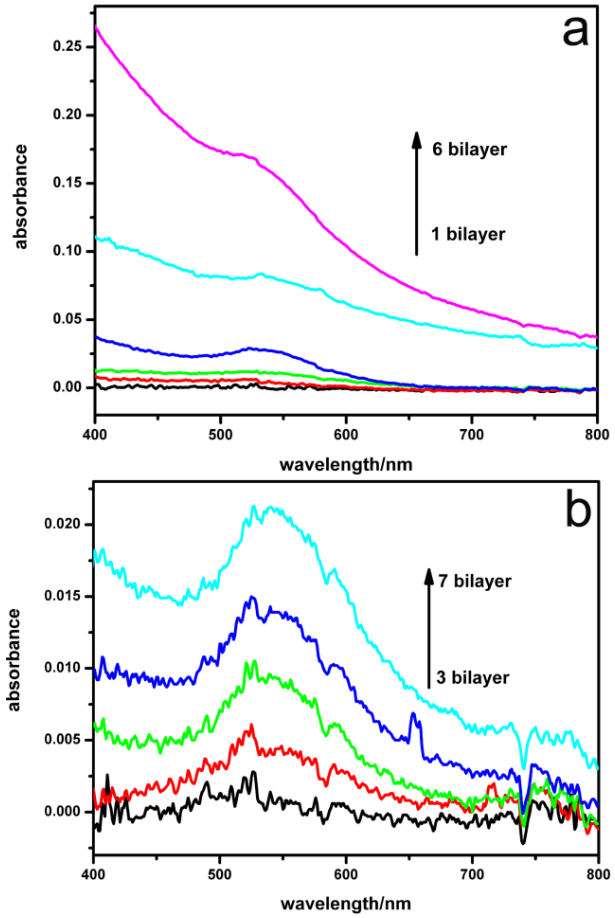

Figure 6.4 UV-vis spectra of PEI/PAA-gold nanoparticles multilayers with different bilayers assembled at PEI (1mg/ml) pH 9.0 (a) and pH 3.5 (b), and PAA (1mg/ml)-gold nanoparticle blend pH 3.2.

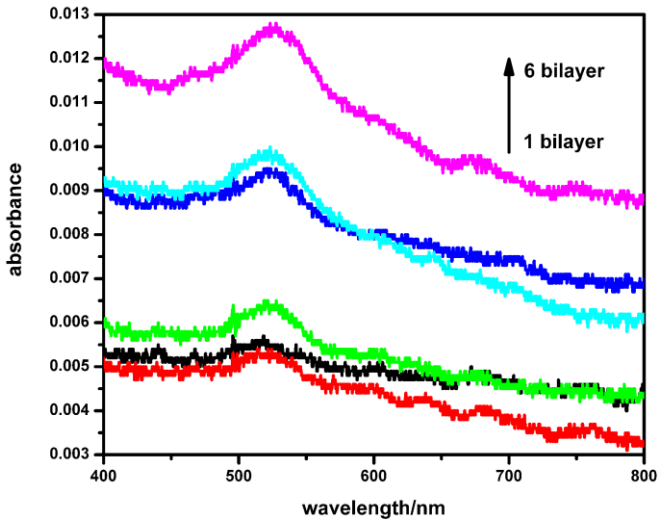

Figure 6.5 UV-vis spectra of PEI/PAA-gold nanoparticles multilayers with different bilayers assembled at PEI pH of 3.5 and PAA pH of 10 and concentration of 0.001mg/ml.

6.4 Characterization of PEI/PAA-gold nanoparticles composite capsules

The PEI/PAA-gold nanoparticles blend multilayers were subsequently assembled on removable $CaCO_3$ microparticles. Three representative concentrations of PAA (0.01 mg/ml, 0.005 mg/ml, 0.001 mg/ml) were tested to investigate the controllable assembly of microcapsules. Figure 6.6 shows the typical CLSM images of the structure of multilayer-coated $CaCO_3$ microparticles and the microcapsules after removal of the $CaCO_3$ microparticles. The fluorescence is distributed over all the core/shell structure but with stronger signals around the microparticles (Figure 6.6a. Only the image of microparticles coated with 0.01 mg/ml PAA assembled films is given. Images of microparticles coated with multilayers assembled at 0.001 mg/ml or 0.005 mg/ml PAA are similar and not shown). It has been reported that the $CaCO_3$ microparticle has a nanoporous structure to allow penetration of polymers into its spheric structure.[270, 275] Thus, the polyelectrolytes and nanoparticles may not only be adsorbed on the $CaCO_3$ surface, but also penetrate into the interior of the sphere structure of the particles. Notably, these multilayer-coated $CaCO_3$ microparticles at all the adopted conditions are well-dispersed. After thorough removal of the $CaCO_3$ core by repeated EDTA treatment and water washing procedure,[74, 270-271] very little fluorescence can be observed in the microparticles for all the PAA concentrations and the dispersion state is still maintained (Figure 6.5b-d), indicating successful formation of well-dispersed hollow capsules. The remaining slight fluorescence is caused by the initially formed complexes in nanopores of $CaCO_3$ particles.[270-271] FE-SEM images of the

nanocomposite (Figure 6.7) show that the structures fabricated at all the conditions collapse, which is due to the ultrathin nanocomposite shell, leading to a very weak mechanical strength. This further confirms the formation of the hollow nanocomposite capsules. The 2-component LbL assembly of PEI and gold nanoparticles without PAA to be blended (same assembly pH and same batch of gold nanoparticles) was also examined and severe aggregation between capsules was observed (Figure 6.8). Moreover, the UV-vis spectra of the two-component polyelectrolyte/nanoparticle multilayers exhibit very strong longitudinal localized surface plasmon coupling peaks at around 625 nm, suggesting serious aggregation between gold nanoparticles inside the individual capsule wall (Figure 6.9).[266, 276] Another phenomenon is that a rather high percentage of broken microcapsules occur (Figure 6.8). This result indicates that the strong tendency of nanoparticles to aggregate could promote the aggregation of the colloidal templates during the assembly process, thus leading to an inhomogeneous coating and even breakage of the multilayer shell. Apparently, the nanoparticle aggregation in the multilayer shell can affect the film continuity. Unlike the 2-component assembled capsules, the nanoparticles are distributed uniformly inside the three-component polyelectrolyte/nanoparticle capsule walls (see TEM results below). The good dispersion and intactness of three-component polyelectrolyte/nanoparticle composite capsules indicate that the PAA component in the blend can not only protect the gold nanoparticles from aggregation, but also significantly improve the wall integrity, thus providing microcapsules much superior to 2-component ones.

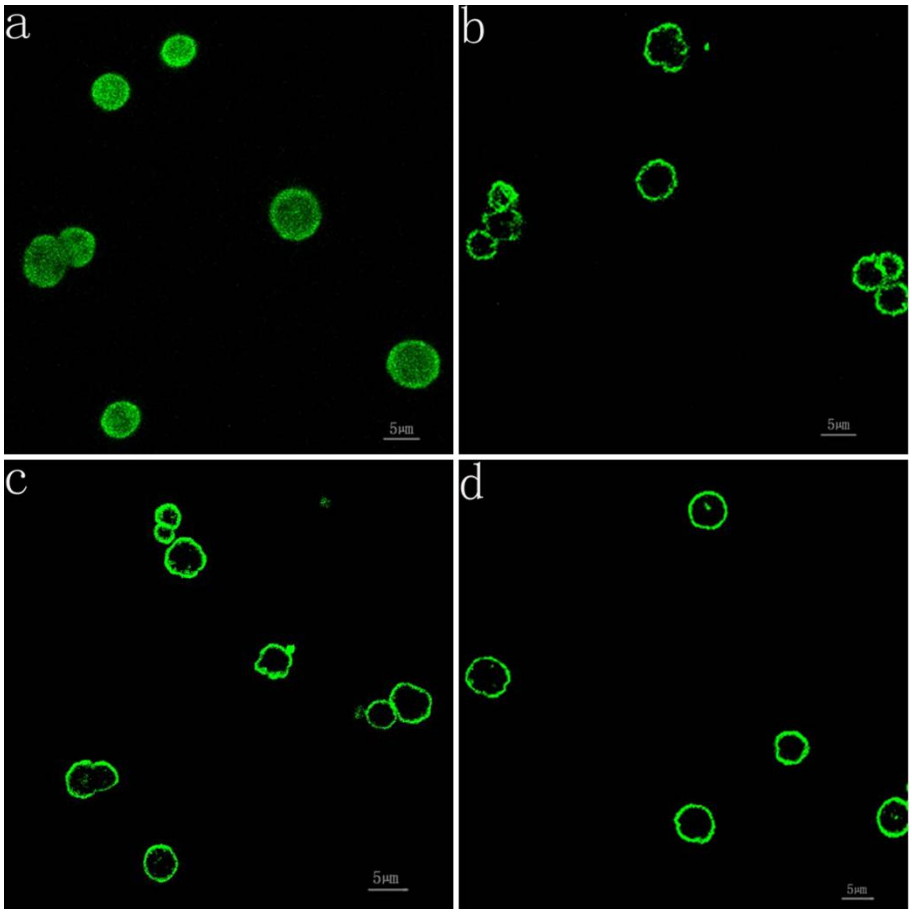

Figure 6.6 CLSM images of microparticles before the core removal (a) and the microcapsules fabricated at 0.001 mg/ml PAA (b), 0.005 mg/ml PAA (c), and 0.01 mg/ml PAA (d).

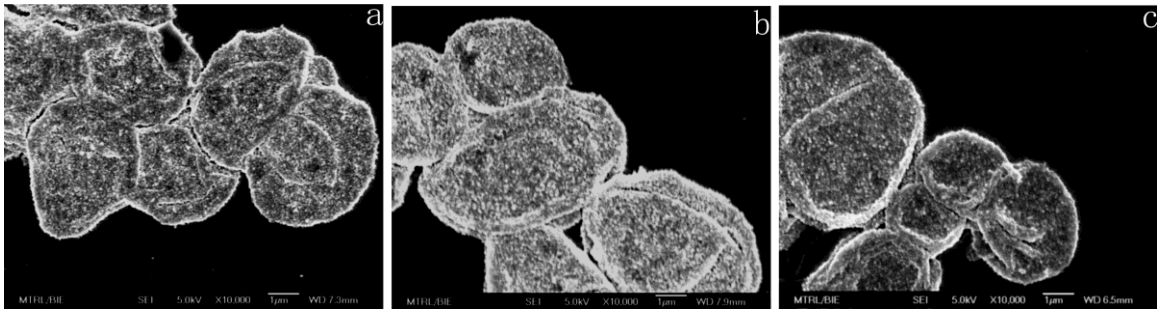

Figure 6.7 FE-SEM images of the microcapsules fabricated at different PAA concentrations. a) 0.001 mg/ml; b) 0.005 mg/ml; c) 0.01 mg/ml.

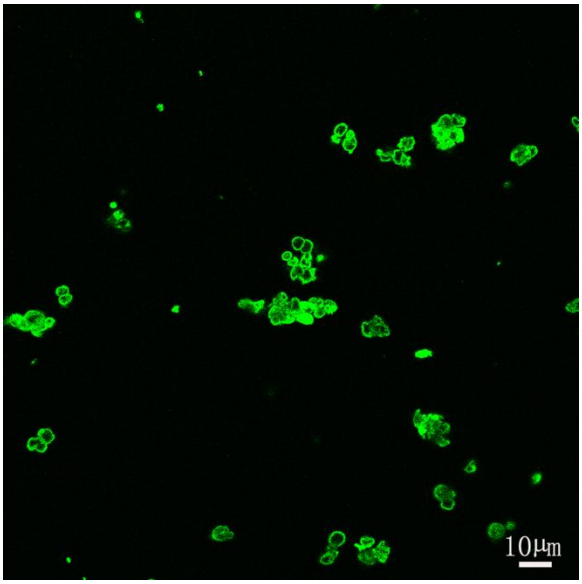

Figure 6.8 CLSM image of the microcapsules fabricated without PAA.

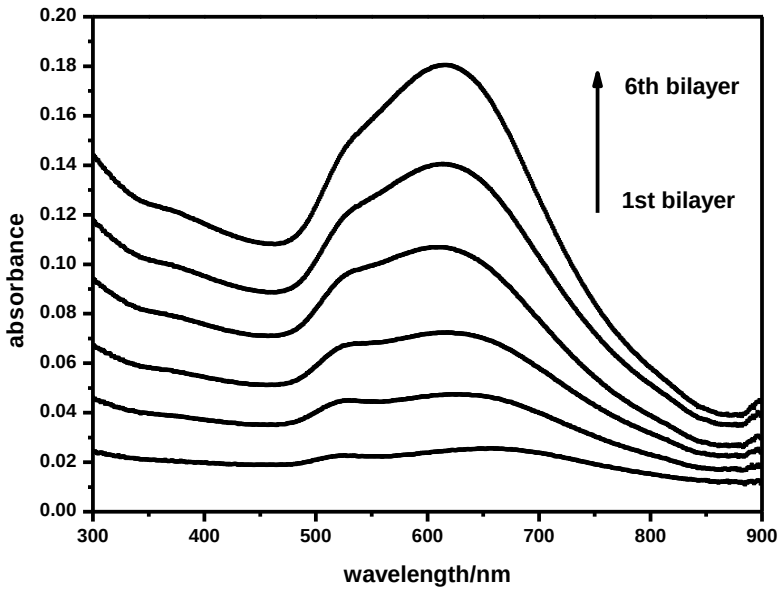

Figure 6.9 UV-vis spectra of PEI/gold nanoparticles multilayers with different bilayers.

TEM was used to study the internal structures of the microcapsules (Figure 6.10). The amount of gold nanoparticles in the capsule wall can be simply controlled by the PAA concentrations. With increase of the PAA concentration, the amount of

the assembled gold nanoparticles significantly decreases (Figure 6.10a-c). The concentration of gold nanoparticles in the capsules can be calculated by dividing the nanoparticle amount with its occupied volume, which is proportional to its occupied thickness. As estimated from AFM result (Figure 6.11), the capsules constructed with 0.01 mg/ml PAA have a thicker wall (41 nm) than the other two types of capsules (28 nm for the 0.001 mg/ml PAA and 17 nm for the 0.005 mg/ml PAA). Thus, the gold nanoparticle concentration in this type of capsule is less than that in the other two types. Although the thickness of capsule walls from 0.001 mg/ml PAA is larger than that from 0.005 mg/ml, nanoparticle amount for 0.001 mg/ml condition is much larger than that for 0.005 mg/ml (~2.5 times), indicating that the gold nanoparticle concentration of capsules fabricated from 0.001 mg/ml PAA is larger than that from 0.005 mg/ml. Therefore, the nanoparticle concentration in the microcapsules can be simply tailored by the PAA assembly concentration. The distribution and interparticle spacing of gold nanoparticles can also be reflected from the TEM images (Figure 6.10). For all the PAA concentrations, the gold nanoparticles distribute homogeneously in their capsule walls. Furthermore, with increase of PAA concentration, the interparticle spacing obviously increases, which should result in a regular shift of LSPR peak position and will be discussed later. To demonstrate the size tunability of the gold nanoparticles assembled into the capsules, the large-sized gold nanoparticles (50 nm) were also used for the capsule fabrication with this three-component LbL assembly process. The capsules also can be fabricated (FE-SEM images shown in Figure 6.12) to incorporate large-sized nanoparticles (Figure 6.10d). Thus, by

tuning the size of nanoparticle used for the assembly, the nanoparticle size in the microcapsules can be easily tuned. It should be noted that the incorporation of such large-sized nanoparticles cannot be easily achieved via other methods such as *in situ* synthesis method due to the strong stabilization effect of the polyelectrolyte shells,[193, 245] direct assembly method due to the aggregation between nanoparticle and colloid,[253, 277] and infiltration method due to the limited pore size of polyelectrolyte multilayers.[256]

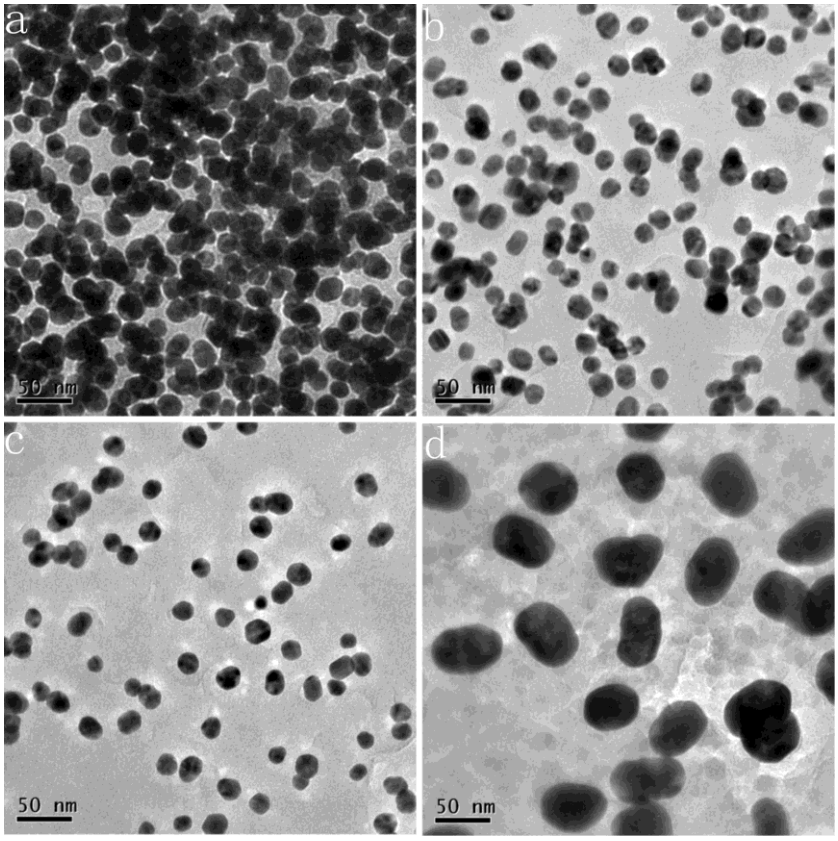

Figure 6.10 TEM images of the microcapsules fabricated at different PAA concentrations and with large gold nanoparticles. a) 0.001 mg/ml; b) 0.005 mg/ml; c) 0.01 mg/ml; d) 0.01 mg/ml with large sized gold nanoparticles.

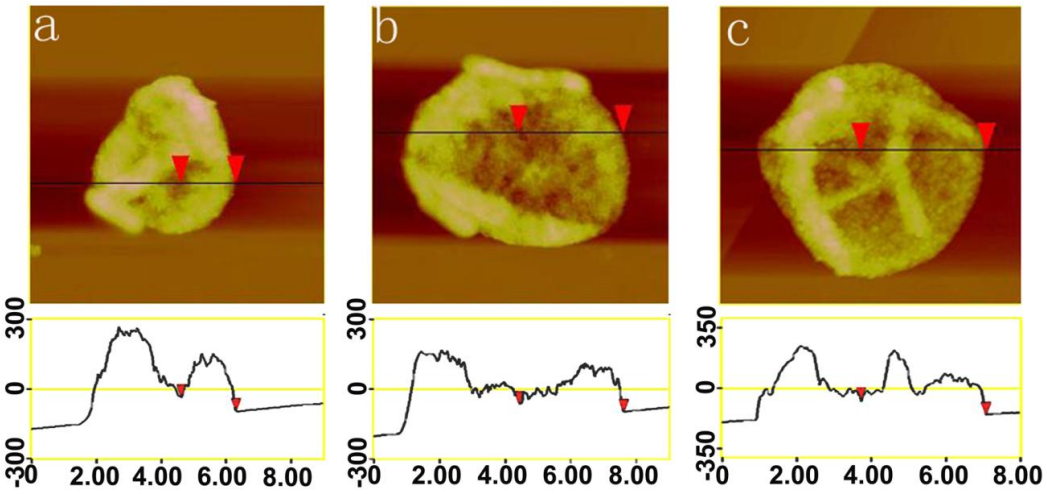

Figure 6.11 AFM images of the microcapsules fabricated at different PAA concentrations. a) 0.001 mg/ml; b) 0.005 mg/ml; c) 0.01 mg/ml.

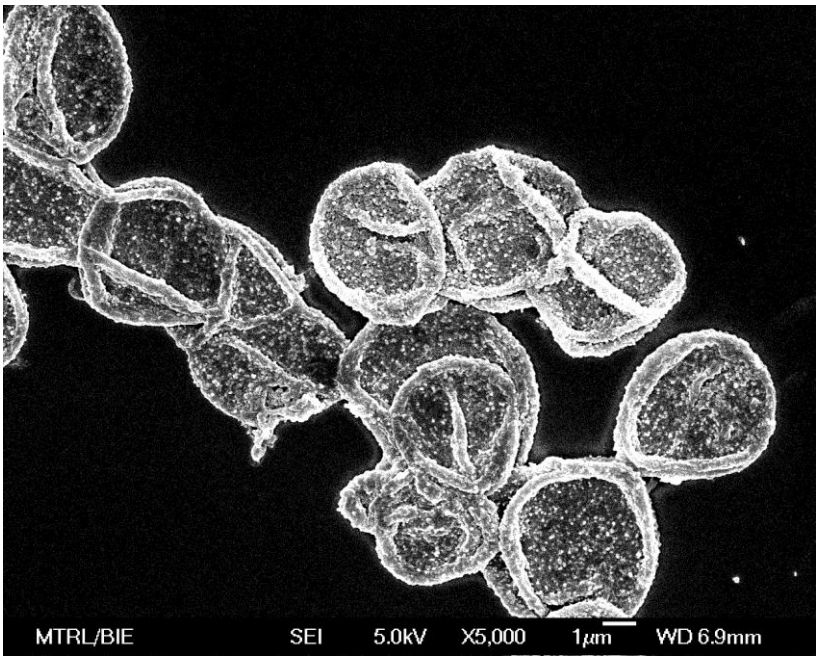

Figure 6.12 FE-SEM images of the microcapsules fabricated with 50 nm gold nanoparticles at PAA concentration of 0.01 mg/ml.

6.5 Synergistic properties of nanocomposite capsules

One important property of metal nanoparticles is their LSPR. The fabrication of nanoparticle assembly on a solid substrate or in a freestanding form with tunable

LSPR is very desirable for many important applications such as laser-responsive drug delivery,[208-209] surface enhanced Raman scattering,[202-203, 278] second harmonic generation,[205, 279] and photonic wave guiding.[206, 280] In the previous chapter, modulation of longitudinal LSPR peak directly on solid substrates with a broad tuning range has been realized.[266] Differently, the LSPR property of the obtained freestanding nanocomposite capsules in this work was investigated. Figure 6.13 shows that the LSPR peak position of the capsules can be simply controlled by the PAA concentrations. With decrease of PAA concentration, the LSPR peak significantly red-shifts from 547 nm to 581 nm. This can be ascribed to the increased nanoparticle filling factor (nanoparticle concentration) and decreased interparticle spacing,[196, 262, 281-282] which is supported by the TEM and AFM result (Figure 6.10 and 6.11). This LSPR tuning range is already among the highest for the gold nanoparticle-loaded polyelectrolyte microcapsules in the reported prior arts,[281] and is expected to be further extended by optimizing the PAA concentration. It is worthy of a note that the good dispersion of gold nanoparticles in the capsules are remained in all tested PAA concentrations (Figure 6.10). The LSPR tunability of polymer/nanoparticle nanocomposite capsule by LbL blend assembly is demonstrated for the first time, and is clearly a synergistic effect of polyelectrolytes and gold nanoparticles, in which the polyelectrolyte plays a role in adjusting the interparticle distance to control interaction between metal nanoparticles in the three-component LbL assembly. Such weak polyelectrolyte/nanoparticle composite capsules with a tunable LSPR property are

particularly promising for smart drug delivery system with biosensing and bioimaging functions.[244, 268, 283-285]

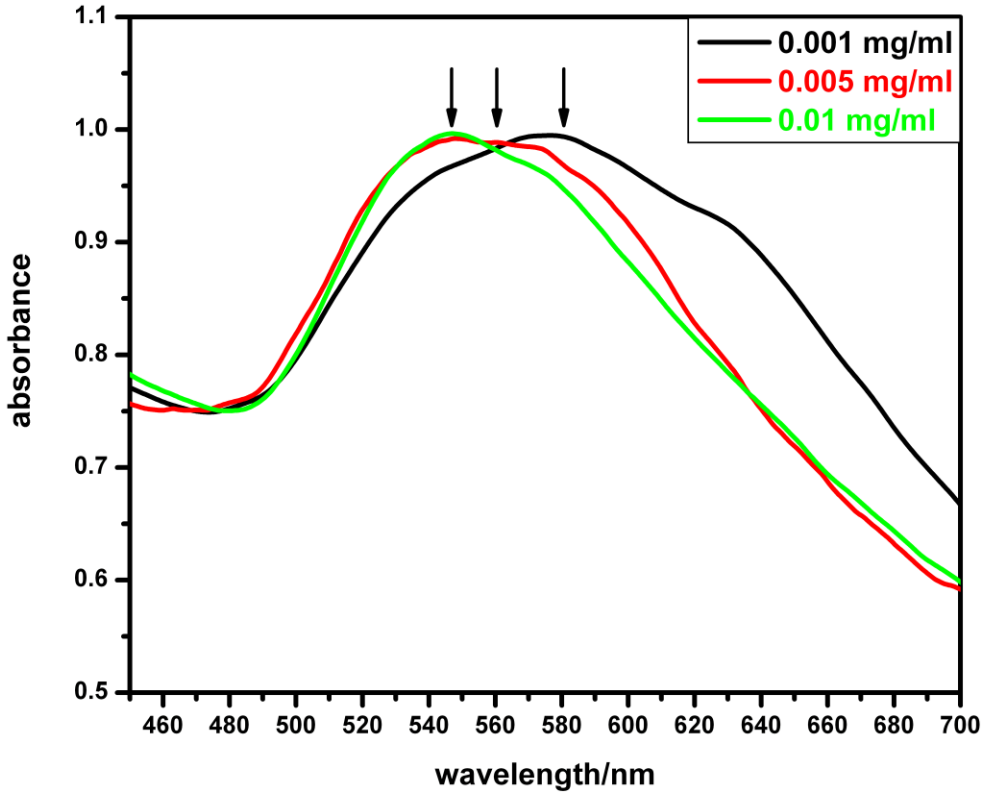

Figure 6.13 The normalized UV-vis spectra of microcapsules assembled at 0.001 mg/ml, 0.005 mg/ml and 0.01 mg/ml PAA concentration.

Permeability is one of the most important properties of the polyelectrolyte hollow capsules for practical applications such as drug delivery and fundamental study to understand the property of the polyelectrolyte multilayer film.[98, 136, 286-289] The assembled polyelectrolyte microcapsules without post-treatment (i.e. under ordinary condition of neutral pH, low salt concentration and room temperature) typically show semipermeability to only small molecules (e.g., PSS/PAH capsule has a typical molecular weight cutoff of ~2 K).[136, 288, 290-291] The polyelectrolyte capsules using porous $CaCO_3$ as a template are more permeable, but the largest molecules reported to permeate till now is FITC-dextran with M~150 K.[292] Thus,

highly permeable microcapsules are required for the loading of high-molecular-weight macromolecules such as DNA and many proteins or even nanoparticles.[136, 288] In addition, it is important to control the permeability for selective loading.[286, 288-289] In this study, the FITC-dextran with molecular weight of 250 K and 2000 K were chosen as probes to test the permeability of microcapsules fabricated with 0.001 mg/ml PAA and 0.01 mg/ml PAA. For the microcapsules with lower PAA concentrations (0.001 mg/ml), even the 2000 K FITC-dextran can permeate through (Figure 6.14a). However, the microcapsules fabricated with 0.01 mg/ml PAA inhibit the penetration of the 2000 K FITC-dextran (Figure 6.14b) while allow the 250 K FITC-dextran passing through easily (Figure 6.14c). This permeability level is much higher than that of reported polyelectrolyte microcapsules.[136, 288, 290-292] The ultrahigh permeability of the weak polyelectrolyte/nanoparticle nanocomposite capsule at low polyelectrolyte concentration (0.001 mg/ml PAA) could be ascribed to the large concentration of gold nanoparticles incorporated, which can introduce significant interparticle interstices.[293-294] With increase of PAA concentration, the gold nanoparticle concentration can be simply reduced with less interparticle interstices to compromise the permeability for particular application requirement. Since lower permeability can be achieved by traditional approaches, the prominent advantage of this work is to provide a method to fabricate highly permeable capsules. Indeed, with this approach even at 0.01 mg/ml PAA concentration at which the content of gold nanoparticles is very low, the permeability is still very high. Thus, the weak polyelectrolytes incorporated should play a role in the high permeability.

Interestingly, FITC-dextran with molecular weight of 250 K can also permeate through the PEI and PAA capsules without incorporating gold nanoparticles (same assembly condition but without addition of gold nanoparticles. Figure 6.15). This might be ascribed to the exponential growth of partially charged PEI and PAA to form a highly loose structure.[76, 78, 130] The unique high permeability of pure weak polyelectrolyte capsule reported here should also be very promising for various applications, which is being further investigated in our lab. However, it could not achieve as high level as that demonstrated in this work (permeable to 2000 K). In addition, without the incorporated nanoparticles, the capsules cannot have the important LSPR properties. To our knowledge, no capsules have been reported to have both such superior and tunable LSPR and permeability. The capsules fabricated in this work provide high, controllable permeability and LSPR, rendering very promising potential for selective encapsulation of macromolecules (or even nanoparticles) for broad practical applications.[136, 271, 289, 295-296] Particularly, with the tunable LSPR property and tunable superior permeability, the weak polyelectrolyte/nanoparticle nanocomposite capsules could have great potential applications in intelligent drug delivery, biosensing and biological imaging. [244, 268, 271, 283-285, 295-296] In our lab, study on the antibody loading for targeted drug delivery and bio-imaging is undergoing using Rabbit anti-goat IgG (cy3 labeled, M_w~160 K) as a model antibody. Preliminary results have been accomplished. After dispersion in cy3-IgG/PBS solution and thoroughly washing with PBS, the cy3-IgG can be very easily spontaneously loaded into the microcapsules (both in the wall and interior) (Figure 6.16).

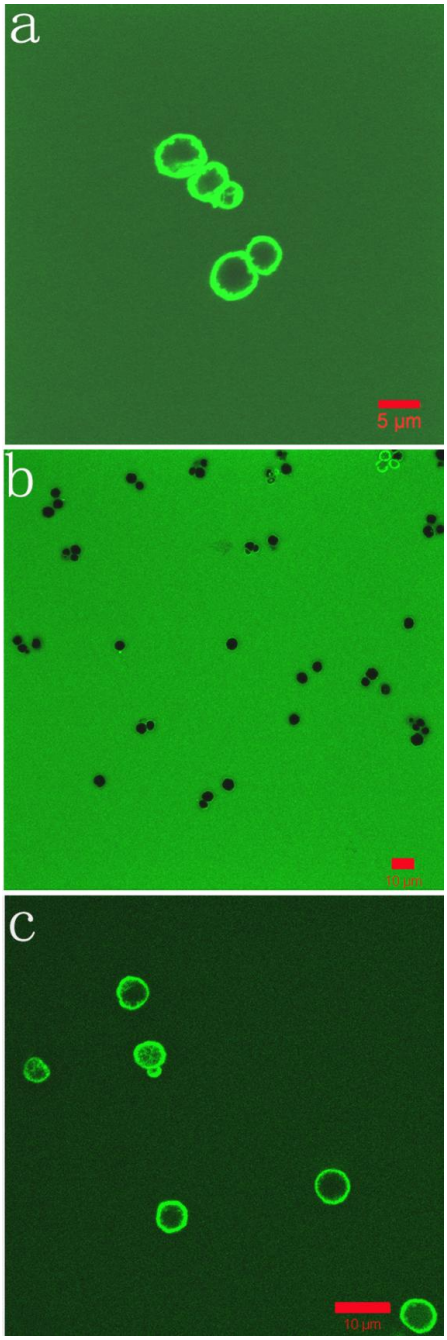

Figure 6.14 The permeability of microcapsules fabricated at different PAA concentrations for FITC-dextran with different molecular weight. a) PAA concentration 0.001 mg/ml, FITC-dextran M=2000 K; b) PAA concentration 0.01 mg/ml, FITC-dextran M=2000 K; c) PAA concentration 0.01 mg/ml, FITC-dextran M=250 K.

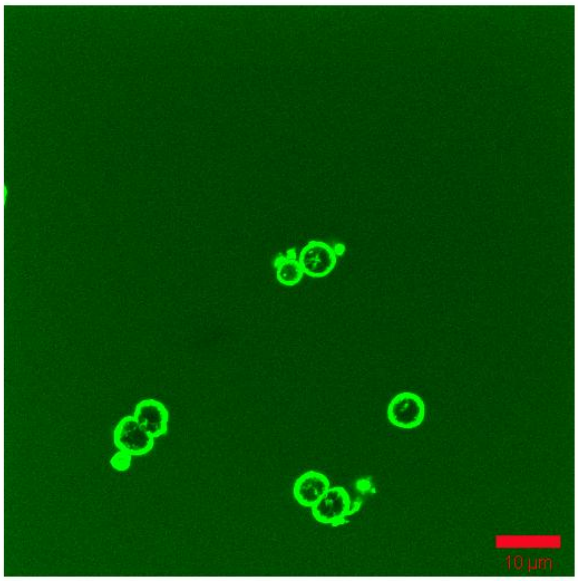

Figure 6.15 Permeability of the microcapsules fabricated at 0.01 mg/ml PAA and without addition of gold nanoparticles for FITC-dextran with a molecular weight of 250 K.

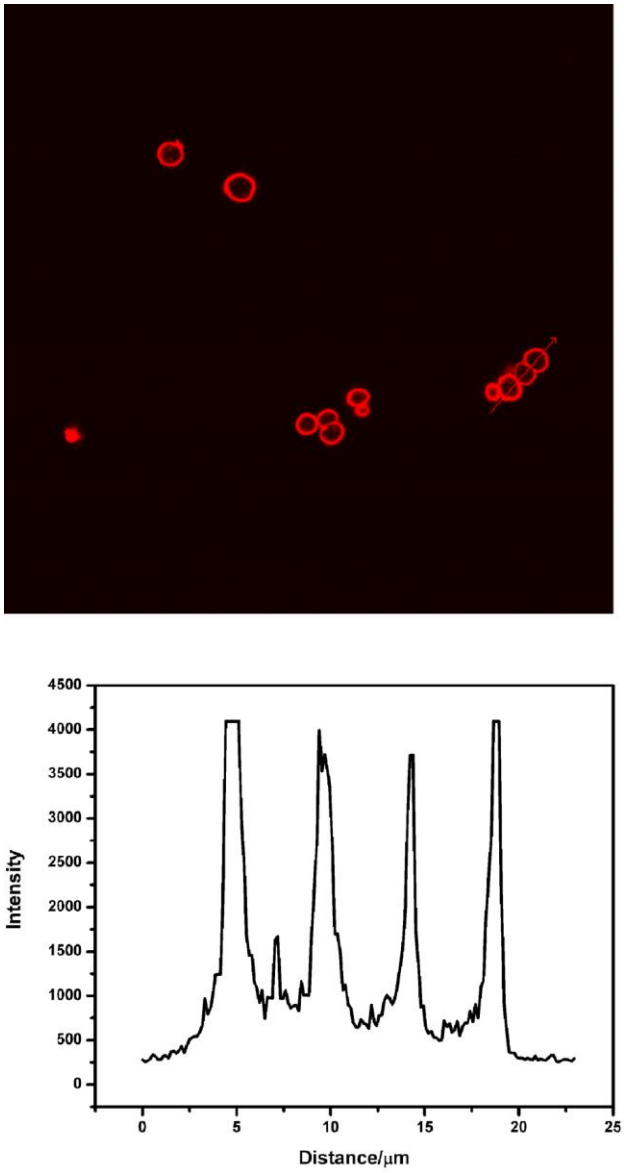

Figure 6.16 CLSM images and the intensity profile of cy3-IgG loaded microcapsules along the line after thoroughly washing with PBS.

6.6 Conclusions

In summary, a nanoparticle-participated three-component LbL assembly using weak polyelectrolyte-nanoparticle blend and another weak polyelectrolyte was used to fabricate polyelectrolyte/nanoparticle hollow composite capsules. The

assembly pH of weak polyelectrolyte and blend ratio of weak polyelectrolyte to nanoparticles were investigated to successfully assemble blend multilayers on colloidal template without aggregation. The microcapsules obtained from removing the cores are well-dispersed, with controllable assembly of nanoparticles including their concentration, size and interparticle spacing. The as-prepared weak polyelectrolyte/nanoparticle nanocomposite capsules demonstrate synergistic superior tunable LSPR and permeability, which are not able to be achieved by traditional pure weak polyelectrolyte capsules, 2-component weak polyelectrolyte/nanoparticle nanocomposite capsules, or even other reported capsules. Importantly, these properties can be simply controlled by the blend ratio of nanoparticle to polyelectrolyte in the blend solution. This work provides not only a novel and universal approach to fabricate well-dispersed microcapsules with controllable incorporation of nanoparticles for various applications, but also scientific insight into the nanoparticle-participated blend LbL assembly process. The weak polyelectrolyte/nanoparticle capsules could have great applications in broad areas, especially in intelligent drug delivery, biosensing, and bioimaging.

Chapter 7 Exponentially growing layer-by-layer assembly to fabricate pH-responsive hierarchical nanoporous polymeric film and its superior controlled release performance

7.1 Introduction

Polymeric nanoporous materials have attracted great interest in recent years due to their great potentials in broad important applications such as catalysis, separation, sensing and controlled drug release.[297-302] A hierarchical nanoporous structure (multi-scale pore sizes with at least one between 1 nm and 100 nm) is particularly desirable for applications such as catalysis and controlled release since the larger pores can enhance target molecule diffusion, while the smaller pores are able to improve loading capacity and molecule-release control.[138, 303-305] Although methods such as template synthesis[299, 303, 306] and lithography[307] have been developed to construct micro- or nano-pores, they are somewhat tedious, costly, and time-consuming, and difficult to fabricate a hierarchical nanoporous structure.

Layer-by-layer (LbL) assembly is a simple and efficient technology to fabricate nanostructured ultrathin films.[179, 308-309] Recently, the exponentially growing LbL (e-LbL) assembly has been fueled up in researches by its great advantages over the linearly growing LbL (l-LbL) one.[310-312] Unlike the l-LbL assembly, by which the assembled chemical species only interact with the outermost layers to form a nanoscale feature, a diffusion in-and-out mechanism of e-LbL assembly enables assembly of much more molecules at each deposition step by interaction with both the outermost layer and the inside multilayer by interdiffusing free molecules, thus

possibly introducing an additional higher-scale structure.[76, 312-313] For the first time, a hierarchical nanoporous multilayer film is directly constructed by the e-LbL assembly approach without any posttreatment and template. Since various weak polyelectrolytes are often used as building blocks in LbL assembly to introduce a pH-controllable and pH-responsive multilayer film,[57, 86, 128] they are selected for the exponentially growing LbL assembly. Particularly, branched high-molecular-weight PEI (BPEI, M_w~750 K) and PAA (M_w~100 K) were used in this work. With a widely pH-tunable charge density of PEI and PAA, the exponentially grown $(PEI/PAA)_n$ multilayers could have pH-dependent charge density and interaction with charged drugs. The drugs are loaded by controlling the pH to enhance the interaction between multilayers and charged drugs, and released when the multilayers are immersed in an environment with a different pH value at which the interaction is weaker. Both the loading and release could be controlled by the solution pH, which forms the basis of pH-controlled drug delivery whether for in vitro or in vivo applications. It needs to be noted that the pH varied greatly from tissue to tissue in human body.[314-315]

7.2 Fabrication of the exponentially grown multilayers

The glass slides or silicon wafer were first immersed into PEI solution with pH at 9.50 for 15 min, rinsed with DI water for 5 times and blown dry with N_2. Subsequently, the substrates were immersed in PAA solutions with pH at 3.20 for 15 min, followed by rinsing with DI water for 5 times and blowing dry with N_2. This cycle was repeated for several times to obtain multilayers with certain bilayer

number. For the thermal cross-linking, the multilayers were incubated for 1 h in a vacuum oven at the temperature of 120˚C.

7.3 Characterization of the exponentially grown multilayers

A very fast exponentially grown multilayer film with highly nanoporous structure was obtained (Figure 7.1). Particularly, a uniform and large-area hierarchical nanoporous structure with well-defined double-scaled pore size (macropores ~200 nm and mesopores ~30 nm) is observed (Figure 7.2). The smaller pores are located in the larger pores, which is one of the most promising hierarchical structures.[303] The experimental results also show that the morphology is highly dependent on the assembly pH. The hierarchical nanoporous structure can be tailored by simply changing the assembly pH (Figure 7.3). Even the micropores can be diminished to form a non-hierarchical uniform nanopore structure through decreasing PEI assembly pH and increasing PAA assembly pH (i. e. increasing the polyelectrolyte charge density) (Figure 7.4). It is noted that the exponential growth is also reduced with increase of the polyelectrolyte charge density (data not shown), suggesting that the formation of the microscale structure is related to the exponential growth. Very high pH of PEI or very low pH of PAA can only assemble a non-homogeneous irregular structure rather than the hierarchical nanoporous film. The as-prepared multilayer film is stable in a solution over a broad pH range from 4.5 to 9.6 without cross-linking, possibly due to the alternate high and low assembly pH conditions.

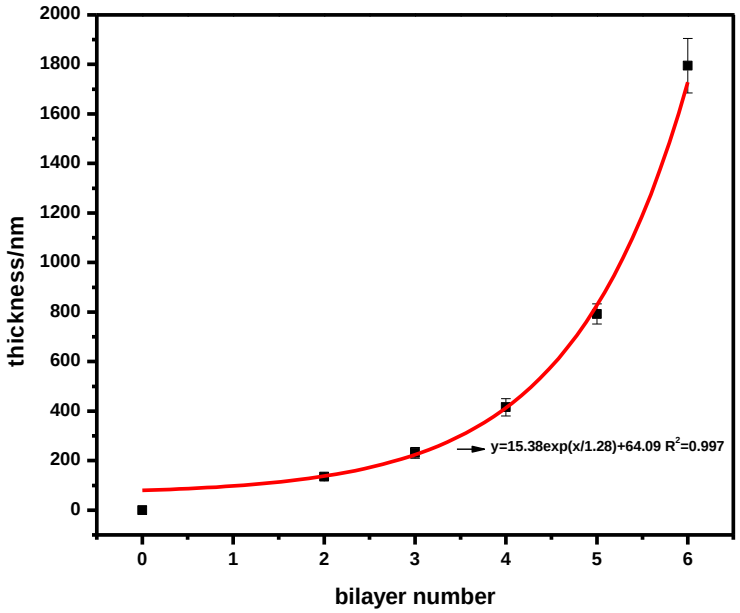

Figure 7.1 Thickness evolution of the multilayers with the bilayer number.

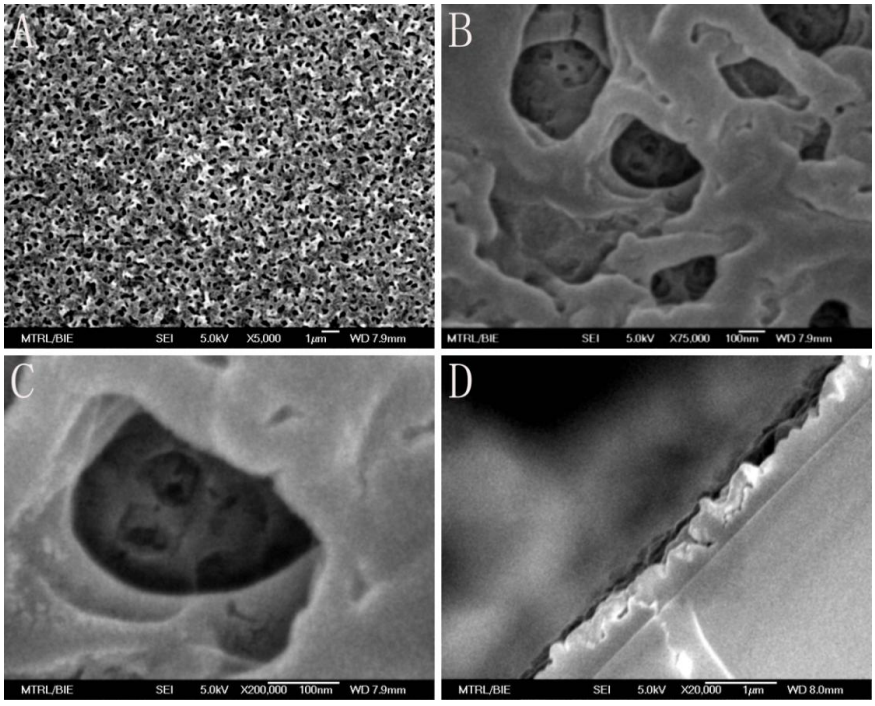

Figure 7.2 FE-SEM top-down images with different magnifications (A-C) and cross-section image (D) of self-assembled hierarchical nanoporous polyelectrolyte multilayers.

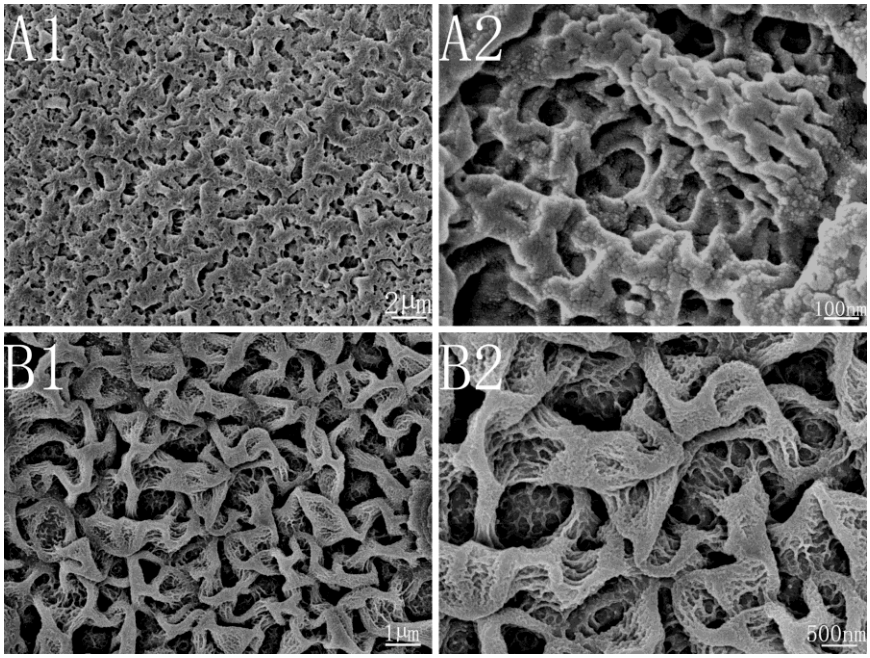

Figure 7.3 Hierarchical nanoporous structure obtained by slight adjustment of assembly pH at low and high magnification: (A1, A2) PEI pH 9.37/PAA pH 3.20, (B1, B2) PEI pH 9.63/PAA pH 3.20.

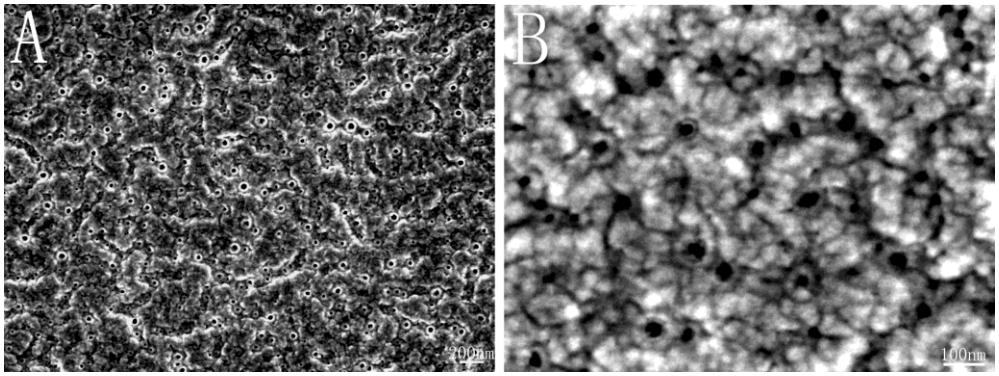

Figure 7.4 Nanoporous structure obtained by changing the assembly pH (PEI pH 8.0 and PAA pH 4.0) at low (A) and high magnification (B).

It has been reported[60, 138, 316] that a weak polyelectrolyte multilayer film could have structure transformation to form nanopores by acid treatment (pH range ~1.75 to ~2.30) possibly contributed from specific molecular reorganization at low pHs. Since the assembly pH can significantly affect the pore structure of the

exponentially grown LbL assembled film, it is also possible that the low assembly pH (PAA, ~ pH 3) could cause the structure change to form hierarchical pores during the self-assembly process. However, the detailed mechanism for formation of the hierarchical pores is still not clear, and needs further investigation.

7.4 MB loading into the hierarchical nanoporous multilayers

The five-bilayer polyelectrolyte film was used to study the loading and release of charged small molecules. Positively charged methylene blue (MB) is used as a model guest molecule, which has been often used as a model drug.[57, 317-319] The fabricated multilayer film demonstrates an important pH-responsive loading capacity (Figure 7.5). With increase of the loading pH, the loading capacity increases tremendously. This is understandable since the increased environmental pH could enhance deprotonization of PEI and ionization of PAA to result in an increased negative charge density, thus increasing the loading capacity of MB. At a high environmental pH such as 9.6, the loading capacity can achieve ~147.2 $\mu g/cm^2$, which is much higher than the linearly grown multilayer films even with a larger bilayer number (~8.25 $\mu g/cm^2$ for a 10.5 bilayer film).[57] To eliminate the effect of film thickness (the exponential growth could increase the thickness to increase the loading) for investigating the role of hierarchical pores in the loading enhancement, the loading capacity is normalized by the film thickness, and ~0.968 g/cm^3 and ~0.208 g/cm^3 for the exponentially grown hierarchical and the linearly grown nonporous films are obtained respectively.[57] It is indeed the best accomplished loading capacity up to date. The remarkably high loading capacity of

the exponentially grown film is very likely to be ascribed to its much optimized hierarchical pore structure, which can eliminate or reduce the dead end nanopores to significantly increase the pore utilization for high loading.

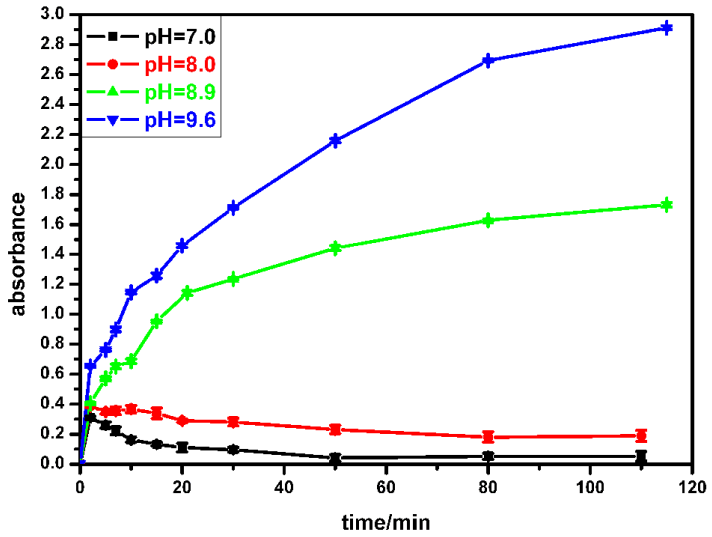

Figure 7.5 MB loading into the nanoporous multilayers at different environmental pH.

7.5 MB release from the hierarchical nanoporous multilayers

The multilayer film was loaded with MB at pH 9.6 for release experiments, demonstrating a pH-responsive release behavior (Figure 7.6). With decrease of the environmental pH, the release rate increases sharply. This can be explained by the same reason as that for the pH-dependent loading capacity, i.e. a decreased environmental pH can enhance both ionization of the PEI and protonization of PAA to decrease the negative charge density. More importantly, the film demonstrates a long release time and also a large linear release range over a broad pH region. For example, the release at pH 9.6 lasts 16 days at least and is linear over 193 hours with R of 0.964 for the linear fitting. The total release time, the linear release time,

and the R value is listed in Table 7.1, showing that the total release time, particularly the linear release time of the film fabricated in this work is much longer than the reported weak polyelectrolyte films, which can only achieve 400 min for the linear release time at the most and in some cases could not release due to trapping in the films.[57, 89] The superior release performance of the film fabricated in this work could be also contributed by its hierarchical nanopore structure, of which the larger pores allows the release mass transport while the smaller pores lower the release rate for a longer linear release time. It has been reported that a nanopore structure can slow the release rate with better linear release property, while exhibiting faster release in a microscale pore structure due to the Fickian diffusion mechanism.[138, 320-321]

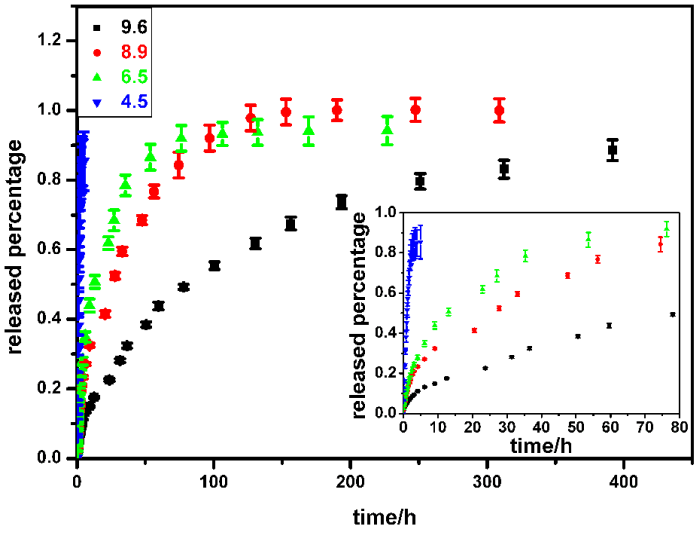

Figure 7.6 MB release from the nanoporous multilayers at different environmental pH. The inset shows release profile at initial stage.

Table 7.1 Total and linear release time at different release pH

Release pH	Total release time	Linear release time	R
pH=9.6	391 h	193 h	0.964
pH=8.9	152 h	74 h	0.962
pH=6.5	76 h	35 h	0.954
pH=4.5	175 min	175 min	0.966

The release from the hierarchical porous film was also performed in a phosphate buffered saline (PBS) solution (pH=7.4 and 10 mM). One of the biggest obstacles experienced in the polyelectrolyte film-based controlled drug release is the short release time in a physiological buffered solution, since the high ionic strength can swell the polyelectrolyte film and shield the electrostatic force between drugs and multilayers to greatly accelerate the drug diffusion out from the film.[57, 317-318] Indeed, the reported weak polyelectrolyte films have burst releases with maximum 10 min-release only in PBS,[57, 317] Figure 7.7 shows that the multilayer film fabricated in this work has a pseudo-linear release profile with a significantly increased release time (~40 min), further demonstrating its superior release property. To enforce the fabricated nanopore structure for further improving its release property in PBS, thermal cross-linking was carried out with the fabricated film and exceptional performance was demonstrated with significant increased release time of ~120 min (Figure 7.7).

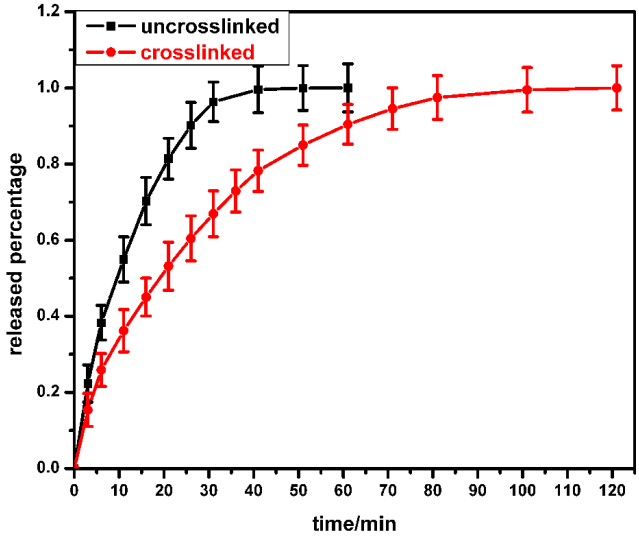

Figure 7.7 MB Release from uncross-linked and cross-linked hierarchical nanoporous multilayers in PBS.

7.6 Conclusions

In conclusion, a hierarchical nanoporous polyelectrolyte multilayer film is fabricated by a pH-controlled LbL assembly of weak polyelectrolyte for the first time. In comparison to the reported weak polyelectrolyte multilayers, the film demonstrates a much higher loading capacity and significantly increased release time and linear range in a broad pH range, while retaining the pH-dependent loading and release behavior. Particularly, in physiological buffered solution the film can also lower the release rate and increase the release time of charged small molecules, and thermal cross-linking of the multilayer film even further significantly increases the release time and improves the release profile in PBS, thus providing a great potential in pH-controlled drug release applications.

Chapter 8 General conclusion and outlook

8.1 General conclusion

This dissertation has systematically reviewed the current status and development of weak polyelectrolyte-based LbL-assembled multilayers. The pH-controllable properties, pH-responsiveness to the environment, and other influential factors for weak polyelectrolyte multilayers have been thoroughly summarized. The pH-dependent properties and synergistic functions obtained from weak polyelectrolyte/other component multilayers have been discussed. As a fast-developing area, weak polyelectrolyte-based exponentially grown multilayers have been reviewed in detail. Additionally, the applications of weak polyelectrolyte-based multilayers have been summarized.

In one of my accomplishments, two natural weak polyelectrolytes, chitosan and alginate, were assembled at different pH levels to form multilayers. It has been found that the surface composition of the films can be controlled by the assembly pH. With a decrease of the assembly pH of alginate, less chitosan could penetrate to the outermost alginate layer to increase the negative charge density from alginate for more antibody immobilization. Moreover, it has been found that the antigen binding activity on the antibody immobilized multilayer film can also be tuned by the assembly pH. With the increase of the assembly pH of alginate, the antigen binding activity decreases. This work can provide more scientific insight into the interaction between protein and polymer matrix and render a simple, novel

approach to building a high-performance biointerface through pH control for potential applications of highly sensitive immunosensors.

For the first time, pH-controllable weak polyelectrolyte/Au nanoparticle nanocomposite films were successfully constructed through LbL assembly to investigate LSPC. The degree of LSPC can be extensively modulated by adjusting the weak polyelectrolyte assembly pH to achieve the largest tuning range of the longitudinal band peak (625 nm to 741.5 nm) to date, thus offering great potential for various applications. The great LSPC modulation in the LbL nanocomposite film can be ascribed to the assembled weak polyelectrolyte, of which the pH-dependent charge density and conformation can easily tailor the interparticle spacing in the nanoparticle clusters. This work provides insights into the effect of morphology on the optical properties of a self-assembled film and opens a simple and economical path to realize the modulation of the optical property directly on substrates. This method can be extended to other weak polyelectrolyte and nanoparticle systems for different devices.

A nanoparticle-participated three-component LbL assembly using a weak polyelectrolyte-nanoparticle blend and another weak polyelectrolyte was employed to fabricate polyelectrolyte/nanoparticle hollow composite capsules. The assembly pH of weak polyelectrolyte and the blend ratio of weak polyelectrolyte to nanoparticles were investigated to successfully assemble blend multilayers on a colloidal template without aggregation. The microcapsules obtained from removing the cores were well-dispersed, with controllable assembly of nanoparticles including their concentration, size, and interparticle spacing. The as-prepared weak

polyelectrolyte/nanoparticle nanocomposite capsules demonstrate synergistic superior tunable LSPR and permeability, which are not achievable by traditional pure weak polyelectrolyte capsules, 2-component weak polyelectrolyte/nanoparticle nanocomposite capsules, or even other reported capsules. These properties can be simply controlled by the blend ratio of nanoparticle to polyelectrolyte in the blend solution. This work provides not only a novel and universal approach to the fabrication of well-dispersed microcapsules with controllable incorporation of nanoparticles for various applications, but also scientific insight into the nanoparticle-participated blend LbL assembly process. The weak polyelectrolyte/nanoparticle capsules could have great applications in broad areas, especially intelligent drug delivery, biosensing, and bioimaging.

A hierarchical nanoporous polyelectrolyte multilayer film has been fabricated by a pH-controlled LbL assembly of weak polyelectrolyte for the first time. In comparison to the reported weak polyelectrolyte multilayers, the film demonstrates a much higher loading capacity and significantly increased release time and linear range in a broad pH range while retaining pH-dependent loading and release behavior. Particularly, in a physiological buffered solution, the film can also lower the release rate and increase the release time of charged small molecules. Thermal cross-linking of the multilayer film further increases the release time and improves the release profile in PBS, thus providing great potential for pH-controlled drug release applications.

In summary, this work has involved the systematic study of several particularly designed weak polyelectrolyte-based multilayers. In so doing, this work has

enriched the scientific knowledge of weak polyelectrolyte multilayer-based assemblies and properties and developed various strategies for the use of LbL assembly in various applications.

8. 2 Outlook

Weak polyelectrolyte-based multilayers have demonstrated their great potential in a variety of advanced applications due to their highly tunable structure at a molecular level, unique properties, and convenience of incorporating functional building blocks. Nevertheless, this research area is still in its infancy with remarkable opportunities ahead.

My PhD work is able to realize the pH-controlled assembly of gold nanoparticles into nanocomposite films. Multi-responsive properties synergistically from the pH-responsive weak polyelectrolyte and optically responsive gold nanoparticles should be investigated for broad applications. In addition, other multi-responsive materials could be designed and fabricated via LbL assembly. Weak polyelectrolytes can provide us the ability to sense the environment via pH response, while the LbL technique can provide a route to incorporate various environmentally responsive building blocks such as temperature-responsive materials, optically active materials, electro-active materials, and magnetically responsive materials. It is possible to have a synergistic functional assembly that is responsive to the environment in dual or multiple ways.

Colloidal sphere has been successfully used as a template for fabricating the weak polyelectrolyte/nanoparticle hollow sphere. The uses of alternative

nanostructured removable materials as templates to generate various weak polyelectrolyte or weak polyelectrolyte/nanoparticle composite nanostructures hold significant promise. Both the multilayer structure and its shape could be controlled with this method. Novel properties such as permeability, fast response to the environment, and large surface area could provide significant possibilities for both fundamental studies and applications.

Much attention has been paid to exponentially grown multilayers, most of which include weak polyelectrolytes. However, the detailed structures such as internal molecular-level structures and formation mechanisms of these multilayers are still not very clear. It is difficult to predict which condition will enhance or reduce exponential growth. The effect of molecular structure and assembly condition on exponential growth in terms of growth rate or multilayer structure is also not understood well. Further study of these topics could result in the evolution and maturation of the method and provide fundamental insights into this unique method of self-assembly for novel applications.

The applications of weak polyelectrolyte-based multilayers need to be extensively explored. The biomedical applications are undoubtedly very promising. The antibody or enzyme immobilized multilayers, for instance, could provide an efficient biointerface for biosensing applications. The weak polyelectrolyte/metal nanoparticle composite film could be used for biosensing or bioimaging. The weak polyelectrolyte/nanoparticle composite capsules are potentially useful for smart, targeted drug delivery. The weak polyelectrolyte multilayers with loose structure (such as exponentially grown multilayers and porous multilayers) could serve as a

potential matrix for pH-controlled drug (such as small-molecule anticancer drugs, therapeutic proteins/peptides and DNA/RNA) delivery. Since various substrates could be used for LbL assembly, different biomedical devices modified with multilayer films could be implanted into tissues of varied pH values,[314-315] which could serve as a stimulus for release of drugs. In the future, the biological test (in vitro/in vivo) will be performed to achieve the real application of these systems for drug delivery. Furthermore, the great tunability of multilayer structures provides a strategy to study the relationship between nanoscale structures and macroscopic biological events. One more important type of application is the development of sustainable energy systems such as solar energy and fuel cells. The LbL assembly is highly compatible with the device applications due to its strong ability to control the nanoscale structure on nearly any substrate. The weak polyelectrolyte-based LbL assembly can be a superior platform to be used to design highly tunable nanoscale blended hybrid for polymer bulk heterojunction solar cell, organic-inorganic hybrid solar cell, or optically active layer for solar cell. It also provides the possibility to improve both ionic conductivity and the performance of electrocatalysts and thus may have great potential as a solid state electrolyte or electrode material for fuel cell applications.

Abbreviations

LbL: Layer-by-Layer
LSPC: localized surface plasmon coupling
LSPR: localized surface plasmon resonance
PAH: poly(allylamine)
PAA: poly(acrylic acid)
PEI: poly(ethyleneimine)
PMAA: poly(methacrylic acid)
PLL: poly(L-lysine)
HA: hyaluronic acid
MB: methylene blue
CG: crocein orange G
PAZO: azobenzene-containing polyelectrolyte
PEO: poly(ethylene oxide)
MEEP: poly[bis(methoxyethoxyethoxy) phosphazene]
CLSM: confocal laser scanning microscopy
PVAm: polyvinylamine
PAArVBA: poly(acrylic acid-ran-vinylbenzyl acrylate)
PSS: poly(styrenesulfonic acid)
PGA: poly(glutamic acid)
PLA: poly(L-aspartic acid)
PVPON: poly(vinylpyrrolidone)
PVCL: poly(N-vinylcaprolactam)
PVME: poly(vinyl methyl ether)
SPR: surface plasmon resonance
ATR: attenuated total reflectance
PDDA: poly(diallyldimethylammonium) chloride
PXV: poly(hexyl viologen)
PAMAM: polyamidoamine
CHI: chitosan
SWNT: single-walled carbon nanotube
MTM: sodium montmorillonite clay nanosheet
Poly(AAc-co-NIPAAm): poly(acrylic acid-co-N-isopropylacrylamide)
polyVAm: poly(vinylamine hydrochloride)
MO: methyl orange
AR: allura red
PAAm: polyacrylamide
SAM: self-assembled monolayer
PAMPS: poly(2-acrylamido-2-methyl-1-propanesulfonic acid)
PEM: polyelectrolyte multilayers
BSA: bovine serum albumin
H-PURET: poly[2-(3-thienyl) ethanol butoxy carbonyl-methyl urethane]
MV^{2+}: methyl viologen
ERα: estrogen receptor α
TGF-β: transforming growth factor β
FE-SEM: field emission scanning electron microscopy
EDX: energy dispersive X-ray analysis
UV-vis: UV-visible spectroscopy
TEM: transmission electron microscopy
QCM: quarz crystal microbalance
AFM: atomic force microscopy
PBS: phosphate buffered saline

References

1. Leclere, P.; Surin, M.; Viville, P.; Lazzaroni, R.; Kilbinger, A. F. M.; Henze, O.; Feast, W. J.; Cavallini, M.; Biscarini, F.; Schenning, A. P. H. J.; Meijer, E. W. About Oligothiophene Self-Assembly: From Aggregation in Solution to Solid-State Nanostructures. *Chem. Mater.* 2004, *16*, 4452-4466.
2. Zhang, E.-Y.; Wang, C.-R. Fullerene self-assembly and supramolecular nanostructures. *Curr. Opin. Colloid Interface Sci.* 2009, *14*, 148-156.
3. Kühnle, A. Self-assembly of organic molecules at metal surfaces. *Curr. Opin. Colloid Interface Sci.* 2009, *14*, 157-168.
4. Leclère, P.; Surin, M.; Brocorens, P.; Cavallini, M.; Biscarini, F.; Lazzaroni, R. Supramolecular assembly of conjugated polymers: From molecular engineering to solid-state properties. *Mater. Sci. Eng., R* 2006, *55*, 1-56.
5. Hammond, P. T. Form and function in multilayer assembly: New applications at the nanoscale. *Adv. Mater.* 2004, *16*, 1271-1293.
6. Tang, Z.; Wang, Y.; Podsiadlo, P.; Kotov, N. A. Biomedical Applications of Layer-by-Layer Assembly: From Biomimetics to Tissue Engineering. *Adv. Mater.* 2006, *18*, 3203-3224.
7. Ariga, K.; Hill, J. P.; Ji, Q. Layer-by-layer assembly as a versatile bottom-up nanofabrication technique for exploratory research and realistic application. *Phys. Chem. Chem. Phys.* 2007, *9*, 2319-2340.
8. Kharlampieva, E.; Kozlovskaya, V.; Sukhishvili, S. A. Layer-by-Layer Hydrogen-Bonded Polymer Films: From Fundamentals to Applications. *Adv. Mater.* 2009, *21*, 3053-3065.
9. Boudou, T.; Crouzier, T.; Ren, K.; Blin, G.; Picart, C. Multiple Functionalities of Polyelectrolyte Multilayer Films: New Biomedical Applications. *Adv. Mater.* 2010, *22*, 441-467.
10. Srivastava, S.; Kotov, N. A. Composite Layer-by-Layer (LBL) Assembly with Inorganic Nanoparticles and Nanowires. *Acc. Chem. Res.* 2008, *41*, 1831-1841.
11. Iler, R. K. Multilayers of colloidal particles. *J. Colloid Interface Sci.* 1966, *21*, 569-594.
12. Decher, G.; Hong, J. D. Buildup of Ultrathin Multilayer Films by a Self-Assembly Process. 1. Consecutive Adsorption of Anionic and Cationic Bipolar Amphiphiles on Charged Surfaces *Makromolekulare Chemie-Macromolecular Symposia* 1991, *46*, 321-327.
13. Decher, G.; Hong, J. D. Buildup of Ultrathin Multilayer Films by a Self-Assembly Process. 2. Consecutive Adsorption of Anionic and Cationic Bipolar Amphiphiles and Polyelectrolytes on Charged Surfaces *Ber. Bunsen-Ges. Phys. Chem. Chem. Phys.* 1991, *95*, 1430-1434.
14. Decher, G.; Hong, J. D.; Schmitt, J. Buildup of ultrathin multilayer films by a self-assembly process: III. Consecutively alternating adsorption of anionic and cationic polyelectrolytes on charged surfaces. *Thin Solid Films* 1992, *210-211*, 831-835.
15. Decher, G. Fuzzy Nanoassemblies: Toward Layered Polymeric Multicomposites. *Science* 1997, *277*, 1232-1237.
16. Wang, Y.; Angelatos, A. S.; Caruso, F. Template Synthesis of Nanostructured Materials via Layer-by-Layer Assembly. *Chem. Mat.* 2007, *20*, 848-858.
17. Amigoni, S.; Taffin de Givenchy, E.; Dufay, M.; Guittard, F. d. r. Covalent Layer-by-Layer Assembled Superhydrophobic Organic−Inorganic Hybrid Films. *Langmuir* 2009, *25*, 11073-11077.
18. Zhang, F.; Srinivasan, M. P. Multilayered Gold-Nanoparticle/Polyimide Composite Thin Film through Layer-by-Layer Assembly. *Langmuir* 2007, *23*, 10102-10108.
19. Cui, X.; Pei, R.; Wang, Z.; Yang, F.; Ma, Y.; Dong, S.; Yang, X. Layer-by-layer assembly of multilayer films composed of avidin and biotin-labeled antibody for immunosensing. *Biosens. Bioelectron.* 2003, *18*, 59-67.
20. Shim, B. S.; Podsiadlo, P.; Lilly, D. G.; Agarwal, A.; Lee, J.; Tang, Z.; Ho, S.; Ingle, P.; Paterson, D.; Lu, W.; Kotov, N. A. Nanostructured Thin Films Made by Dewetting Method of Layer-By-Layer Assembly. *Nano Lett.* 2007, *7*, 3266-3273.
21. Podsiadlo, P.; Michel, M.; Critchley, K.; Srivastava, S.; Qin, M.; Lee, Jung W.; Verploegen, E.; Hart, A. J.; Qi, Y.; Kotov, Nicholas A. Diffusional Self-Organization in Exponential Layer-By-Layer Films with Micro- and Nanoscale Periodicity13. *Angew. Chem. Int. Ed.* 2009, *48*, 7073-7077.
22. Nolte, A. J.; Rubner, M. F.; Cohen, R. E. Creating Effective Refractive Index Gradients within Polyelectrolyte Multilayer Films: Molecularly Assembled Rugate Filters. *Langmuir* 2004, *20*,

3304-3310.
23. Yoo, D.; Shiratori, S. S.; Rubner, M. F. Controlling bilayer composition and surface wettability of sequentially adsorbed multilayers of weak polyelectrolytes. *Macromolecules* 1998, *31*, 4309-4318.
24. Nolte, A. J.; Cohen, R. E.; Rubner, M. F. A Two-Plate Buckling Technique for Thin Film Modulus Measurements: Applications to Polyelectrolyte Multilayers. *Macromolecules* 2006, *39*, 4841-4847.
25. Miller, M. D.; Bruening, M. L. Controlling the Nanofiltration Properties of Multilayer Polyelectrolyte Membranes through Variation of Film Composition. *Langmuir* 2004, *20*, 11545-11551.
26. Hiller, J. A.; Mendelsohn, J. D.; Rubner, M. F. Reversibly erasable nanoporous anti-reflection coatings from polyelectrolyte multilayers. *Nat. Mater.* 2002, *1*, 59-63.
27. Durstock, M. F.; Rubner, M. F. Dielectric Properties of Polyelectrolyte Multilayers. *Langmuir* 2001, *17*, 7865-7872.
28. Cui, T.; Lvov, Y. In *Nano self-assembly for MEMS and microelectronics applications*, Masayoshi, E.; Zhaoying, Z., Eds. SPIE: 2006; p 603202.
29. Kang, H.; Evmenenko, G.; Dutta, P.; Clays, K.; Song, K.; Marks, T. J. X-shaped electro-optic chromophore with remarkably blue-shifted optical absorption. synthesis, characterization, linear/nonlinear optical properties, self-assembly, and thin film microstructural characteristics. *J. Am. Chem. Soc.* 2006, *128*, 6194-6205.
30. Benten, H.; Ogawa, M.; Ohkita, H.; Ito, S. Design of Multilayered Nanostructures and Donor-Acceptor Interfaces in Solution-Processed Thin-Film Organic Solar Cells. *Adv. Funct. Mater.* 2008, *18*, 1563-1572.
31. Lutkenhaus, J. L.; Hammond, P. T. Electrochemically enabled polyelectrolyte multilayer devices: from fuel cells to sensors. *Soft Matter* 2007, *3*, 804-816.
32. Lichter, J. A.; Thompson, M. T.; Delgadillo, M.; Nishikawa, T.; Rubner, M. F.; Van Vliet, K. J. Substrata Mechanical Stiffness Can Regulate Adhesion of Viable Bacteria. *Biomacromolecules* 2008, *9*, 1571-1578.
33. Shiratori, S. S.; Rubner, M. F. pH-dependent thickness behavior of sequentially adsorbed layers of weak polyelectrolytes. *Macromolecules* 2000, *33*, 4213-4219.
34. Mendelsohn, J. D.; Barrett, C. J.; Chan, V. V.; Pal, A. J.; Mayes, A. M.; Rubner, M. F. Fabrication of microporous thin films from polyelectrolyte multilayers. *Langmuir* 2000, *16*, 5017-5023.
35. Burke, S. E.; Barrett, C. J. pH-Responsive Properties of Multilayered Poly(l-lysine)/Hyaluronic Acid Surfaces. *Biomacromolecules* 2003, *4*, 1773-1783.
36. Mendelsohn, J. D.; Yang, S. Y.; Hiller, J. A.; Hochbaum, A. I.; Rubner, M. F. Rational Design of Cytophilic and Cytophobic Polyelectrolyte Multilayer Thin Films. *Biomacromolecules* 2002, *4*, 96-106.
37. Hiller, J. A.; Rubner, M. F. Reversible Molecular Memory and pH-Switchable Swelling Transitions in Polyelectrolyte Multilayers. *Macromolecules* 2003, *36*, 4078-4083.
38. Yang, S. Y.; Mendelsohn, J. D.; Rubner, M. F. New Class of Ultrathin, Highly Cell-Adhesion-Resistant Polyelectrolyte Multilayers with Micropatterning Capabilities. *Biomacromolecules* 2003, *4*, 987-994.
39. Decher, G.; Hong, J. D. Buildup of Ultrathin Multilayer Films by a Self-Assembly Process. 1. Consecutive Adsorption of Anionic and Cationic Bipolar Amphiphiles on Charged Surfaces. *Makromolekulare Chemie-Macromolecular Symposia* 1991, *46*, 321-327.
40. Ariga, K.; Hill, J. P.; Ji, Q. M. Layer-by-layer assembly as a versatile bottom-up nanofabrication technique for exploratory research and realistic application. *Phys. Chem. Chem. Phys.* 2007, *9*, 2319-2340.
41. Jaber, J. A.; Schlenoff, J. B. Recent developments in the properties and applications of polyelectrolyte multilayers. *Curr. Opin. Colloid Interface Sci.* 2006, *11*, 324-329.
42. Balasubramanian, S.; Wang, X. G.; Wang, H. C.; Yang, K.; Kumar, J.; Tripathy, S. K.; Li, L. Azochromophore-functionalized polyelectrolytes. 2. Acentric self-assembly through a layer-by-layer deposition process. *Chem. Mat.* 1998, *10*, 1554-1560.
43. Liu, Y. J.; Wang, Y. X.; Lu, H. X.; Claus, R. O. Electrostatic self-assembly of highly-uniform micrometer-thick fullerene films. *J. Phys. Chem. B* 1999, *103*, 2035-2036.

44. Shchukin, D. G.; Patel, A. A.; Sukhorukov, G. B.; Lvov, Y. M. Nanoassembly of biodegradable microcapsules for DNA encasing. *J. Am. Chem. Soc.* 2004, *126*, 3374-3375.
45. Shchukin, D. G.; Shutava, T.; Shchukina, E.; Sukhorukov, G. B.; Lvov, Y. M. Modified polyelectrolyte microcapsules as smart defense systems. *Chem. Mat.* 2004, *16*, 3446-3451.
46. Crespilho, F. N.; Zucolotto, V.; Siqueira, J. R.; Constantino, C. J. L.; Nart, F. C.; Oliveira, O. N. Immobilization of humic acid in nanostructured layer-by-layer films for sensing applications. *Environ. Sci. Technol.* 2005, *39*, 5385-5389.
47. Wang, S.; Granick, S.; Zhao, J. Charge on a weak polyelectrolyte. *J. Chem. Phys.* 2008, *129*, 241102.
48. Dobrynin, A. V.; Rubinstein, M. Theory of polyelectrolytes in solutions and at surfaces. *Prog. Polym. Sci.* 2005, *30*, 1049-1118.
49. Wang, Z.; Feng, Z.; Gao, C. Stepwise Assembly of the Same Polyelectrolytes Using Host−Guest Interaction To Obtain Microcapsules with Multiresponsive Properties. *Chem. Mater.* 2008, *20*, 4194-4199.
50. Park, M.-K.; Deng, S.; Advincula, R. C. pH-Sensitive Bipolar Ion-Permselective Ultrathin Films. *J. Am. Chem. Soc.* 2004, *126*, 13723-13731.
51. Wosnick, J. H.; Liao, J. H.; Swager, T. M. Layer-by-Layer Poly(phenylene ethynylene) Films on Silica Microspheres for Enhanced Sensory Amplification. *Macromolecules* 2005, *38*, 9287-9290.
52. Sun, B.; Jewell, C. M.; Fredin, N. J.; Lynn, D. M. Assembly of Multilayered Films Using Well-Defined, End-Labeled Poly(acrylic acid): Influence of Molecular Weight on Exponential Growth in a Synthetic Weak Polyelectrolyte System. *Langmuir* 2007, *23*, 8452-8459.
53. Chollakup, R.; Smitthipong, W.; Eisenbach, C. D.; Tirrell, M. Phase Behavior and Coacervation of Aqueous Poly(acrylic acid)−Poly(allylamine) Solutions. *Macromolecules* 2010, *43*, 2518-2528.
54. Sadeghpour, A.; Vaccaro, A.; Rentsch, S.; Borkovec, M. Influence of alkali metal counterions on the charging behavior of poly(acrylic acid). *Polymer* 2009, *50*, 3950-3954.
55. Dong, R.; Lindau, M.; Ober, C. K. Dissociation Behavior of Weak Polyelectrolyte Brushes on a Planar Surface. *Langmuir* 2009, *25*, 4774-4779.
56. Su, Y.; Sun, M.; Wang, L.; Jiang, Z. Ion-Pair Formation and Ion-Specific Flux of a Weak Polyelectrolyte Membrane. *J. Phys. Chem. B* 2009, *113*, 9454-9460.
57. Chung, A. J.; Rubner, M. F. Methods of Loading and Releasing Low Molecular Weight Cationic Molecules in Weak Polyelectrolyte Multilayer Films. *Langmuir* 2002, *18*, 1176-1183.
58. Zhai, L.; Nolte, A. J.; Cohen, R. E.; Rubner, M. F. pH-Gated Porosity Transitions of Polyelectrolyte Multilayers in Confined Geometries and Their Application as Tunable Bragg Reflectors. *Macromolecules* 2004, *37*, 6113-6123.
59. Burke, S. E.; Barrett, C. J. Controlling the physicochemical properties of weak polyelectrolyte multilayer films through acid/base equilibria. *Pure Appl. Chem.* 2004, *76*, 1387-1398.
60. Lutkenhaus, J. L.; McEnnis, K.; Hammond, P. T. Nano- and Microporous Layer-by-Layer Assemblies Containing Linear Poly(ethylenimine) and Poly(acrylic acid). *Macromolecules* 2008, *41*, 6047-6054.
61. Chia, K.-K.; Rubner, M. F.; Cohen, R. E. pH-Responsive Reversibly Swellable Nanotube Arrays†. *Langmuir* 2009, *25*, 14044-14052.
62. Fery, A.; Schöler, B.; Cassagneau, T.; Caruso, F. Nanoporous Thin Films Formed by Salt-Induced Structural Changes in Multilayers of Poly(acrylic acid) and Poly(allylamine). *Langmuir* 2001, *17*, 3779-3783.
63. Kujawa, P.; Moraille, P.; Sanchez, J.; Badia, A.; Winnik, F. M. Effect of Molecular Weight on the Exponential Growth and Morphology of Hyaluronan/Chitosan Multilayers: A Surface Plasmon Resonance Spectroscopy and Atomic Force Microscopy Investigation. *J. Am. Chem. Soc.* 2005, *127*, 9224-9234.
64. Olugebefola, S. C.; Ryu, S.-W.; Nolte, A. J.; Rubner, M. F.; Mayes, A. M. Photo-cross-linkable Polyelectrolyte Multilayers for 2-D and 3-D Patterning. *Langmuir* 2006, *22*, 5958-5962.
65. Farhat, T. R.; Hammond, P. T. Designing a New Generation of Proton-Exchange Membranes Using Layer-by-Layer Deposition of Polyelectrolytes. *Adv. Funct. Mater.* 2005, *15*, 945-954.

66. Wang, X.; Kim, Y.-G.; Drew, C.; Ku, B.-C.; Kumar, J.; Samuelson, L. A. Electrostatic Assembly of Conjugated Polymer Thin Layers on Electrospun Nanofibrous Membranes for Biosensors. *Nano Lett.* 2004, *4*, 331-334.
67. Wang, T. C.; Rubner, M. F.; Cohen, R. E. Polyelectrolyte Multilayer Nanoreactors for Preparing Silver Nanoparticle Composites: Controlling Metal Concentration and Nanoparticle Size. *Langmuir* 2002, *18*, 3370-3375.
68. Boddohi, S.; Killingsworth, C. E.; Kipper, M. J. Polyelectrolyte Multilayer Assembly as a Function of pH and Ionic Strength Using the Polysaccharides Chitosan and Heparin. *Biomacromolecules* 2008, *9*, 2021-2028.
69. Elzbieciak, M.; Zapotoczny, S.; Nowak, P.; Krastev, R.; Nowakowska, M.; Warszyński, P. Influence of pH on the Structure of Multilayer Films Composed of Strong and Weak Polyelectrolytes. *Langmuir* 2009, *25*, 3255-3259.
70. Lutkenhaus, J. L.; Hrabak, K. D.; McEnnis, K.; Hammond, P. T. Elastomeric Flexible Free-Standing Hydrogen-Bonded Nanoscale Assemblies. *J. Am. Chem. Soc.* 2005, *127*, 17228-17234.
71. Argun, A. A.; Ashcraft, J. N.; Herring, M. K.; Lee, D. K. Y.; Allcock, H. R.; Hammond, P. T. Ion Conduction and Water Transport in Polyphosphazene-Based Multilayers. *Chem. Mater.* 2009, *22*, 226-232.
72. Li, Y.-C.; Schulz, J.; Grunlan, J. C. Polyelectrolyte/Nanosilicate Thin-Film Assemblies: Influence of pH on Growth, Mechanical Behavior, and Flammability. *ACS Appl. Mater. Interfaces* 2009, *1*, 2338-2347.
73. Jiang, G.; Baba, A.; Ikarashi, H.; Xu, R.; Locklin, J.; Kashif, K. R.; Shinbo, K.; Kato, K.; Kaneko, F.; Advincula, R. Signal Enhancement and Tuning of Surface Plasmon Resonance in Au Nanoparticle/Polyelectrolyte Ultrathin Films. *J. Phys. Chem. C* 2007, *111*, 18687-18694.
74. Geest, B. G. D.; Skirtach, A. G.; Beer, T. R. M. D.; Sukhorukov, G. B.; Bracke, L.; Baeyens, W. R. G.; Demeester, J.; Smedt, S. C. D. Stimuli-Responsive Multilayered Hybrid Nanoparticle/Polyelectrolyte Capsules. *Macromol. Rapid Commun.* 2007, *28*, 88-95.
75. Quinn, A.; Such, G. K.; Quinn, J. F.; Caruso, F. Polyelectrolyte Blend Multilayers: A Versatile Route to Engineering Interfaces and Films. *Adv. Funct. Mater.* 2008, *18*, 17-26.
76. Fu, J.; Ji, J.; Shen, L.; Küller, A.; Rosenhahn, A.; Shen, J.; Grunze, M. pH-Amplified Exponential Growth Multilayers: A Facile Method to Develop Hierarchical Micro- and Nanostructured Surfaces. *Langmuir* 2008, *25*, 672-675.
77. Yoo, P. J.; Nam, K. T.; Qi, J.; Lee, S.-K.; Park, J.; Belcher, A. M.; Hammond, P. T. Spontaneous assembly of viruses on multilayered polymer surfaces. *Nat. Mater.* 2006, *5*, 234-240.
78. Picart, C.; Mutterer, J.; Richert, L.; Luo, Y.; Prestwich, G. D.; Schaaf, P.; Voegel, J.-C.; Lavalle, P. Molecular basis for the explanation of the exponential growth of polyelectrolyte multilayers. *PNAS* 2002, *99*, 12531-12535.
79. Richert, L.; Lavalle, P.; Payan, E.; Shu, X. Z.; Prestwich, G. D.; Stoltz, J.-F.; Schaaf, P.; Voegel, J.-C.; Picart, C. Layer by Layer Buildup of Polysaccharide Films: Physical Chemistry and Cellular Adhesion Aspects. *Langmuir* 2003, *20*, 448-458.
80. Abalde-Cela, S.; Ho, S.; Rodríguez-González, B.; Correa-Duarte, Miguel A.; Álvarez-Puebla, Ramón A.; Liz-Marzán, Luis M.; Kotov, Nicholas A. Loading of Exponentially Grown LBL Films with Silver Nanoparticles and Their Application to Generalized SERS Detection13. *Angew. Chem. Int. Ed.* 2009, *48*, 5326-5329.
81. Wang, X.; Ji, J. Postdiffusion of Oligo-Peptide within Exponential Growth Multilayer Films for Localized Peptide Delivery. *Langmuir* 2009, *25*, 11664-11671.
82. Srivastava, S.; Podsiadlo, P.; Critchley, K.; Zhu, J.; Qin, M.; Shim, B. S.; Kotov, N. A. Single-Walled Carbon Nanotubes Spontaneous Loading into Exponentially Grown LBL Films. *Chem. Mater.* 2009, *21*, 4397-4400.
83. Laugel, N.; Boulmedais, F.; El Haitami, A. E.; Rabu, P.; Rogez, G.; Voegel, J.-C.; Schaaf, P.; Ball, V. Tunable Synthesis of Prussian Blue in Exponentially Growing Polyelectrolyte Multilayer Films. *Langmuir* 2009, *25*, 14030-14036.
84. Podsiadlo, P.; Michel, M.; Lee, J.; Verploegen, E.; Wong Shi Kam, N.; Ball, V.; Lee, J.; Qi, Y.; Hart, A. J.; Hammond, P. T.; Kotov, N. A. Exponential Growth of LBL Films with Incorporated Inorganic Sheets. *Nano Lett.* 2008, *8*, 1762-1770.
85. Vodouhê, C.; Guen, E. L.; Garza, J. M.; Francius, G.; Dégugnat, C.; Ogier, J.; Schaaf, P.; Voegel, J.-C.; Lavalle, P. Control of drug accessibility on functional polyelectrolyte multilayer films.

Biomaterials 2006, *27*, 4149-4156.
86. Yuan, W.; Dong, H.; Li, C. M.; Cui, X.; Yu, L.; Lu, Z.; Zhou, Q. pH-Controlled Construction of Chitosan/Alginate Multilayer Film: Characterization and Application for Antibody Immobilization. *Langmuir* 2007, *23*, 13046-13052.
87. Fu, J.; Ji, J.; Yuan, W.; Shen, J. Construction of anti-adhesive and antibacterial multilayer films via layer-by-layer assembly of heparin and chitosan. *Biomaterials* 2005, *26*, 6684-6692.
88. Miller, M. D.; Bruening, M. L. Correlation of the Swelling and Permeability of Polyelectrolyte Multilayer Films. *Chem. Mater.* 2005, *17*, 5375-5381.
89. Burke, S. E.; Barrett, C. J. pH-Dependent Loading and Release Behavior of Small Hydrophilic Molecules in Weak Polyelectrolyte Multilayer Films. *Macromolecules* 2004, *37*, 5375-5384.
90. Tanchak, O. M.; Barrett, C. J. Swelling Dynamics of Multilayer Films of Weak Polyelectrolytes. *Chem. Mater.* 2004, *16*, 2734-2739.
91. Burke, S. E.; Barrett, C. J. Swelling Behavior of Hyaluronic Acid/Polyallylamine Hydrochloride Multilayer Films. *Biomacromolecules* 2005, *6*, 1419-1428.
92. Pavoor, P. V.; Bellare, A.; Strom, A.; Yang, D.; Cohen, R. E. Mechanical Characterization of Polyelectrolyte Multilayers Using Quasi-Static Nanoindentation. *Macromolecules* 2004, *37*, 4865-4871.
93. Thompson, M. T.; Berg, M. C.; Tobias, I. S.; Rubner, M. F.; Van Vliet, K. J. Tuning compliance of nanoscale polyelectrolyte multilayers to modulate cell adhesion. *Biomaterials* 2005, *26*, 6836-6845.
94. Mermut, O.; Lefebvre, J.; Gray, D. G.; Barrett, C. J. Structural and Mechanical Properties of Polyelectrolyte Multilayer Films Studied by AFM. *Macromolecules* 2003, *36*, 8819-8824.
95. DeLongchamp, D. M.; Hammond, P. T. Fast Ion Conduction in Layer-By-Layer Polymer Films. *Chem. Mater.* 2003, *15*, 1165-1173.
96. Lutkenhaus, J. L.; McEnnis, K.; Hammond, P. T. Tuning the Glass Transition of and Ion Transport within Hydrogen-Bonded Layer-by-Layer Assemblies. *Macromolecules* 2007, *40*, 8367-8373.
97. Mauser, T.; Déjugnat, C.; Sukhorukov, G. B. Balance of Hydrophobic and Electrostatic Forces in the pH Response of Weak Polyelectrolyte Capsules. *J. Phys. Chem. B* 2006, *110*, 20246-20253.
98. Tong, W.; Gao, C.; Möhwald, H. Stable Weak Polyelectrolyte Microcapsules with pH-Responsive Permeability. *Macromolecules* 2005, *39*, 335-340.
99. Illergård, J.; Enarsson, L.-E.; Wågberg, L.; Ek, M. Interactions of Hydrophobically Modified Polyvinylamines: Adsorption Behavior at Charged Surfaces and the Formation of Polyelectrolyte Multilayers with Polyacrylic Acid. *ACS Appl. Mater. Interfaces* 2010, *2*, 425-433.
100. Dai, J.; Jensen, A. W.; Mohanty, D. K.; Erndt, J.; Bruening, M. L. Controlling the Permeability of Multilayered Polyelectrolyte Films through Derivatization, Cross-Linking, and Hydrolysis. *Langmuir* 2001, *17*, 931-937.
101. Kovačevic, D.; van der Burgh, S.; de Keizer, A.; Cohen Stuart, M. A. Specific Ionic Effects on Weak Polyelectrolyte Multilayer Formation†. *J. Phys. Chem. B* 2003, *107*, 7998-8002.
102. Nolte, A. J.; Takane, N.; Hindman, E.; Gaynor, W.; Rubner, M. F.; Cohen, R. E. Thin Film Thickness Gradients and Spatial Patterning via Salt Etching of Polyelectrolyte Multilayers. *Macromolecules* 2007, *40*, 5479-5486.
103. Schneider, A.; Francius, G.; Obeid, R.; Schwinté, P.; Hemmerlé, J.; Frisch, B.; Schaaf, P.; Voegel, J.-C.; Senger, B.; Picart, C. Polyelectrolyte Multilayers with a Tunable Young's Modulus: Influence of Film Stiffness on Cell Adhesion. *Langmuir* 2005, *22*, 1193-1200.
104. Ren, K.; Crouzier, T.; Roy, C.; Picart, C. Polyelectrolyte Multilayer Films of Controlled Stiffness Modulate Myoblast Cell Differentiation. *Adv. Funct. Mater.* 2008, *18*, 1378-1389.
105. Cho, J.; Quinn, J. F.; Caruso, F. Fabrication of Polyelectrolyte Multilayer Films Comprising Nanoblended Layers. *J. Am. Chem. Soc.* 2004, *126*, 2270-2271.
106. Hübsch, E.; Ball, V.; Senger, B.; Decher, G.; Voegel, J.-C.; Schaaf, P. Controlling the Growth Regime of Polyelectrolyte Multilayer Films: Changing from Exponential to Linear Growth by Adjusting the Composition of Polyelectrolyte Mixtures. *Langmuir* 2004, *20*, 1980-1985.
107. Quinn, A.; Tjipto, E.; Yu, A. M.; Gengenbach, T. R.; Caruso, F. Polyelectrolyte blend multilayer films: Surface morphology, wettability, and protein adsorption characteristics. *Langmuir*

2007, *23*, 4944-4949.
108. Francius, G.; Hemmerlé, J.; Voegel, J.-C.; Schaaf, P.; Senger, B.; Ball, V. Anomalous Thickness Evolution of Multilayer Films Made from Poly-l-lysine and Mixtures of Hyaluronic Acid and Polystyrene Sulfonate. *Langmuir* 2007, *23*, 2602-2607.
109. Quinn, J. F.; Yeo, J. C. C.; Caruso, F. Layer-by-Layer Assembly of Nanoblended Thin Films: Poly(allylamine hydrochloride) and a Binary Mixture of a Synthetic and Natural Polyelectrolyte. *Macromolecules* 2004, *37*, 6537-6543.
110. Debreczeny, M.; Ball, V.; Boulmedais, F.; Szalontai, B.; Voegel, J.-C.; Schaaf, P. Multilayers Built from Two Component Polyanions and Single Component Polycation Solutions: A Way To Engineer Films with Desired Secondary Structure. *J. Phys. Chem. B* 2003, *107*, 12734-12739.
111. Choi, J.; Rubner, M. F. Influence of the Degree of Ionization on Weak Polyelectrolyte Multilayer Assembly. *Macromolecules* 2004, *38*, 116-124.
112. Meng, S.; Liu, Z.; Shen, L.; Guo, Z.; Chou, L. L.; Zhong, W.; Du, Q.; Ge, J. The effect of a layer-by-layer chitosan-heparin coating on the endothelialization and coagulation properties of a coronary stent system. *Biomaterials* 2009, *30*, 2276-2283.
113. Ruan, Q.; Zhu, Y.; Li, F.; Xiao, J.; Zeng, Y.; Xu, F. Investigation of layer-by-layer assembled heparin and chitosan multilayer films via electrochemical spectroscopy. *J. Colloid Interface Sci.* 2009, *333*, 725-733.
114. Zacharia, N. S.; DeLongchamp, D. M.; Modestino, M.; Hammond, P. T. Controlling Diffusion and Exchange in Layer-by-Layer Assemblies. *Macromolecules* 2007, *40*, 1598-1603.
115. Zacharia, N. S.; Modestino, M.; Hammond, P. T. Factors Influencing the Interdiffusion of Weak Polycations in Multilayers. *Macromolecules* 2007, *40*, 9523-9528.
116. Laugel, N.; Betscha, C.; Winterhalter, M.; Voegel, J.-C.; Schaaf, P.; Ball, V. Relationship between the Growth Regime of Polyelectrolyte Multilayers and the Polyanion/Polycation Complexation Enthalpy. *J. Phys. Chem. B* 2006, *110*, 19443-19449.
117. Kharlampieva, E.; Sukhishvili, S. A. Ionization and pH Stability of Multilayers Formed by Self-Assembly of Weak Polyelectrolytes. *Langmuir* 2003, *19*, 1235-1243.
118. Kozlovskaya, V.; Yakovlev, S.; Libera, M.; Sukhishvili, S. A. Surface Priming and the Self-Assembly of Hydrogen-Bonded Multilayer Capsules and Films. *Macromolecules* 2005, *38*, 4828-4836.
119. Sukhishvili, S. A.; Granick, S. Layered, Erasable Polymer Multilayers Formed by Hydrogen-Bonded Sequential Self-Assembly. *Macromolecules* 2001, *35*, 301-310.
120. DeLongchamp, D. M.; Hammond, P. T. Highly ion conductive poly(ethylene oxide)-based solid polymer electrolytes from hydrogen bonding layer-by-layer assembly. *Langmuir* 2004, *20*, 5403-5411.
121. Yang, S.; Zhang, Y.; Guan, Y.; Tan, S.; Xu, J.; Cheng, S.; Zhang, X. Water uptake behavior of hydrogen-bonded PVPON-PAA LBL film. *Soft Matter* 2006, *2*, 699-704.
122. Kharlampieva, E.; Kozlovskaya, V.; Tyutina, J.; Sukhishvili, S. A. Hydrogen-Bonded Multilayers of Thermoresponsive Polymers. *Macromolecules* 2005, *38*, 10523-10531.
123. Millstone, J. E.; Hurst, S. J.; Métraux, G. S.; Cutler, J. I.; Mirkin, C. A. Colloidal Gold and Silver Triangular Nanoprisms. *Small* 2009, *5*, 646-664.
124. Gao, J.; Gu, H.; Xu, B. Multifunctional Magnetic Nanoparticles: Design, Synthesis, and Biomedical Applications. *Acc. Chem. Res.* 2009, *42*, 1097-1107.
125. Kotov, N. A.; Winter, J. O.; Clements, I. P.; Jan, E.; Timko, B. P.; Campidelli, S.; Pathak, S.; Mazzatenta, A.; Lieber, C. M.; Prato, M.; Bellamkonda, R. V.; Silva, G. A.; Kam, N. W. S.; Patolsky, F.; Ballerini, L. Nanomaterials for Neural Interfaces. *Adv. Mater.* 2009, *21*, 3970-4004.
126. Lu, X.; Wang, C.; Wei, Y. One-Dimensional Composite Nanomaterials: Synthesis by Electrospinning and Their Applications. *Small* 2009, *5*, 2349-2370.
127. Hicks, J. F.; Seok-Shon, Y.; Murray, R. W. Layer-by-Layer Growth of Polymer/Nanoparticle Films Containing Monolayer-Protected Gold Clusters. *Langmuir* 2002, *18*, 2288-2294.
128. Yuan, W.; Li, C. M. Direct Modulation of Localized Surface Plasmon Coupling of Au Nanoparticles on Solid Substrates via Weak Polyelectrolyte-Mediated Layer-by-Layer Self Assembly. *Langmuir* 2009, *25*, 7578-7585.
129. Schlenoff, J. B. Retrospective on the Future of Polyelectrolyte Multilayers. *Langmuir* 2009,

25, 14007-14010.
130. Srivastava, S.; Ball, V.; Podsiadlo, P.; Lee, J.; Ho, P.; Kotov, N. A. Reversible Loading and Unloading of Nanoparticles in "Exponentially" Growing Polyelectrolyte LBL Films. *J. Am. Chem. Soc*. 2008, *130*, 3748-3749.
131. Lavalle, P.; Vivet, V.; Jessel, N.; Decher, G.; Voegel, J.-C.; Mesini, P. J.; Schaaf, P. Direct Evidence for Vertical Diffusion and Exchange Processes of Polyanions and Polycations in Polyelectrolyte Multilayer Films. *Macromolecules* 2004, *37*, 1159-1162.
132. Hoda, N.; Larson, R. G. Modeling the Buildup of Exponentially Growing Polyelectrolyte Multilayer Films. *J. Phys. Chem. B* 2009, *113*, 4232-4241.
133. Salomäki, M.; Vinokurov, I. A.; Kankare, J. Effect of Temperature on the Buildup of Polyelectrolyte Multilayers. *Langmuir* 2005, *21*, 11232-11240.
134. Yoo, P. J.; Zacharia, N. S.; Doh, J.; Nam, K. T.; Belcher, A. M.; Hammond, P. T. Controlling Surface Mobility in Interdiffusing Polyelectrolyte Multilayers. *ACS Nano* 2008, *2*, 561-571.
135. Hoffmann, K.; Tieke, B. Layer-by-layer assembled membranes containing hexacyclen-hexaacetic acid and polyethyleneimine N-acetic acid and their ion selective permeation behaviour. *J. Membr. Sci.* 2009, *341*, 261-267.
136. Antipov, A. A.; Sukhorukov, G. B. Polyelectrolyte multilayer capsules as vehicles with tunable permeability. *Adv. Colloid Interface Sci.* 2004, *111*, 49-61.
137. Serizawa, T.; Matsukuma, D.; Akashi, M. Loading and Release of Charged Dyes Using Ultrathin Hydrogels. *Langmuir* 2005, *21*, 7739-7742.
138. Berg, M. C.; Zhai, L.; Cohen, R. E.; Rubner, M. F. Controlled Drug Release from Porous Polyelectrolyte Multilayers. *Biomacromolecules* 2005, *7*, 357-364.
139. Joly, S.; Kane, R.; Radzilowski, L.; Wang, T.; Wu, A.; Cohen, R. E.; Thomas, E. L.; Rubner, M. F. Multilayer Nanoreactors for Metallic and Semiconducting Particles. *Langmuir* 1999, *16*, 1354-1359.
140. Manca, L.; et al. Controlled synthesis of pure and doped ZnS nanoparticles in weak polyion assemblies: growth characteristics and fluorescence properties. *Nanotechnology* 2009, *20*, 275601.
141. Chia, K.-K.; Cohen, R. E.; Rubner, M. F. Amine-Rich Polyelectrolyte Multilayer Nanoreactors for in Situ Gold Nanoparticle Synthesis. *Chem. Mater.* 2008, *20*, 6756-6763.
142. Yuan, W.; Fu, J.; Su, K.; Ji, J. Self-assembled chitosan/heparin multilayer film as a novel template for in situ synthesis of silver nanoparticles. *Colloids Surf. B. Biointerfaces* 2010, *76*, 549-555.
143. Yuan, W.; Ji, J.; Fu, J.; Shen, J. A facile method to construct hybrid multilayered films as a strong and multifunctional antibacterial coating. *J. Biomed. Mater. Res. B* 2008, *85B*, 556-563.
144. Choi, W. S.; Koo, H. Y.; Park, J.-H.; Kim, D.-Y. Synthesis of Two Types of Nanoparticles in Polyelectrolyte Capsule Nanoreactors and Their Dual Functionality. *J. Am. Chem. Soc.* 2005, *127*, 16136-16142.
145. Kidambi, S.; Bruening, M. L. Multilayered Polyelectrolyte Films Containing Palladium Nanoparticles: Synthesis, Characterization, and Application in Selective Hydrogenation. *Chem. Mater.* 2004, *17*, 301-307.
146. Jiang, M.; Wang, E.; Kang, Z.; Lian, S.; Wu, A.; Li, Z. In situ controllable synthesis of polyoxometalate nanoparticles in polyelectrolyte multilayers. *J. Mater. Chem.* 2003, *13*, 647-649.
147. Aravind, U. K.; Mathew, J.; Aravindakumar, C. T. Transport studies of BSA, lysozyme and ovalbumin through chitosan/polystyrene sulfonate multilayer membrane. *J. Membr. Sci.* 2007, *299*, 146-155.
148. Sung, W.-C.; Chang, C.-C.; Makamba, H.; Chen, S.-H. Long-Term Affinity Modification on Poly(dimethylsiloxane) Substrate and Its Application for ELISA Analysis. *Anal. Chem.* 2008, *80*, 1529-1535.
149. Sung, W.-C.; Chen, H.-H.; Makamba, H.; Chen, S.-H. Functionalized 3D-Hydrogel Plugs Covalently Patterned Inside Hydrophilic Poly(dimethylsiloxane) Microchannels for Flow-Through Immunoassays. *Anal. Chem.* 2009, *81*, 7967-7973.
150. Zhou, X. C.; Zhou, J. Z. Protein microarrays on hybrid polymeric thin films prepared by self-assembly of polyelectrolytes for multiple-protein immunoassays. *Proteomics* 2006, *6*, 1415-1426.

151. Bai, Y. L.; Koh, C. G.; Boreman, M.; Juang, Y. J.; Tang, I. C.; Lee, L. J.; Yang, S. T. Surface modification for enhancing antibody binding on polymer-based microfluidic device for enzyme-linked immunosorbent assay. *Langmuir* 2006, *22*, 9458-9467.
152. Ha, T. H.; Jung, S. O.; Lee, J. M.; Lee, K. Y.; Lee, Y.; Park, J. S.; Chung, B. H. Oriented immobilization of antibodies with GST-fused multiple F-c-specific B-domains on a gold surface. *Anal. Chem.* 2007, *79*, 546-556.
153. Vareiro, M. L. M.; Liu, J.; Knoll, W.; Zak, K.; Williams, D.; Jenkins, A. T. A. Surface plasmon fluorescence measurements of human chorionic gonadotrophin: Role of antibody orientation in obtaining enhanced sensitivity and limit of detection. *Anal. Chem.* 2005, *77*, 2426-2431.
154. Chen, L. L.; Deng, L.; Liu, L. L.; Peng, Z. H. Immunomagnetic separation and MS/SPR end-detection combined procedure for rapid detection of Staphylococcus aureus and protein A. *Biosens. Bioelectron.* 2007, *22*, 1487-1492.
155. Xu, H.; Lu, J. R.; Williams, D. E. Effect of surface packing density of interfacially adsorbed monoclonal antibody on the binding of hormonal antigen human chorionic gonadotrophin. *J. Phys. Chem. B* 2006, *110*, 1907-1914.
156. Roach, P.; Farrar, D.; Perry, C. C. Surface tailoring for controlled protein adsorption: Effect of topography at the nanometer scale and chemistry. *J. Am. Chem. Soc.* 2006, *128*, 3939-3945.
157. Bernard, A.; Michel, B.; Delamarche, E. Micromosaic immunoassays. *Anal. Chem.* 2001, *73*, 8-12.
158. Ferretti, S.; Paynter, S.; Russell, D. A.; Sapsford, K. E.; Richardson, D. J. Self-assembled monolayers: a versatile tool for the formulation of bio-surfaces. *Trac-Trends Anal. Chem.* 2000, *19*, 530-540.
159. Tang, Z. Y.; Wang, Y.; Podsiadlo, P.; Kotov, N. A. Biomedical applications of layer-by-layer assembly: From biomimetics to tissue engineering. *Adv. Mater.* 2006, *18*, 3203-3224.
160. Stigter, E. C. A.; de Jong, G. J.; van Bennekom, W. P. An improved coating for the isolation and quantitation of interferon-gamma in spiked plasma using surface plasmon resonance (SPR). *Biosens. Bioelectron.* 2005, *21*, 474-482.
161. Masson, J. F.; Battaglia, T. M.; Kim, Y. C.; Prakash, A.; Beaudoin, S.; Booksh, K. S. Preparation of analyte-sensitive polymeric supports for biochemical sensors. *Talanta* 2004, *64*, 716-725.
162. Thierry, B.; Winnik, F. M.; Merhi, Y.; Silver, J.; Tabrizian, M. Bioactive coatings of endovascular stents based on polyelectrolyte multilayers. *Biomacromolecules* 2003, *4*, 1564-1571.
163. Wang, T. C.; Rubner, M. F.; Cohen, R. E. Polyelectrolyte multilayer nanoreactors for preparing silver nanoparticle composites: Controlling metal concentration and nanoparticle size. *Langmuir* 2002, *18*, 3370-3375.
164. Park, M. K.; Deng, S. X.; Advincula, R. C. pH-sensitive bipolar ion-permselective ultrathin films. *J. Am. Chem. Soc.* 2004, *126*, 13723-13731.
165. Choi, J.; Rubner, M. F. Influence of the degree of ionization on weak polyelectrolyte multilayer assembly. *Macromolecules* 2005, *38*, 116-124.
166. Itano, K.; Choi, J. Y.; Rubner, M. F. Mechanism of the pH-induced discontinuous swelling/deswelling transitions of poly(allylamine hydrochloride)-containing polyelectrolyte multilayer films. *Macromolecules* 2005, *38*, 3450-3460.
167. Kaschak, D. M.; Lean, J. T.; Waraksa, C. C.; Saupe, G. B.; Usami, H.; Mallouk, T. E. Photoinduced energy and electron transfer reactions in lamellar polyanion/polycation thin films: Toward an inorganic "leaf". *J. Am. Chem. Soc.* 1999, *121*, 3435-3445.
168. Caruso, F.; Niikura, K.; Furlong, D. N.; Okahata, Y. Ultrathin multilayer polyelectrolyte films on gold: Construction and thickness determination .1. *Langmuir* 1997, *13*, 3422-3426.
169. Michel, M.; Vautier, D.; Voegel, J. C.; Schaaf, P.; Ball, V. Layer by layer self-assembled polyelectrolyte multilayers with embedded phospholipid vesicles. *Langmuir* 2004, *20*, 4835-4839.
170. Wood, K. C.; Boedicker, J. Q.; Lynn, D. M.; Hammon, P. T. Tunable drug release from hydrolytically degradable layer-by-layer thin films. *Langmuir* 2005, *21*, 1603-1609.
171. Yuan, W.; Ji, J.; Fu, J.; Shen, J. A facile method to construct hybrid multilayered films as a strong and multifunctional antibacterial coating. *J. Biomed. Mater. Res. B* 2008, *85B*, 556-563.
172. Rinaudo, M. Chitin and chitosan: Properties and applications. *Prog. Polym. Sci.* 2006, *31*, 603-632.

173. George, M.; Abraham, T. E. Polyionic hydrocolloids for the intestinal delivery of protein drugs: Alginate and chitosan - a review. *J. Control. Release* 2006, *114*, 1-14.
174. Ye, S. Q.; Wang, C. Y.; Liu, X. X.; Tong, Z.; Ren, B.; Zeng, F. New loading process and release properties of insulin from polysaccharide microcapsules fabricated through layer-by-layer assembly. *J. Control. Release* 2006, *112*, 79-87.
175. Wilson, W. D. Analyzing biomolecular interactions. *Science* 2002, *295*, 2103-2105.
176. Hu, W. H.; Li, C. M.; Cui, X. Q.; Dong, H.; Zhou, Q. In situ studies of protein adsorptions on poly(pyrrole-co-pyrrole propylic acid) film by electrochemical surface plasmon resonance. *Langmuir* 2007, *23*, 2761-2767.
177. Stenberg, E.; Persson, B.; Roos, H.; Urbaniczky, C. Quantitative-Determination of Surface Concentration of Protein with Surface Plasmon Resonance Using Radiolabeled Proteins *J. Colloid Interface Sci.* 1991, *143*, 513-526.
178. Lu, Z. S.; Li, C. M.; Zhou, Q.; Bao, Q. L.; Cui, X. Q. Covalently linked DNA/protein multilayered film for controlled DNA release. *J. Colloid Interface Sci.* 2007, *314*, 80-88.
179. Wei, H.; Ma, N.; Shi, F.; Wang, Z. Q.; Zhang, X. Artificial nacre by alternating preparation of layer-by-layer polymer films and CaCO3 strata. *Chem. Mat.* 2007, *19*, 1974-1978.
180. Debruijn, H. E.; Altenburg, B. S. F.; Kooyman, R. P. H.; Greve, J. Determination of Thickness and Dielectric Constant of Thin Transparent Dielectric Layers Using Surface Plasmon Resonance. *Opt. Commun.* 1991, *82*, 425-432.
181. Fu, J. H.; Ji, J.; Yuan, W. Y.; Shen, J. C. Construction of anti-adhesive and antibacterial multilayer films via layer-by-layer assembly of heparin and chitosan. *Biomaterials* 2005, *26*, 6684-6692.
182. Wu, X. Z.; Huang, T. M.; Mullett, W. M.; Yeung, J. M.; Pawliszyn, J. Determination of isoelectric point and investigation of immunoreaction in peanut allergenic proteins-rabbit IgG antibody system by whole-column imaged capillary isoelectric focusing. *J. Microcolumn Sep.* 2001, *13*, 322-326.
183. Salloum, D. S.; Schlenoff, J. B. Protein adsorption modalities on polyelectrolyte multilayers. *Biomacromolecules* 2004, *5*, 1089-1096.
184. Caruso, F.; Niikura, K.; Furlong, D. N.; Okahata, Y. Assembly of alternating polyelectrolyte and protein multilayer films for immunosensing .2. *Langmuir* 1997, *13*, 3427-3433.
185. Chen, S. F.; Liu, L. Y.; Zhou, J.; Jiang, S. Y. Controlling antibody orientation on charged self-assembled monolayers. *Langmuir* 2003, *19*, 2859-2864.
186. Hu, X. G.; Dong, S. J. Metal nanomaterials and carbon nanotubes - synthesis, functionalization and potential applications towards electrochemistry. *J. Mater. Chem.* 2008, *18*, 1279-1295.
187. Seydack, M. Nanoparticle labels in immunosensing using optical detection methods. *Biosens. Bioelectron.* 2005, *20*, 2454-2469.
188. Cheng, W. L.; Dong, S. J.; Wang, E. K. Two- and three-dimensional Au nanoparticle/CoTMPyP self-assembled nanotructured materials: Film structure, tunable electrocatalytic activity, and plasmonic properties. *J. Phys. Chem. B* 2004, *108*, 19146-19154.
189. Aslan, K.; Gryczynski, I.; Malicka, J.; Matveeva, E.; Lakowicz, J. R.; Geddes, C. D. Metal-enhanced fluorescence: an emerging tool in biotechnology. *Curr. Opin. Biotechnol.* 2005, *16*, 55-62.
190. Huang, X. H.; Jain, P. K.; El-Sayed, I. H.; El-Sayed, M. A. Gold nanoparticles: interesting optical properties and recent applications in cancer diagnostic and therapy. *Nanomedicine* 2007, *2*, 681-693.
191. Chen, D.; Wang, G.; Li, J. H. Interfacial bioelectrochemistry: Fabrication, properties and applications of functional nanostructured biointerfaces. *J. Phys. Chem. C* 2007, *111*, 2351-2367.
192. Huang, C. C.; Yang, Z.; Lee, K. H.; Chang, H. T. Synthesis of highly fluorescent gold nanoparticles for sensing Mercury(II). *Angew. Chem. Int. Edit.* 2007, *46*, 6824-6828.
193. Schuetz, P.; Caruso, F. Semiconductor and Metal Nanoparticle Formation on Polymer Spheres Coated with Weak Polyelectrolyte Multilayers. *Chem. Mater.* 2004, *16*, 3066-3073.
194. Jain, P. K.; Huang, X.; El-Sayed, I. H.; El-Sayad, M. A. Review of some interesting surface plasmon resonance-enhanced properties of noble metal nanoparticles and their applications to biosystems. *Plasmonics* 2007, *2*, 107-118.
195. Yang, Y.; Matsubara, S.; Nogami, M.; Shi, J. L.; Huang, W. M. One-dimensional self-

assembly of gold nanoparticles for tunable surface plasmon resonance properties. *Nanotechnology* 2006, *17*, 2821-2827.
196. Verma, A.; Srivastava, S.; Rotello, V. M. Modulation of the interparticle spacing and optical behavior of nanoparticle ensembles using a single protein spacer. *Chem. Mat.* 2005, *17*, 6317-6322.
197. Rechberger, W.; Hohenau, A.; Leitner, A.; Krenn, J. R.; Lamprecht, B.; Aussenegg, F. R. Optical properties of two interacting gold nanoparticles. *Opt. Commun.* 2003, *220*, 137-141.
198. Mirkin, C. A.; Letsinger, R. L.; Mucic, R. C.; Storhoff, J. J. A DNA-based method for rationally assembling nanoparticles into macroscopic materials. *Nature* 1996, *382*, 607-609.
199. Jain, P. K.; Huang, W. Y.; El-Sayed, M. A. On the universal scaling behavior of the distance decay of plasmon coupling in metal nanoparticle pairs: A plasmon ruler equation. *Nano Lett.* 2007, *7*, 2080-2088.
200. Shi, C. S.; Tian, L. F.; Wu, L. L.; Zhu, J. Layered aggregates of gold nanoparticles: Solution and surface-assembled structures. *J. Phys. Chem. C* 2007, *111*, 1243-1247.
201. Kneipp, K.; Kneipp, H.; Kneipp, J. Surface-Enhanced Raman Scattering in Local Optical Fields of Silver and Gold NanoaggregatesFrom Single-Molecule Raman Spectroscopy to Ultrasensitive Probing in Live Cells. *Acc. Chem. Res.* 2006, *39*, 443-450.
202. Aroca, R. F.; Alvarez-Puebla, R. A.; Pieczonka, N.; Sanchez-Cortez, S.; Garcia-Ramos, J. V. Surface-enhanced Raman scattering on colloidal nanostructures. *Adv. Colloid Interface Sci.* 2005, *116*, 45-61.
203. Goulet, P. J. G.; dos Santos, D. S.; Alvarez-Puebla, R. A.; Oliveira, O. N.; Aroca, R. F. Surface-enhanced Raman scattering on dendrimer/metallic nanoparticle layer-by-layer film substrates. *Langmuir* 2005, *21*, 5576-5581.
204. Hayakawa, T.; Usui, Y.; Bharathi, S.; Nogami, M. Second harmonic generation from coupled surface-plasmon resonances in self-assembled gold-nanoparticle monolayers coated with an aminosilane. *Adv. Mater.* 2004, *16*, 1408-1412.
205. Ishifuji, M.; Mitsuishi, M.; Miyashita, T. Enhanced optical second harmonic generation in hybrid polymer nanoassemblies based on coupled surface plasmon resonance of a gold nanoparticle array. *Appl. Phys. Lett.* 2006, *89*.
206. Maier, S. A.; Kik, P. G.; Atwater, H. A.; Meltzer, S.; Harel, E.; Koel, B. E.; Requicha, A. A. G. Local detection of electromagnetic energy transport below the diffraction limit in metal nanoparticle plasmon waveguides. *Nat. Mater.* 2003, *2*, 229-232.
207. Maier, S. A.; Brongersma, M. L.; Kik, P. G.; Meltzer, S.; Requicha, A. A. G.; Atwater, H. A. Plasmonics - A route to nanoscale optical devices. *Adv. Mater.* 2001, *13*, 1501-1505.
208. Skirtach, A. G.; Javier, A. M.; Kreft, O.; Kohler, K.; Alberola, A. P.; Mohwald, H.; Parak, W. J.; Sukhorukov, G. B. Laser-induced release of encapsulated materials inside living cells. *Angew. Chem. Int. Ed.* 2006, *45*, 4612-4617.
209. Skirtach, A. G.; Dejugnat, C.; Braun, D.; Susha, A. S.; Rogach, A. L.; Parak, W. J.; Mohwald, H.; Sukhorukov, G. B. The role of metal nanoparticles in remote release of encapsulated materials. *Nano Lett.* 2005, *5*, 1371-1377.
210. Reinhard, B. M.; Siu, M.; Agarwal, H.; Alivisatos, A. P.; Liphardt, J. Calibration of dynamic molecular rule based on plasmon coupling between gold nanoparticles. *Nano Lett.* 2005, *5*, 2246-2252.
211. Jain, P. K.; El-Sayed, M. A. Noble Metal Nanoparticle Pairs: Effect of Medium for Enhanced Nanosensing. *Nano Lett.* 2008, *8*, 4347-4352.
212. Jiang, C. Y.; Markutsya, S.; Tsukruk, V. V. Collective and individual plasmon resonances in nanoparticle films obtained by spin-assisted layer-by-layer assembly. *Langmuir* 2004, *20*, 882-890.
213. Lu, C.; Mohwald, H.; Fery, A. Plasmon resonance tunable by deaggregation of gold nanoparticles in multilayers. *J. Phys. Chem. C* 2007, *111*, 10082-10087.
214. Frankamp, B. L.; Uzun, O.; Ilhan, F.; Boal, A. K.; Rotello, V. M. Recognition-mediated assembly of nanoparticles into micellar structures with diblock copolymers. *J. Am. Chem. Soc.* 2002, *124*, 892-893.
215. Schmid, G.; Baumle, M.; Beyer, N. Ordered two-dimensional monolayers of Au-55 clusters. *Angew. Chem. Int. Edit.* 2000, *39*, 181-183.
216. Boal, A. K.; Galow, T. H.; Ilhan, F.; Rotello, V. M. Binary and ternary polymer-mediated "bricks and mortar" self-assembly of gold and silica nanoparticles. *Adv. Funct. Mater.* 2001, *11*,

461-465.
217. Shenhar, R.; Norsten, T. B.; Rotello, V. M. Polymer-mediated nanoparticle assembly: Structural control and applications. *Adv. Mater.* 2005, *17*, 657-669.
218. Boal, A. K.; Frankamp, B. L.; Uzun, O.; Tuominen, M. T.; Rotello, V. M. Modulation of spacing and magnetic properties of iron oxide nanoparticles through polymer-mediated "bricks and mortar" self-assembly. *Chem. Mat.* 2004, *16*, 3252-3256.
219. Boal, A. K.; Ilhan, F.; DeRouchey, J. E.; Thurn-Albrecht, T.; Russell, T. P.; Rotello, V. M. Self-assembly of nanoparticles into structured spherical and network aggregates. *Nature* 2000, *404*, 746-748.
220. Frankamp, B. L.; Boal, A. K.; Rotello, V. M. Controlled interparticle spacing through self-assembly of Au nanoparticles and poly(amidoamine) dendrimers. *J. Am. Chem. Soc.* 2002, *124*, 15146-15147.
221. Ung, T.; Liz-Marzan, L. M.; Mulvaney, P. Optical properties of thin films of Au@SiO2 particles. *J. Phys. Chem. B* 2001, *105*, 3441-3452.
222. Phillips, K. S.; Han, J. H.; Martinez, M.; Wang, Z. Z.; Carter, D.; Cheng, Q. Nanoscale glassification of gold substrates for surface plasmon resonance analysis of protein toxins with supported lipid membranes. *Anal. Chem.* 2006, *78*, 596-603.
223. Yuan, W.; Ji, J.; Fu, J. H.; Shen, J. C. A facile method to construct hybrid multilayered films as a strong and multifunctional antibacterial coating. *J. Biomed. Mater. Res. B* 2008, *85B*, 556-563.
224. Hiller, J.; Rubner, M. F. Reversible molecular memory and pH-switchable swelling transitions in polyelectrolyte multilayers. *Macromolecules* 2003, *36*, 4078-4083.
225. Mendelsohn, J. D.; Yang, S. Y.; Hiller, J.; Hochbaum, A. I.; Rubner, M. F. Rational design of cytophilic and cytophobic polyelectrolyte multilayer thin films. *Biomacromolecules* 2003, *4*, 96-106.
226. Grabar, K. C.; Freeman, R. G.; Hommer, M. B.; Natan, M. J. Preparation and Characterization of Au Colloid Monolayers *Anal. Chem.* 1995, *67*, 735-743.
227. Rahme, K.; Gauffre, F.; Marty, J. D.; Payre, B.; Mingotaud, C. A systematic study of the stabilization in water of gold nanoparticles by poly(ethylene oxide)-poly(propylene oxide)-poly(ethylene oxide) triblock copolymers. *J. Phys. Chem. C* 2007, *111*, 7273-7279.
228. Singh, N.; Lyon, L. A. Au nanoparticle templated synthesis of pNIPAm nanogels. *Chem. Mat.* 2007, *19*, 719-726.
229. Schmitt, J.; Machtle, P.; Eck, D.; Mohwald, H.; Helm, C. A. Preparation and optical properties of colloidal gold monolayers. *Langmuir* 1999, *15*, 3256-3266.
230. Lebrun, L.; Vallee, F.; Alexandre, B.; Nguyen, Q. T. Preparation of chelating membranes to remove metal cations from aqueous solutions. *Desalination* 2007, *207*, 9-23.
231. Tang, Z. Y.; Wang, Y.; Kotov, N. A. Semiconductor nanoparticles on solid substrates: Film structure, intermolecular interactions, and polyelectrolyte effects. *Langmuir* 2002, *18*, 7035-7040.
232. Zhu, T.; Fu, X. Y.; Mu, T.; Wang, J.; Liu, Z. F. pH-dependent adsorption of gold nanoparticles on p-aminothiophenol-modified gold substrates. *Langmuir* 1999, *15*, 5197-5199.
233. Ostrander, J. W.; Mamedov, A. A.; Kotov, N. A. Two modes of linear layer-by-layer growth of nanoparticle-polylectrolyte multilayers and different interactions in the layer-by-layer deposition. *J. Am. Chem. Soc.* 2001, *123*, 1101-1110.
234. Abu-Sharkh, B. Structure and mechanism of the deposition of multilayers of polyelectrolytes and nanoparticles. *Langmuir* 2006, *22*, 3028-3034.
235. Licha, K.; Olbrich, C. Optical imaging in drug discovery and diagnostic applications. *Adv. Drug Deliv. Rev.* 2005, *57*, 1087-1108.
236. Weissleder, R. A clearer vision for in vivo imaging. *Nat. Biotechnol.* 2001, *19*, 316-317.
237. Storhoff, J. J.; Lazarides, A. A.; Mucic, R. C.; Mirkin, C. A.; Letsinger, R. L.; Schatz, G. C. What controls the optical properties of DNA-linked gold nanoparticle assemblies? *J. Am. Chem. Soc.* 2000, *122*, 4640-4650.
238. Zhong, Z. Y.; Patskovskyy, S.; Bouvrette, P.; Luong, J. H. T.; Gedanken, A. The surface chemistry of Au colloids and their interactions with functional amino acids. *J. Phys. Chem. B* 2004, *108*, 4046-4052.
239. Harris, N.; Arnold, M. D.; Blaber, M. G.; Ford, M. J. Plasmonic Resonances of Closely Coupled Gold Nanosphere Chains. *J. Phys. Chem. C* 2009, *113*, 2784-2791.

240. Howe, A. M.; Wesley, R. D.; Bertrand, M.; Cote, M.; Leroy, J. Controlled association in suspensions of charged nanoparticles with a weak polyelectrolyte. *Langmuir* 2006, *22*, 4518-4525.
241. Kotov, N. A.; Haraszti, T.; Turi, L.; Zavala, G.; Geer, R. E.; Dekany, I.; Fendler, J. H. Mechanism of and defect formation in the self-assembly of polymeric polycation-montmorillonite ultrathin films. *J. Am. Chem. Soc.* 1997, *119*, 6821-6832.
242. Correa-Duarte, M. A.; Giersig, M.; Kotov, N. A.; Liz-Marzan, L. M. Control of packing order of self-assembled monolayers of magnetite nanoparticles with and without SiO2 coating by microwave irradiation. *Langmuir* 1998, *14*, 6430-6435.
243. Lou, X. W.; Archer, L. A.; Yang, Z. Hollow Micro-/Nanostructures: Synthesis and Applications. *Adv. Mater.* 2008, *20*, 3987-4019.
244. Geest, B. G. D.; Koker, S. D.; Sukhorukov, G. B.; Kreft, O.; Parak, W. J.; Skirtach, A. G.; Demeester, J.; Smedt, S. C. D.; Hennink, W. E. Polyelectrolyte microcapsules for biomedical applications. *Soft Matter* 2009, *5*, 282-291.
245. Lee, D.; Rubner, M. F.; Cohen, R. E. Formation of Nanoparticle-Loaded Microcapsules Based on Hydrogen-Bonded Multilayers. *Chem. Mater.* 2005, *17*, 1099-1105.
246. Correa-Duarte, M. A.; Kosiorek, A.; Kandulski, W.; Giersig, M.; Liz-Marzan, L. M. Layer-by-Layer Assembly of Multiwall Carbon Nanotubes on Spherical Colloids. *Chem. Mater.* 2005, *17*, 3268-3272.
247. Zebli, B.; Susha, A. S.; Sukhorukov, G. B.; Rogach, A. L.; Parak, W. J. Magnetic targeting and cellular uptake of polymer microcapsules simultaneously functionalized with magnetic and luminescent nanocrystals. *Langmuir* 2005, *21*, 4262-4265.
248. Skirtach, A. G.; Dejugnat, C.; Braun, D.; Susha, A. S.; Rogach, A. L.; Parak, W. J.; Möhwald, H.; Sukhorukov, G. B. The Role of Metal Nanoparticles in Remote Release of Encapsulated Materials. *Nano Lett.* 2005, *5*, 1371-1377.
249. Shchukin, D. G.; Sukhorukov, G. B.; Möhwald, H. Smart Inorganic/Organic Nanocomposite Hollow Microcapsules13. *Angew. Chem. Int. Ed.* 2003, *42*, 4472-4475.
250. Sukhorukov, G. B.; Möhwald, H. Multifunctional cargo systems for biotechnology. *Trends Biotechnol.* 2007, *25*, 93-98.
251. Johnston, A. P. R.; Cortez, C.; Angelatos, A. S.; Caruso, F. Layer-by-layer engineered capsules and their applications. *Curr. Opin. Colloid Interface Sci.* 2006, *11*, 203-209.
252. Wang, Y.; Angelatos, A. S.; Caruso, F. Template Synthesis of Nanostructured Materials via Layer-by-Layer Assembly†. *Chem. Mater.* 2007, *20*, 848-858.
253. Skirtach, A. G.; Déjugnat, C.; Braun, D.; Susha, A. S.; Rogach, A. L.; Sukhorukov, G. B. Nanoparticles Distribution Control by Polymers: Aggregates versus Nonaggregates. *J. Phys. Chem. C* 2006, *111*, 555-564.
254. Kato, N.; Schuetz, P.; Fery, A.; Caruso, F. Thin multilayer films of weak polyelectrolytes on colloid particles. *Macromolecules* 2002, *35*, 9780-9787.
255. Yang, S. Y.; Lee, D.; Cohen, R. E.; Rubner, M. F. Bioinert solution-cross-linked hydrogen-bonded multilayers on colloidal particles. *Langmuir* 2004, *20*, 5978-5981.
256. Gaponik, N.; Radtchenko, I. L.; Sukhorukov, G. B.; Rogach, A. L. Luminescent Polymer Microcapsules Addressable by a Magnetic Field. *Langmuir* 2004, *20*, 1449-1452.
257. Sui, Z.; Schlenoff, J. B. Phase Separations in pH-Responsive Polyelectrolyte Multilayers: Charge Extrusion versus Charge Expulsion. *Langmuir* 2004, *20*, 6026-6031.
258. Cho, J.; Quinn, J. F.; Caruso, F. Fabrication of Polyelectrolyte Multilayer Films Comprising Nanoblended Layers. *J. Am. Chem. Soc.* 2004, *126*, 2270-2271.
259. Quinn, A.; Tjipto, E.; Yu, A.; Gengenbach, T. R.; Caruso, F. Polyelectrolyte Blend Multilayer Films: Surface Morphology, Wettability, and Protein Adsorption Characteristics. *Langmuir* 2007, *23*, 4944-4949.
260. Yap, H. P.; Quinn, J. F.; Johnston, A. P. R.; Caruso, F. Compositional Engineering of Polyelectrolyte Blend Capsules. *Macromolecules* 2007, *40*, 7581-7589.
261. Crouzier, T.; Szarpak, A.; Boudou, T.; Auzély-Velty, R.; Picart, C. Polysaccharide-Blend Multilayers Containing Hyaluronan and Heparin as a Delivery System for rhBMP-2. *Small* 2010, *6*, 651-662.
262. Schmitt, J.; Mächtle, P.; Eck, D.; Möhwald, H.; Helm, C. A. Preparation and Optical Properties of Colloidal Gold Monolayers. *Langmuir* 1999, *15*, 3256-3266.
263. Peng, C.; Thio, Y. S.; Gerhardt, R. A. Enhancing the Layer-by-Layer Assembly of Indium

Tin Oxide Thin Films by Using Polyethyleneimine. *J. Phys. Chem. C* 2010, *114*, 9685-9692.
264. Lvov, Y.; Ariga, K.; Onda, M.; Ichinose, I.; Kunitake, T. A careful examination of the adsorption step in the alternate layer-by-layer assembly of linear polyanion and polycation. *Colloids Surf., A* 1999, *146*, 337-346.
265. Hu, W.; Lu, Z.; Liu, Y.; Li, C. M. In Situ Surface Plasmon Resonance Investigation of the Assembly Process of Multiwalled Carbon Nanotubes on an Alkanethiol Self-Assembled Monolayer for Efficient Protein Immobilization and Detection. *Langmuir* 2010, *26*, 8386-8391.
266. Yuan, W. Y.; Li, C. M. Direct Modulation of Localized Surface Plasmon Coupling of Au Nanoparticles on Solid Substrates via Weak Polyelectrolyte-Mediated Layer-by-Layer Self Assembly. *Langmuir* 2009, *25*, 7578-7585.
267. Daniel, M.-C.; Astruc, D. Gold Nanoparticles: Assembly, Supramolecular Chemistry, Quantum-Size-Related Properties, and Applications toward Biology, Catalysis, and Nanotechnology. *Chem. Rev.* 2003, *104*, 293-346.
268. Jain, P.; Huang, X.; El-Sayed, I.; El-Sayed, M. Review of Some Interesting Surface Plasmon Resonance-enhanced Properties of Noble Metal Nanoparticles and Their Applications to Biosystems. *Plasmonics* 2007, *2*, 107-118.
269. Grabar, K. C.; Freeman, R. G.; Hommer, M. B.; Natan, M. J. PREPARATION AND CHARACTERIZATION OF AU COLLOID MONOLAYERS. *Anal. Chem.* 1995, *67*, 735-743.
270. Volodkin, D. V.; Larionova, N. I.; Sukhorukov, G. B. Protein encapsulation via porous CaCO3 microparticles templating. *Biomacromolecules* 2004, *5*, 1962-1972.
271. Volodkin, D. V.; Petrov, A. I.; Prevot, M.; Sukhorukov, G. B. Matrix polyelectrolyte microcapsules: New system for macromolecule encapsulation. *Langmuir* 2004, *20*, 3398-3406.
272. Ball, V.; Bernsmann, F.; Betscha, C.; Maechling, C.; Kauffmann, S.; Senger, B.; Voegel, J.-C.; Schaaf, P.; Benkirane-Jessel, N. Polyelectrolyte Multilayer Films Built from Poly(l-lysine) and a Two-Component Anionic Polysaccharide Blend. *Langmuir* 2009, *25*, 3593-3600.
273. Lu, C.; Möhwald, H.; Fery, A. Plasmon Resonance Tunable by Deaggregation of Gold Nanoparticles in Multilayers. *J. Phys. Chem. C* 2007, *111*, 10082-10087.
274. Li, Q.; Quinn, J. F.; Wang, Y.; Caruso, F. Preparation of Nanoporous Polyelectrolyte Multilayer Films via Nanoparticle Templating. *Chem. Mater.* 2006, *18*, 5480-5485.
275. Sukhorukov, G. B.; Volodkin, D. V.; Gunther, A. M.; Petrov, A. I.; Shenoy, D. B.; Mohwald, H. Porous calcium carbonate microparticles as templates for encapsulation of bioactive compounds. *J. Mater. Chem.* 2004, *14*, 2073-2081.
276. Jiang, C.; Markutsya, S.; Tsukruk, V. V. Collective and Individual Plasmon Resonances in Nanoparticle Films Obtained by Spin-Assisted Layer-by-Layer Assembly. *Langmuir* 2003, *20*, 882-890.
277. Caruso, F.; Caruso, R. A.; Mohwald, H. Production of Hollow Microspheres from Nanostructured Composite Particles. *Chem. Mater.* 1999, *11*, 3309-3314.
278. Kneipp, K.; Kneipp, H.; Kneipp, J. Surface-Enhanced Raman Scattering in Local Optical Fields of Silver and Gold NanoaggregatesFrom Single-Molecule Raman Spectroscopy to Ultrasensitive Probing in Live Cells. *Acc. Chem. Res.* 2006, *39*, 443-450.
279. Hayakawa, T.; Usui, Y.; Bharathi, S.; Nogami, M. Second harmonic generation from coupled surface-plasmon resonances in self-assembled gold-nanoparticle monolayers coated with an aminosilane. *Adv. Mater.* 2004, *16*, 1408-1412.
280. Maier, S. A.; Brongersma, M. L.; Kik, P. G.; Meltzer, S.; Requicha, A. A. G.; Atwater, H. A. Plasmonics - A route to nanoscale optical devices. *Adv. Mater.* 2001, *13*, 1501-1505.
281. Dong, W.-F.; Sukhorukov, G. B.; Mohwald, H. Enhanced Raman imaging and optical spectra of gold nanoparticle doped microcapsules. *Phys. Chem. Chem. Phys.* 2003, *5*, 3003-3012.
282. Ung, T.; Liz-Marzan, L. M.; Mulvaney, P. Optical Properties of Thin Films of Au@SiO2 Particles. *J. Phys. Chem. B* 2001, *105*, 3441-3452.
283. Jain, P. K.; Lee, K. S.; El-Sayed, I. H.; El-Sayed, M. A. Calculated absorption and scattering properties of gold nanoparticles of different size, shape, and composition: Applications in biological imaging and biomedicine. *J. Phys. Chem. B* 2006, *110*, 7238-7248.
284. Sharma, P.; Brown, S.; Walter, G.; Santra, S.; Moudgil, B. Nanoparticles for bioimaging. *Adv. Colloid Interface Sci.* 2006, *123-126*, 471-485.
285. Gil, P. R.; del Mercato, L. L.; del_Pino, P.; Muñoz_Javier, A.; Parak, W. J. Nanoparticle-modified polyelectrolyte capsules. *Nano Today 3*, 12-21.

286. Krishna, G.; Shutava, T.; Lvov, Y. Lipid modified polyelectrolyte microcapsules with controlled diffusion. *Chem. Commun.* 2005, 2796-2798.
287. An, Z.; Möhwald, H.; Li, J. pH Controlled Permeability of Lipid/Protein Biomimetic Microcapsules. *Biomacromolecules* 2006, *7*, 580-585.
288. Kozlovskaya, V.; Sukhishvili, S. A. pH-Controlled Permeability of Layered Hydrogen-Bonded Polymer Capsules. *Macromolecules* 2006, *39*, 5569-5572.
289. Ma, Y.; Dong, W.-F.; Hempenius, M. A.; Mohwald, H.; Julius Vancso, G. Redox-controlled molecular permeability of composite-wall microcapsules. *Nat. Mater.* 2006, *5*, 724-729.
290. Shi, X.; Caruso, F. Release Behavior of Thin-Walled Microcapsules Composed of Polyelectrolyte Multilayers. *Langmuir* 2001, *17*, 2036-2042.
291. Bergbreiter, D. E. Self-Assembled, Sub-Micrometer Diameter Semipermeable Capsules. *Angew. Chem. Int. Ed.* 1999, *38*, 2870-2872.
292. Wang, Z.; Qian, L.; Wang, X.; Yang, F.; Yang, X. Construction of hollow DNA/PLL microcapsule as a dual carrier for controlled delivery of DNA and drug. *Colloids Surf., A* 2008, *326*, 29-36.
293. Dun, H. J.; Zhang, W. Q.; Wei, Y.; Song, X. Q.; Li, Y. M.; Chen, L. R. Layer-by-layer self-assembly of multilayer zirconia nanoparticles on silica spheres for HPLC packings. *Anal. Chem.* 2004, *76*, 5016-5023.
294. Xihong, G.; et al. Myoglobin-loaded layer-by-layer films containing SiO 2 nanoparticles studied using electrochemistry. *Nanotechnology* 2008, *19*, 055709.
295. Ibarz, G.; Dahne, L.; Donath, E.; Mohwald, H. Resealing of polyelectrolyte capsules after core removal. *Macromol. Rapid Commun.* 2002, *23*, 474-478.
296. Kozlovskaya, V.; Kharlampieva, E.; Mansfield, M. L.; Sukhishvili, S. A. Poly(methacrylic acid) Hydrogel Films and Capsules: Response to pH and Ionic Strength, and Encapsulation of Macromolecules. *Chem. Mater.* 2005, *18*, 328-336.
297. Sharma, A. C.; Borovik, A. S. Design, Synthesis, and Characterization of Templated Metal Sites in Porous Organic Hosts: Application to Reversible Dioxygen Binding. *J. Am. Chem. Soc.* 2000, *122*, 8946-8955.
298. Li, Y. Y.; Cunin, F.; Link, J. R.; Gao, T.; Betts, R. E.; Reiver, S. H.; Chin, V.; Bhatia, S. N.; Sailor, M. J. Polymer Replicas of Photonic Porous Silicon for Sensing and Drug Delivery Applications. *Science* 2003, *299*, 2045-2047.
299. Wang, Y.; Angelatos, A. S.; Caruso, F. Template Synthesis of Nanostructured Materials via Layer-by-Layer Assembly†. *Chem. Mater.* 2007, *20*, 848-858.
300. Jang, J.; Bae, J. Fabrication of mesoporous polymer using soft template method. *Chem. Commun.* 2005, 1200-1202.
301. Zhang, L.; Sun, J. Layer-by-layer deposition of polyelectrolyte complexes for the fabrication of foam coatings with high loading capacity. *Chem. Commun.* 2009, 3901-3903.
302. Du, X.; Sun, Y.; Tan, B.; Teng, Q.; Yao, X.; Su, C.; Wang, W. Troger's base-functionalised organic nanoporous polymer for heterogeneous catalysis. *Chem. Commun.* 2010, *46*, 970-972.
303. Yuan, Z.-Y.; Su, B.-L. Insights into hierarchically meso-macroporous structured materials. *J. Mater. Chem.* 2006, *16*, 663-677.
304. Bernards, D. A.; Desai, T. A. Nanoscale porosity in polymer films: fabrication and therapeutic applications. *Soft Matter* 2010, *6*, 1621-1631.
305. Gultepe, E.; Nagesha, D.; Sridhar, S.; Amiji, M. Nanoporous inorganic membranes or coatings for sustained drug delivery in implantable devices. *Adv. Drug Del. Rev.* 2010, *62*, 305-315.
306. Sun, X.; Zheng, C.; Qiao, M.; Yan, J.; Wang, X.; Guan, N. Bioinspired synthesis of hierarchical macro-mesoporous titania with tunable macroporous morphology using cell-assemblies as macrotemplates. *Chem. Commun.* 2009, 4750-4752.
307. Jang, J.-H.; Jhaveri, S. J.; Rasin, B.; Koh, C.; Ober, C. K.; Thomas, E. L. Three-Dimensionally-Patterned Submicrometer-Scale Hydrogel/Air Networks That Offer a New Platform for Biomedical Applications. *Nano Lett.* 2008, *8*, 1456-1460.
308. Yang, M.; Lu, S. F.; Lu, J. L.; Jiang, S. P.; Xiang, Y. Layer-by-layer self-assembly of PDDA/PWA-Nafion composite membranes for direct methanol fuel cells. *Chem. Commun.* 2010, *46*, 1434-1436.
309. Manna, U.; Dhar, J.; Nayak, R.; Patil, S. Multilayer single-component thin films and microcapsules via covalent bonded layer-by-layer self-assembly. *Chem. Commun.* 2010, *46*, 2250-

2252.
310. Srivastava, S.; Ball, V.; Podsiadlo, P.; Lee, J.; Ho, P.; Kotov, N. A. Reversible Loading and Unloading of Nanoparticles in "Exponentially" Growing Polyelectrolyte LBL Films. *J. Am. Chem. Soc*. 2008, *130*, 3748-3749.
311. Podsiadlo, P.; Michel, M.; Lee, J.; Verploegen, E.; Wong Shi Kam, N.; Ball, V.; Lee, J.; Qi, Y.; Hart, A. J.; Hammond, P. T.; Kotov, N. A. Exponential Growth of LBL Films with Incorporated Inorganic Sheets. *Nano Lett.* 2008, *8*, 1762-1770.
312. Picart, C.; Mutterer, J.; Richert, L.; Luo, Y.; Prestwich, G. D.; Schaaf, P.; Voegel, J.-C.; Lavalle, P. Molecular basis for the explanation of the exponential growth of polyelectrolyte multilayers. *PNAS* 2002, *99*, 12531-12535.
313. Ren, K.; Ji, J.; Shen, J. Construction and enzymatic degradation of multilayered poly-l-lysine/DNA films. *Biomaterials* 2006, *27*, 1152-1159.
314. Pernaut, J.-M.; Reynolds, J. R. Use of Conducting Electroactive Polymers for Drug Delivery and Sensing of Bioactive Molecules. A Redox Chemistry Approach. *J. Phys. Chem. B* 2000, *104*, 4080-4090.
315. Langer, R. New methods of drug delivery. *Science* 1990, *249*, 1527-1533.
316. Zhai, L.; Cebeci, F. C.; Cohen, R. E.; Rubner, M. F. Stable superhydrophobic coatings from polyelectrolyte multilayers. *Nano Lett.* 2004, *4*, 1349-1353.
317. Zhong, Y.; Whittington, C. F.; Zhang, L.; Haynie, D. T. Controlled loading and release of a model drug from polypeptide multilayer nanofilms. *Nanomedicine: NBM* 2007, *3*, 154-160.
318. Chunder, A.; Sarkar, S.; Yu, Y.; Zhai, L. Fabrication of ultrathin polyelectrolyte fibers and their controlled release properties. *Colloids Surf., B* 2007, *58*, 172-179.
319. Huang, X.; Lowe, T. L. Biodegradable Thermoresponsive Hydrogels for Aqueous Encapsulation and Controlled Release of Hydrophilic Model Drugs. *Biomacromolecules* 2005, *6*, 2131-2139.
320. Salehi, P.; Sarazin, P.; Favis, B. D. Porous devices derived from co-continuous polymer blends as a route for controlled drug release. *Biomacromolecules* 2008, *9*, 1131-1138.
321. Kuznetsova, A.; Yates, J. T.; Liu, J.; Smalley, R. E. Physical adsorption of xenon in open single walled carbon nanotubes: Observation of a quasi-one-dimensional confined Xe phase. *J. Chem. Phys.* 2000, *112*, 9590-9598.

Author's CV

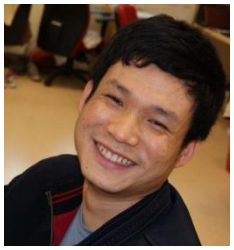

Weiyong Yuan received his Bachelor's degree in Polymeric Materials and Engineering from Zhejiang University in 2004, and obtained his Master's degree in Materials Science and Engineering from Zhejiang University in 2006 under the co-supervision of Prof. Jiacong Shen and Prof. Jian Ji. After that he joined Nanyang Technological University to pursue his Ph. D study under the supervision of Prof. Chang Ming Li.

Publication List in Ph. D study

1. **Yuan, W.**; Dong, H.; Li, C. M.; Cui, X.; Yu, L.; Lu, Z.; Zhou, Q. pH-Controlled Construction of Chitosan/Alginate Multilayer Film: Characterization and Application for Antibody Immobilization. *Langmuir* 2007, 23, 13046-13052.
2. **Yuan, W.**; Li, C. M. Direct Modulation of Localized Surface Plasmon Coupling of Au Nanoparticles on Solid Substrates via Weak Polyelectrolyte-Mediated Layer-by-Layer Self Assembly. *Langmuir* 2009, 25, 7578-7585.
3. **Yuan, W.**; Lu, Z.; Li, C. M. Superior Tunability and Synergistic Properties of Controllablly Layer-by-Layer Assembled Polyelectrolytes/Nanoparticle Blend Hollow Capsules. *Journal of Materials chemistry* Accecpted.
4. **Yuan, W.**; Li, C. M. Exponentially growing layer-by-layer assembly to fabricate pH-responsive hierarchical nanoporous polymeric film and its superior controlled release performance. *Chemical Communications* 2010, 46, 9161-9163.

5. Chen, L. H.; Chan, C. C.; **Yuan, W.**; Goh, S. K.; Sun, J. High performance chitosan diaphragm-based fiber-optic acoustic sensor. *Sensors and Actuators A*: *Physical* doi:10.1016/j.sna.2010.06.023.
6. **Yuan, W.**; Li, C. M. Exponentially growing weak polyelectrolyte multilayers for protein delivery. *The 2nd International Conference on Cellular & Molecular Bioengineering* 2010.
7. **Yuan, W.**; Li, C. M. Fabrication of Non-UV Induced Superhydrophilic, Antifogging, and Antibacterial Multilayer Coating via Self-assembly. In patent application.
8. **Yuan, W.**; Liu, J.; Li, C. M.; Wang, H. Fabrication of Substrate-attached Large-area and high-density polyelectrolyte nanotube arrays via ZnO-nanowire-array-templated self-assembly. In preparation.
9. **Yuan, W.**; Li, C. M. Fabrication of high-density gold nanoparticle arrays on solid substrates via a sacrificial pH-amplified exponentially grown multilayer template. In preparation.
10. **Yuan, W.**; Li, C. M. Exponentially Grown Multilayers for Reversible Loading and Release of Protein. In preparation.
11. **Yuan, W.**; Lu, Z.; Li, C. M. Self-assembled hierarchical ZnO nanoflower multilayers with non-UV induced superhydrophilicity, antifogging, and antibacterial properties. In preparation.
12. **Yuan, W.**; Li, C. M. Ultrafast exponentially growing weak polyelectrolyte multilayers for small-molecule delivery: amphoteric property, ultrahigh loading capacity and pH-responsiveness. In preparation.

13. **Yuan, W.**; Li, C. M. Weak Polyelectrolyte-Based Multilayers via Layer-by-Layer Assembly: Insights and Applications. In preparation.